Long chain branching analysis of polyethylene using advanced fractionation methods

by

Petronella Zabesuthu Ndlovu

Thesis presented in partial fulfilment of the degree of
Master of Science (Polymer Science)

at the

University of Stellenbosch

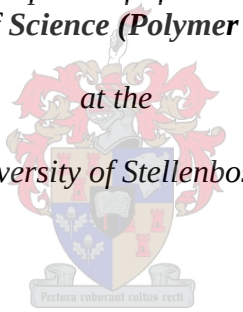

Supervisor: Prof. Harald Pasch **December 2021**

Declaration

By submitting this thesis electronically, I declare that the entirety of the work contained therein is my own, original work, that I am the sole author thereof (save to the extent explicitly otherwise stated), that reproduction and publication thereof by Stellenbosch University will not infringe any third-party rights and that I have not previously in its entirety or in part submitted it for obtaining any qualification.

Dedication

To my parents, siblings, and colleagues.

Abstract

Polyolefins (POs) have contributed immensely to the quality of life since their commercialization in the mid-1950s and they are modified continuously to suit new applications. PO homopolymer properties for materials such as polyethylene (PE) are strongly influenced by molar mass (MM), molar mass distribution (MMD), as well as branching types and branching distributions. These distributions influence the processability as well as the physical and mechanical properties of the PO; in turn affecting its end-use properties.

In the first part of this study, three commercial low density polyethylenes (LDPES) and four long chain branched PEs (LCBPEs) are comprehensively analyzed using various advanced analytical techniques to elucidate their MM and branching structures. Fourier-transform infrared spectroscopy (FTIR) and high-resolution carbon-thirteen nuclear magnetic resonance spectroscopy (^{13}C-NMR) were used for average chemical composition determination. ^{13}C-NMR enabled the identification and quantification of the diverse short chain branches (SCB) e.g., methyl, ethyl, butyl amyl groups as well as long chain branches (LCB). High-temperature quadruple-detector size exclusion chromatography (HT-SEC-d4) revealed the branching differences via specific conformation plots. The differences in the LCB contents of the LCBPEs was readily identified in HT-SEC-d4 using Mark-Houwink-Sakurada (MHS) plots. These LCBs are estimated to be longer than C_{50} or C_{60} and this information cannot be readily obtained from ^{13}C-NMR. LDPEs also showed deviation, although less significant, from linear behaviour and influences of both SCB and LCB could be readily identified. It was shown that in the absence of SCB, LCBs encourage formation of compact structures with low chain entanglement. High melting (T_m) and crystallization temperatures (T_c) as well as crystallinities (X_c) for LCBPEs which were different to LDPEs (where SCB was dominant) were obtained using differential scanning calorimetry (DSC). Interaction chromatography (HT-IC) was used to separate differently branched molecules on two different stationary phases using two interaction modes. Owing to the strong adsorptive force on porous graphitic carbon (PGC), the components in the LDPEs and LCBPEs could not be separated efficiently using temperature gradient interaction chromatography (TGIC). However, a solvent gradient (SGIC) could resolve the copolymer and homopolymer components. TGIC was more efficient in separating the differently branched chains when silica was used as the stationary phase due to the absence of a strong adsorptive force. The differences in SCB of the LDPEs could be readily recognised

using TGIC wherein silica was used as the stationary phase. These differences were linked to tensile strength and Young's moduli of the samples. Hyphenation of HT-IC in the first dimension to HT-SEC in the second dimension as in high-temperature two-dimensional liquid chromatography (HT-2D-LC) confirmed the molar mass of the eluting components.

In the second part of the study the bulk samples are fractionated using preparative molar mass fractionation (p-MMF) to obtain fractions with distinctly different molar masses. HT-SEC-d4 used for molar mass and branching analyses confirmed ^{13}C-NMR findings that SCB is inherent across the MM fractions of the LDPEs. On the other hand, LCB content was shown to increase with decrease in the fraction molar mass of LCBPE fractions. Chemical composition analyses using HT-TGIC showed that multiple branching distributions were present in the LCBPE fractions as seen in the multimodal elution patterns. Further fractionation of fractions and bulk samples exhibiting multimodal elution behaviours could possibly be carried out to investigate the underlying complex compositions.

Opsomming

Polyolefiene (POs) het sedert die kommersialisering daarvan in die middel van die vyftigerjare geweldig bygedra tot die lewensgehalte. Dit word deurlopend aangepas om by nuwe toepassings te pas. PO-homopolimeer-eienskappe vir materiale soos poliëtileen (PE) word sterk beïnvloed deur molêre massa (MM), molêre massaverdeling (MMD), sowel as vertakkingstipes en vertakkingsverspreidings. Hierdie verspreidings beïnvloed die verwerkbaarheid sowel as die fisiese en meganiese eienskappe van die PO. Op die einde beïnvloed dit die eindgebruiks eienskappe daarvan.

In die eerste deel van hierdie studie word drie kommersiële lae-digtheid poliëtielenes (LDPES) en vier langkettingvertakte PE's (LCBPE's) breedvoerig geanaliseer. Dit word geanaliseer met die hulp van verskillende gevorderde analitiese tegnieke om die MM en vertakkingsstrukture toe te lig. Fourier-transform infrarooi spektroskopie (FTIR) en hoë-resolusie koolstof-13 kernmagnetiese resonansspektroskopie (13C-NMR) is gebruik vir die gemiddelde bepaling van chemiese samestellings. 13C-NMR het die identifisering en kwantifisering van die verskillende kortkettingtakke (SCB) moontlik gemaak, bv., metiel-, etiel-, butielamilgroepe sowel as langkettingtakke (LCB). Hoë temperatuur grootte uitsluiting chromatografie met 'n viervoudige detektor (HT-SEC-d4) het die vertakkingsverskille via spesifieke bouvormplotte aan die lig gebring. Die verskille in die LCB-inhoud van die LCBPE's is geïdentifiseer met HT-SEC-d4 met behulp van Mark-Houwink-Sakurada (MHS) erwe. Na raming is hierdie LCB's langer as C50 of C60 dan kan hierdie inligting nie maklik verkry word van 13C-NMR nie. LDPE's het ook afwyking getoon, hoewel minder betekenisvol, van lineêre gedrag. Die beinvloed van beide die SCB en LCB kon maklik geïdentifiseer word. Daar is aangetoon dat LCB's in die afwesigheid van SCB, die vorming van kompakte strukture met 'n lae ketting verstrengeling aanmoedig. hoë smelt- (Tm) en kristallisasietemperature (Tc) sowel as kristalliniteite (Xc) vir LCBPE's, wat verskil van LDPE's (waar SCB oorheersend was), is verkry met behulp van differensiële skandering kalorimetrie (DSC). Interaksiechromatografie (HT-IC) word gebruik om verskillende vertakte molekules te skei. Dit word op twee verskillende stilstaande fases met behulp van twee interaksiemetodes gedoen. As gevolg van die sterk adsorptiewe krag op poreuse grafitiese koolstof (PGC), kon die komponente in die LDPE's en LCBPE's nie doeltreffend geskei word met behulp van temperatuur gradiënteinteraksiechromatografie (TGIC) nie.'n Oplosmiddelgradiënt (SGIC) kan egter die

kopolimeer- en homopolymer komponente oplos. TGIC was meer doëltreffend om die verskillende vertakte kettings te skei as silika as die stilstaande fase gebruik is weens die afwesigheid van 'n sterk adsorptiewe krag. Die verskille in SCB van die LDPE's kan maklik herken word met behulp van TGIC waarin silika as die stilstaande fase gebruik is. Hierdie verskille is gekoppel aan trek sterkte en Young se moduli van die monsters. Die gebruik van HT-IC in die eerste dimensie en HT-SEC in die tweede dimensie, het die molêre massa van die eluerende komponente bevestig.

In die tweede deel van die studie word die grootmaat monsters gefrakteer met behulp van voorbereidende molêre massa-fraksionering (p-MMF) om breuke met verskillende molêre massas te verkry. HT-SEC-d4 wat gebruik word vir molêre massa en vertakkingsanalises, het 13C-NMR bevindings bevestig dat SCB inherent is aan die MM-breuke van die LDPE's. Aan die ander kant is dit aangetoon dat die LCB-inhoud toeneem met die afname in die fraksie molêre massa van LCBPE-breuke. Chemiese samestellingsanalises met behulp van HT-TGIC het getoon dat meervoudige takverdelings in die LCBPE-breuke teenwoordig was. Dit is waargeneem in die multimodale elusiepatrone. Verdere fraksionering van breuke en grootmaat monsters met multimodale elusiegedrag kan moontlik uitgevoer word om die onderliggende komplekse samestellings te ondersoek.

Acknowledgements

Firstly, I want to thank God for granting me this opportunity and seeing me throughout this study.

My sincerest gratitude goes to **Prof. Harald Pasch** for the guidance, patience, supervision, and encouragement for the duration of this MSc study. The conversations we had were educative and enlightening. I am grateful for the opportunity to learn and grow as an academic as well as the financial support.

My sincere thanks go to:

Dr. Anthony Ndiripo for being a patient academic mentor.

Dr. Andy Roediger and Ms. Illana Bergh of Roediger Agencies for the permission to use their facilities as well as the assistance with the mechanical analyses.

Dr. Andreas Albrecht (Borealis, Linz Austria) for supplying the long chain branched polyethylene samples.

Prof. Albena Lederer for her mentorship sessions.

Dr. Jaco Brand and **Mrs Elsa Malherbe** for the immense help with the high-resolution NMR analyses.

All the staff at the Department of Chemistry and Polymer Science, **Mrs. Erinda Cooper, Mr. Jim Motshweni, Mr. Calvin Maart and Mr. Mbuso Dludlu.**

All members of the Pasch's group present: **Helen**, **Mawande, Joshua, Ndumiso, Paul, Chelsea, Zahn and Zanelle.**

Family and friends

Table of Contents

List of Figures

List of Tables

List of Symbols

M_w	Weight-average molar mass
M_n	Number-average molar mass
M_p	Peak molar mass
Đ	Molar mass dispersity
V_e	Elution volume
α	Selectivity factor
R_g	Radius of gyration
η	Intrinsic viscosity
g	Contraction factor
g'	Contraction factor
X_c	Crystallinity
T_m	Melting temperature
T_c	Crystallisation temperature

List of abbreviations

CC	Chemical composition
CCD	Chemical composition distribution
^{13}C-NMR	Carbon-thirteen nuclear magnetic resonance spectroscopy
CRYSTAF	Crystallization analysis fractionation
SCB	Short chain branching
SCBD	Short chain branching distribution
DSC	Differential scanning calorimetry
ESL	Ethylene sequence length
ESLD	Ethylene sequence length distribution
FTIR	Fourier transform infrared spectroscopy
HDPE	High density polyethylene
HT-2D-LC	High temperature two-dimensional liquid chromatography
IC	Interaction chromatography
LDPE	Low density polyethylene
LLDPE	Linear low density polyethylene
LCBPE	Long chain branched polyethylene
MFI	Melt flow index
MM	Molar mass
MMD	Molar mass distribution
HT-HPLC	High-temperature high performance liquid chromatography
HT-SEC	High-temperature size exclusion chromatography
HT-SGIC	High-temperature solvent gradient interaction chromatography
HT-TGIC	High-temperature temperature gradient interaction chromatography
HT-SEC-d4	High temperature quadruple detector size exclusion chromatography
PE	Polyethylene
PP	Polypropylene
PS	Polystyrene
SGIC	Solvent gradient interaction chromatography
TGIC	Temperature gradient interaction chromatography
TREF	Temperature rising elution fractionation

Chapter 1 : Introduction and objectives

This chapter introduces the challenges that will be addressed in the present work and lists the objectives to be addressed.

1.1 Introduction

Polyethylene (PE) is a synthetic polyolefin material that is widely used, making up one third of the total thermoplastics market[1,2]. Its properties are strongly influenced by molar mass (MM), molar mass distribution (MMD), as well as branching types and branching distributions. Amongst the types of PE, low density polyethylene (LDPE) is an industrially important material exhibiting complex branching distributions[3]. Globally, LDPE production and consumption rates are quite high and were reported to reach 20.3 million tons in 2015. Market studies reveal that consumption rates will steadily increase annually.[4] For this reason, studies on LDPE and PE indicate that improvements in production and molecular analysis of LDPE have a high priority[5-8].

The first PE that was produced industrially was LDPE using free radical polymerization with traces of oxygen as the initiator under harsh conditions of high pressure and temperature[9]. Commercial LDPE manufactured by either tubular or stirred reactors has gained popularity as one of the most used polymers[10]. With time, PE with short-chain branches (SCBs) and long-chain branches (LCBs) was produced via intra- or intermolecular radical chain transfer during polymerization. LDPE contains both LCB and SCB having different impacts on the materials properties irrespective of their amount/quantity. LCB allows for good processability whereas SCB gives the polymer a low degree of crystallinity. Different methods have been used to produce long-chain branched polyethylene.

The advancement in olefin polymerization catalysis has led to the expansion of commercial production of polyolefins beyond conventional linear or branched architectures.[11] Notably, progress has been achieved in the controlled synthesis of long chain branched polyolefins with diverse MM, MMD, tacticity, chemical composition (CC), chemical composition distribution (CCD), and long-chain branching[12]. More and better catalyst systems have evolved providing refined macromonomer formation and insertion ability. These include metallocenes, constraint geometry catalysts (CGC), ansa-metallocenes, and late transition metal catalytic systems (Pd

and Ni).[13] However, a notable challenge remains in comprehensively characterizing these classes of polyolefins with regard to their molecular composition.

Crystallization-based techniques are a stronghold of polyolefin characterization. These fractionation techniques have been used to separate polyolefins according to their varying structures[14]. Crystallization analysis fractionation (CRYSTAF), crystallization elution fractionation (CEF) and temperature rising elution fractionation (TREF) are commonly used to determine CCD of semi-crystalline olefin copolymers utilizing the relationship between comonomer content and crystallizability in a hot dilute solution as per Flory's theory. These techniques, however, are limited to semi-crystalline polyolefins, so they fail when applied to polyolefins with low crystallinity or amorphous materials.

There is a wide variety of characterization methods that can be used to unravel the microstructure of polyolefins. Amongst various liquid chromatography (LC) techniques employed for the characterization of polymers in general, high-temperature size exclusion chromatography (HT-SEC) is the most used for molar mass characterization of polyolefins making use of good solvents like 1,2,4-trichlorobenzene (TCB) as the mobile phase.[15,16] When coupled to multiple detectors, information on chemical composition and/or branching is obtained as a function of elution volume. The main disadvantage with SEC is the co-elution of branched and linear chains as it only separates macromolecules according to hydrodynamic volume.[17,18] Furthermore, the separation is based on size instead of functionality. The recent introduction of high-temperature interaction chromatography HT-IC has paved way for new ways of probing into the microstructure of polyolefins. Previous analysis of these materials had only been limited to HT-SEC, which by its very nature separates macromolecules according to size and provides very limited information on chemical composition/branching distributions.

Interaction chromatography is more efficient in the separation of polyolefins according to chemical composition/branching as it uses enthalpic interactions to control adsorption or partition of solute molecules on the stationary phase. It has been shown repeatedly that van der Waals interactions occur on porous graphitic carbon (PGC) used as the stationary phase.[19,20] In this case, the separation mechanism is more sensitive to the chemical and topological nature of the polyolefin molecules. The interactive forces are influenced by the methylene sequence length of the polyolefin chain rather than its crystallinity. The interactions on PGC are controlled by london dispersion forces which are overcome by applying a solvent or

temperature gradient.[2] High-temperature solvent gradient interaction chromatography (HT-SGIC) and high-temperature temperature gradient interaction chromatography (HT-TGIC) have been employed for the separation and characterization of polyolefins and are excellent platforms to assist the method development specifically for LDPEs[21].

Preparative fractionation techniques have been used to simplify the complex composition of bulk samples by providing narrow dispersed fractions that can be independently analyzed. Amongst these, preparative temperature rising elution fractionation (p-TREF), preparative molar mass fractionation (p-MMF), and preparative solution crystallization fractionation (p-SCF) are the most frequently used. These methods aid in providing narrowly distributed fractions and fractions with homogenous chemical composition or molar mass. Subsequent to the preparative fractionation, the obtained fractions are subjected to in-depth analysis using chromatographic and spectroscopic techniques which give information on branching, MMD, and CCD. These techniques include Fourier transform infrared spectroscopy (FTIR) and nuclear magnetic resonance (NMR) spectroscopy.

1.2 Problem statement

LDPEs and other long chain branched polyethylenes are complex polyolefin materials that exhibit complex branching and molar mass distributions. These distributions influence the processability and mechanical properties of the polymer, which in turn affects its end-use. Different techniques are being used to analyze LDPE to understand its structure. Unlike crystallization-based analytical techniques such as CRYSTAF, TREF and DSC, that are limited to crystallizable materials, interaction chromatography has proven to be more reliable in characterizing LDPEs according to chemical composition and branching.

Several analytical techniques must be combined complementary to acquire comprehensive knowledge on the microstructure of the polyolefin. Preparative molar mass fractionation (p-MMF) is an important tool as it separates the polymer chains based on their solubility in a solvent system suitable for separating the polymer irrespective of its crystallinity. In the present study, a suitable analytical method for the comprehensive characterization of long chain branched LDPE will be developed.

1.3 Aims and objectives

Branched polyethylene characterization is an interesting area of research because of the complex structure of LDPE, which is dependent on the reaction conditions. This study aims at analyzing several branched polyethylene samples using novel methodologies and new approaches by applying advanced analytical techniques. The following objectives are defined:

- Obtain LDPEs from different producers as a sample toolbox (commercial and lab synthesized).
- Analyze the bulk samples using advanced analytical techniques (HT-SEC, HT-IC, HT-2D-LC, DSC, CRYSTAF, FTIR and ^{13}C-NMR).
- Fractionate the bulk samples using preparative molar mass fractionation (p-MMF) to obtain fractions for further analysis.
- Analyze fractions using several advanced analytical techniques to obtain more data regarding the microstructure of the polymer.
- Perform mechanical analyses on the bulk samples to correlate to microstructure.
- Develop tailored analysis conditions for comprehensive results.

1.4 Thesis layout

Chapter 1

Information on the complex structure of polyethylene is presented alongside synthesis techniques, suitable analytical techniques that are used for polyolefin characterization, the aim, and the objectives of the present work.

Chapter 2

Relevant literature on branched polyethylene together with different synthesizing techniques, characterization, and fractionation methods are discussed.

Chapter 3

Details on experimental and instrumental procedures are given here in detail. Techniques for processing the acquired data are also introduced.

Chapter 4

Results obtained from the analyses of bulk samples of four laboratory synthesized long chain branched PE samples and three commercial LDPE samples with varying branching contents are presented herein.

Chapter 5

This chapter presents and discusses results obtained from the analyses of p-MMF fractions of laboratory and commercial LDPE polymers with varying branching and chemical composition distributions.

Chapter 6

The results obtained from the present work are summarized in the present chapter. Conclusions are presented and recommendations are offered for future work.

1.5 References

(1) Kokko, E. *Metallocene-catalyzed ethene polymerization: long-chain branched polyethene*. Ph.D. thesis, Helsinki University of Technology, Helsinki, 2002.

(2) Pasch, H.; Malik, M. I. *Advanced separation techniques for polyolefins*; Springer: Switzerland, 2014, p 179.

(3) Kesti, S. S. *J. Adv. Sci. Res.* **2019**, *10*, 30–34.

(4) Azmi, A.; Sata, S.; Rohman, F.; Aziz, N. In *J. Phys. Conf. Ser.* ; IOP Publishing, 2019, p 012094.

(5) Bungu, P. E.; Pasch, H. *Polym. Chem.* **2018**, *9*, 1116–1131.

(6) Muhammad, D.; Aziz, N. *Chem. Eng. Trans.* **2017**, *56*, 757–762.

(7) Azmi, A.; Aziz, N. *Procedia Eng.* **2016**, *148*, 1170–1176.

(8) Junkar, I.; Modic, M.; Mozeti, M. *Open Chem.* **2014**, *13*, 490–496.

(9) Fawcett, E.; Gibson, R.; Perrin, M.; Patton, J.; Williams, E. *Pat* **1937**, *2*, 816–883.

(10) Cui, Y.; Shao, C.; Sun, W.-H. *Open Chem.* **2003**, *1*, 325–338.

(11) Orski, S. V.; Kassekert, L. A.; Farrell, W. S.; Kenlaw, G. A.; Hillmyer, M. A.; Beers, K. L. *Macromolecules* **2020**, *53*, 2344–2353.

(12) Liu, P.; Liu, W.; Wang, W. J.; Li, B. G.; Zhu, S. *Macromol. React. Eng.* **2017**, *11*, 1600012.

(13) Liu, P.; Liu, W.; Wang, W. J.; Li, B. G.; Zhu, S. *Macromol. React. Eng.* **2016**, *10*, 156–179.

(14) Wild, L.; Ryle, T.; Knobeloch, D.; Peat, I. *J. Polym. Sci., Part B: Polym. Phys.* **1982**, *20*, 441–455.

(15) Carbognani, L. *J. Chromatogr. A* **1997**, *788*, 63–73.

(16) Mori, S.; Barth, H. G. In *Size Exclusion Chromatography*; Springer, 1999, pp 55–76.

(17) Plüschke, L.; Mundil, R.; Sokolohorskyj, A.; Merna, J.; Sommer, J.-U.; Lederer, A. *Anal. Chem.* **2018**, *90*, 6178–6186.

(18) Pasch, H. *Polym. Chem.* **2013**, *4*, 2628–2650.

(19) Ndiripo, A.; Albrecht, A.; Pasch, H. *RSC Adv.* **2020**, *10*, 17942–17950.

(20) West, C.; Elfakir, C.; Lafosse, M. *J. Chromatogr. A* **2010**, *1217*, 3201–3216.

(21) Cong, R.; deGroot, A. W.; Parrott, A.; Yau, W.; Hazlitt, L.; Brown, R.; Cheatham, M.; Miller, M. D.; Zhou, Z. *Macromol. Symp.* **2012**, *312*, 108–114.

Chapter 2 : Literature review

This chapter reviews the literature on polyolefins and polyethylene characterization with a particular emphasis on long chain branching. The historical background and recent developments in characterization of polyolefins are also addressed.

2.1 Introduction

Polyolefins are thermoplastics prepared by the polymerization of olefins containing predominantly hydrogen and carbon. The most common polyolefins are polyethylene (PE) and polypropylene (PP). They are produced mainly from natural gas and oil by a process of polymerization of ethylene and propylene, respectively. They have evolved to be the most popular plastics in use today for packaging. PE has evolved into a global leader with a demand that increases annually and a share of 36% of total polymer production.[1]

PE is commonly categorized into several types that include low density polyethylene (LDPE), linear low density polyethylene (LLDPE), and high density polyethylene (HDPE). Branching (LCB and SCB) is prime subject in polyolefin research as the type, length, density, and distribution of branches have a considerable effect on the polymer flow behaviour (rheology) and processability.[2] One of the major achievements in polymer science has been finding suitable catalysts that allow for the production of polymers with desired microstructure and properties. The material properties of PE such as molar mass dispersity, chemical composition, and topology are affected by the method of synthesis which entails the process, the catalyst, and the reactor type used. A summary of the properties of PE is shown in Table 2.1.

2.2 Brief history of PE

The history of PE as shown in Fig 2.1 is traced back to 1898 when the first traces of PE were reported by Hans von Pechman as a side product of the thermal decomposition of diazomethane[3]. This product was not stable enough to be used industrially. Later, in the 1920s, Hermann Staudinger introduced the high molar mass concept of macromolecules hence defining the polymerization process to be the linking together of individual molecules (monomers) by the covalent bonds. A few years later in 1933, the first solid polyethylene

polymer was produced by E. W. Fawcett and R. O. Gibson who at the time were working for the Imperial Chemical Company.[4]

Table 2.1 Summary of different polyethylenes and their microstructural characteristics as well as applications.

	LDPE	**LLDPE**	**HDPE**
Branch type	• SCB • LCB	SCB	Linear
Catalyst	• Peroxide • Oxygen • Azo compounds	• Ziegler-Natta • Metallocene	• Ziegler-Natta • Metallocene
Synthesis	High-pressure free radical polymerization of ethylene, with pressures up to 200 MPa and temperatures up to 300 °C.	Low-pressure polymerization technology using Ziegler-Natta catalyst or metallocene catalyst	Low pressures by slurry or gas-phase processes using Ziegler-Natta catalyst in: single-stage polymerization, multi-stage polymerization or a Cr or Phillips-type catalyst
Properties	• Density ~ 0.91 – 0.94 g/cm^3 • Melting point: ~105 to 115 °C • Good processability • Poor toughness • Good clarity and ductility	• Density ~ 0.91 – 0.93 g/cm^3 • Very flexible with high impact strength • Toughness • Poor flow properties	• Density ~0.94 – 0.97 g/cm^3 • Melting point: 120 to 140 °C • High strength • Toughness • Low stretching • Poor flow properties
Applications	• Thin clarity films • Laminates, general packaging	• Stretch wraps • Thin films	• Pipes • Thick films
Structure			

PE was obtained by chance due to a leakage that allowed traces of oxygen to contaminate the ethylene batch, and, at high temperatures, it decomposed to provide free radicals hence enabling polyethylene formation through free radical polymerization. The intra- and intermolecular chain transfer in the free radical process led to the formation of LDPE with short

and long chain branching by employing high temperatures (200 to 300 °C) and high pressures (1000 to 4000 bars).

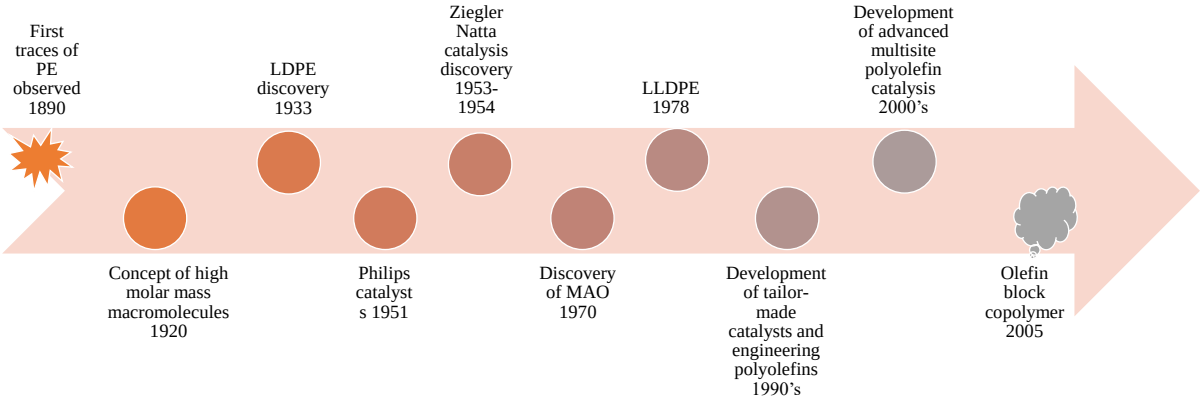

Figure 2.1 Major advances in polyolefin development (modified from reference [5]).

With more advanced technology, extensive studies were performed on the chemistry of polyethylene. In the 1950s there were some breakthroughs such as the discovery of an ethylene polymerization mechanism by Karl Ziegler in 1951 where the reaction conditions were lowered. Ziegler managed to generate solid polyethylene at low pressures and temperatures by utilizing a catalyst[5]. Shortly after Ziegler's discovery, another group of researchers working at Phillips Petroleum Inc. found catalysts that produced similar results as Ziegler's process. Philips catalysts became popular because of their ability to produce small amounts of long-chain branching (LCB) via macromer insertion.[6,7]

In the mid-1970s, another chemical species that transformed the world of polymerization catalysis was discovered by Kaminsky and Sinn[8], methyl aluminoxane, referred to as MAO. It was shown that it can be used to operate a broad range of molecular complexes and late transition metals, thus leading to a new group of catalysts with custom-made properties.[5,9] This led to the discovery of metallocene catalysts which present a remarkable control over molar mass and chemical composition.

2.2.1 Low density polyethylene

Low density polyethylene (LDPE) is generated by free radical polymerization of ethylene under harsh conditions of high pressures (≤3.5 kbar) and high temperatures (between 132 and 332 °C).[10,11] Trace contaminates of oxygen/peroxides are supplemented to initiate the ethylene reaction. This is done either in a stirred autoclave reactor or a tube reactor. The polymerization proceeds by a chain reaction, initiation through the addition of a free radical of ethylene and propagation by repeated additions of monomer (Scheme 2.1).

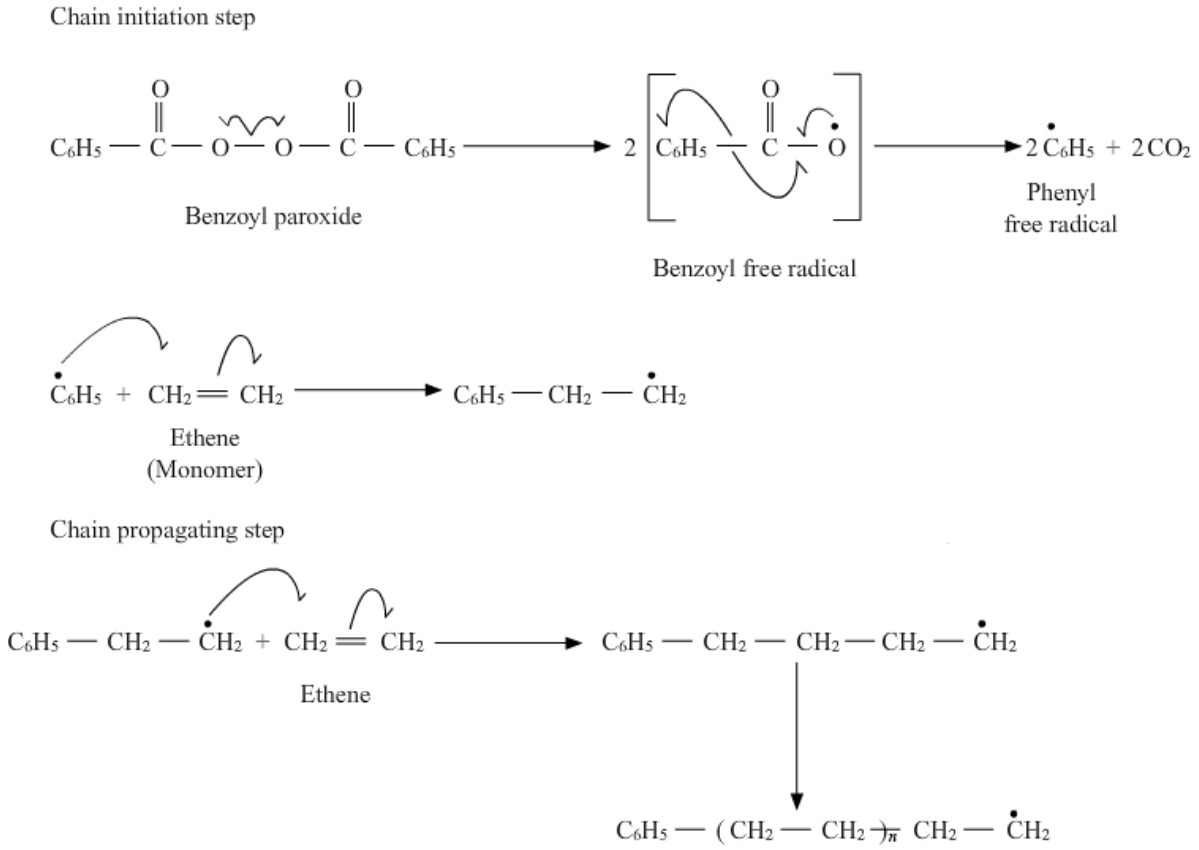

Scheme 2.1. Free radical polymerization of ethylene.

According to Roedel[12], short chain branching in LDPE is due to back-biting mechanisms. A propagating macroradical in this mechanism transfers the active center from a terminal to the 4th or 5th carbon atom hence producing a short chain branch which occurs after further propagation (Scheme 2.2) being an intramolecular transfer. Long chain branching is due to intermolecular transfer, thus occurring between the radical and an internal carbon from another chain. Different methods have been used to introduce long chain branches to the polymer backbone. One of the methods is grafting and will be discussed in detail in the next section.

SCB does not exceed a length of 6 carbons and the longer chains are called LCB as determined by ^{13}C-NMR to have six carbons and more.

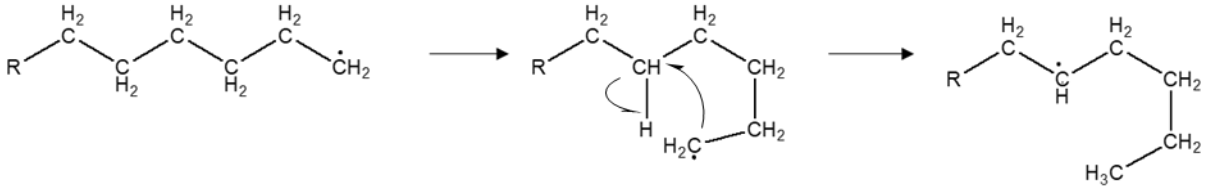

Scheme 2.2. Back-biting mechanism for short chain branch formation.

The conditions used during the synthesis of LDPE determine its properties. Temperature affects the density or crystallinity of the polymer produced, pressure and concentration of chain transfer agents (1-olefins) affect molar mass and molar mass distribution.[10] Besides using chain transfer agents, adjusting temperature and pressure may also help to vary the molar mass.

The molecular structure of LDPE is characterized by long chain branching which in turn gives it a more complex structure when compared to other PE types. Molar mass increases with increased pressure or decreased temperature whereas LCB increases with an increase in temperature. The total number of branching per 1000 carbons (NBr) ranges between 10 – 30 branches per 1000 carbons and for SCB, the main types present are n-butyl (5 – 10 br/1000C) followed by ethyl (2 – 8) and n-amyl (1 – 3) chains for different types of LDPE.[13] Controlling levels of long chain branching is a challenge resulting in batches that may differ remarkably. LDPE resembles a highly branched structure with a central backbone from which many branches are affixed. It is a tough and flexible polymer characterized by long branches that do not fit well into crystallite structures. These branches are broadly distributed in size and it is challenging to determine the branch lengths and spacing between them.[14] The entanglements formed, even in very low quantities, have an acute impact on rheological properties including melt elasticity, melt viscosity, shear-thinning, and extension thickening.

A high level of LCB increases impact strength and environmental resistance, whereas a low level enhances drawdown, tear strength and optical properties. SCB controls the melting and crystallization behaviour of the polymer and reduces the polymer density by adjusting the packing of the molecules.[15] Generally, LDPE with a wide MMD exhibits a high degree of long chain branching which in turn affects crystallinity.[16,17]

In general, polyolefins are classified as semi-crystalline or amorphous materials depending on the polymer in context. The physical properties of polyethylene are influenced by the formation and presence of crystals, and in turn, crystallization is governed by the shape and size of substituent groups on the polymer backbone. The packing of chains during crystallization is in an orderly manner that forms spherulites from the lamellae produced (Fig. 2.2). LDPE is a semi-crystalline polymer as it contains both amorphous and crystalline regions.

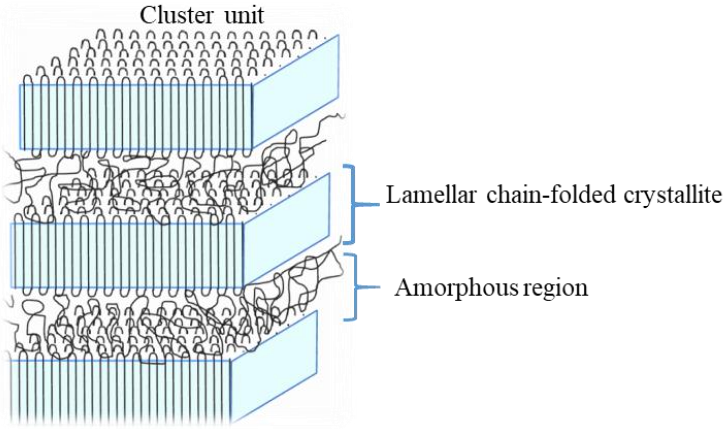

Figure 2.2 Depiction of the packing of polymer chains in a unit cell of a semi-crystalline polyethylene.

Different techniques are utilised to determine the crystallinity of PE samples, amongst these the commonly used ones are DSC[18], solid-state ^{13}C NMR[19], and X-ray diffraction[20]. In the present work, the DSC technique was used for determining the crystallinity of polyethylene samples by integrating the melting/crystallization peaks and comparing them to the peak integrals of 100% crystalline polyethylene.[21] Equation 2.1 was used for calculating crystallinity.

$$Xc = \frac{\Delta \mathrm{Hm}}{\Delta \mathrm{Hm}^{\theta}} \times 100\% \qquad (2.1)$$

$X_c = percentage\ crystallinity$

$\Delta Hm^{0} = heat\ of\ fusion\ of$ 100 % $crystalline\ PE$ = 293 J/g

$\Delta Hm = heat\ of\ fusion\ of\ sample$

2.2.2 High density polyethylene

High density polyethylene (HDPE) is highly linear with dispersed small contents of side chains (Table 2.1). It is synthesized at a pressure between 5 – 25 bar and temperatures between 50 and 250 °C. Philipps and Ziegler catalysts are used in this synthesis, and they produce similar PE structures. High molar mass polymers arise from chromium-based components whereas products obtained from Ziegler catalysis have a relatively narrow MM range.[22] The densities of these polymers differ as Phillips-type materials have densities of 0.956 – 0.965 g/cm³ and are more compact than their counterparts from Ziegler catalysis (density of 0.94 – 0.95 g/cm³).[23] This gives rise to different processing procedures. Blow molding is used for Phillips-type catalyzed HDPEs, whereas for Ziegler catalysis injection molding techniques are utilized. Unlike LDPE, HDPE has a high degree of crystallinity that arises from strong intermolecular interactions (van der Waals forces) and parallel macromolecular alignments. The number of branches in HDPE is quite low with NBr = 0 – 2Br/1000C, resulting to a high degree of crystallinity of 70 – 90 %.[2,24] It is evident that the degree of branching is inversely proportional to crystallinity; as the number of branches decreases, the degree of crystallinity increases. High branching interrupts the regular packing of the polymer chains hence lowering the degree of crystallinity.

2.2.3 Linear low density polyethylene

The production of linear low density polyethylene (LLDPE) came at a huge cost and a low-cost alternative was needed, hence the development of the UNIPOL™ process. The process was flexible enough to have a binary feeding of the reactor, therefore, the gas phase process was soon extended to produce copolymers.

LLDPE is produced by introducing SCB into a linear PE, which is attained by co-feeding α-olefins such as octene, hexene, or butene. Its branching density (BD) is highly dependent on the type and content of the added comonomer. NBr in LLDPE varies between 10 – 30 Br/1000C.[25,26] Due to polymerization mechanisms, this type of PE does not have LCB, however, it has SCB with a BD that depends on the type of catalyst used. The LLDPEs obtained from Ziegler-type catalysts show some multimodality, while LLDPEs obtained from metallocenes are homogeneous.[27,28] The differences are due to the differences in the accessibility of the Ziegler catalyst active centres whereas single-site catalysts allow for

homogeneous chain growth. LLDPE is more flexible and stretchable as compared to other PEs earning its use in thin film applications.

2.3 Characterization techniques

Polyolefins exhibit a complex molecular structure that is typified by distributions in molecular size, constitution, conformation, and configuration. Depending on the conditions of polymerization (the type of catalyst and reactor), polyethylene is highly heterogeneous concerning MM, chemical composition, functionality, and architecture. The characterization of these features is tricky as most analytical methods focus on only one or a few attributes of the macromolecular properties. Multiple characterization steps must be utilized to gain information to generate an overall view on the sample.

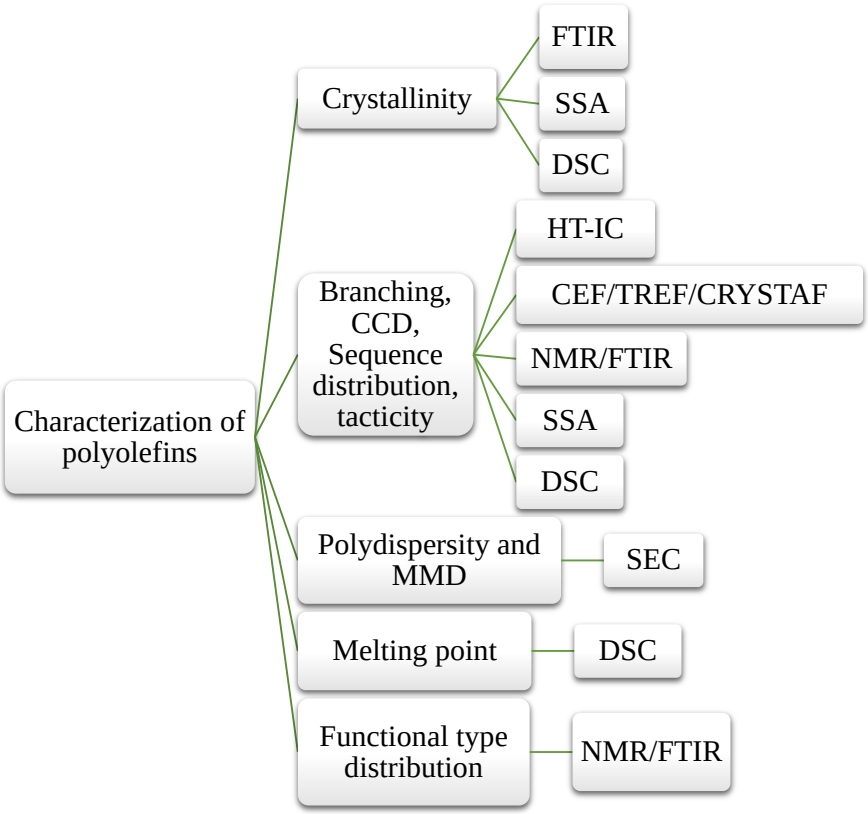

Figure 2.3 Some of the analytical tools used for the comprehensive description of polyolefin microstructure.

Different methods as shown in Fig. 2.3 are used to characterize the complex structures of branched PEs: crystallization-based techniques which relate crystallization and melting behaviour to molecular properties like branching and comonomer content, chromatographic

column-based techniques which separate polyolefins according to their CCD or size, and spectroscopic methods which analyze branching and chemical composition in polyolefins.[29,30]

2.3.1 Crystallization-based techniques

Crystallization-based techniques determine CCD as a function of crystallizability and solubility of polyolefin chains in dilute solutions. The major techniques are temperature rising elution fractionation (TREF),[31,32] crystallization analysis fractionation (CRYSTAF),[33] and crystallization elution fractionation (CEF)[34]. All these techniques distinguish polyolefins by differences in their crystallizability as a function of temperature. This is accomplished by fractionating the polyolefin according to the principle that higher amounts of α-olefin comonomer or other molecular defects result in lower crystallization temperatures and *vice versa*.[35] Flory's equilibrium theory indicates that the crystallization temperature is highly related to the comonomer content of an olefin copolymer.

Table 2.2 Key features of TREF, CRYSTAF, and CEF.

Tool	Characteristics
TREF	• Column fractionation technique • Zero solvent flow in the crystallization step • Detection only during the elution step • Lengthy analysis times
CRYSTAF	• Is a batch technique • Detection during the crystallization step • No elution step • Shorter analysis times in contrast to TREF
CEF	• Column fractionation technique • Solvent flow during crystallization • Detection during the elution step • Shorter analysis times unlike in TREF and CRYSTAF

Fractionation is accomplished using a dilute solution of the polyolefin in e.g., 1,2,4-trichlorobenzene or ortho- dichlorobenzene by gradually reducing the temperature of the solution in either an agitated vessel (CRYSTAF) or a loaded column (TREF and CEF). Table 2.2 shows a comparison of the characteristics of these techniques. CEF was developed to have a higher resolution than TREF and a faster analysis time than CRYSTAF. The limiting factor of TREF and CRYSTAF is the co-crystallization of polymer chains with distinct chemical structures but having similar crystallizabilities. This lowers the resolution in those separation processes. CEF separates polyolefins with significantly lower co-crystallization effects in comparison to TREF and CRYSTAF and has a better resolution than TREF as demonstrated in Fig. 2.4.[36] Besides the significant time consumption, another disadvantage of crystallization techniques is that just the crystallizable part of the sample can be fractionated.[37]

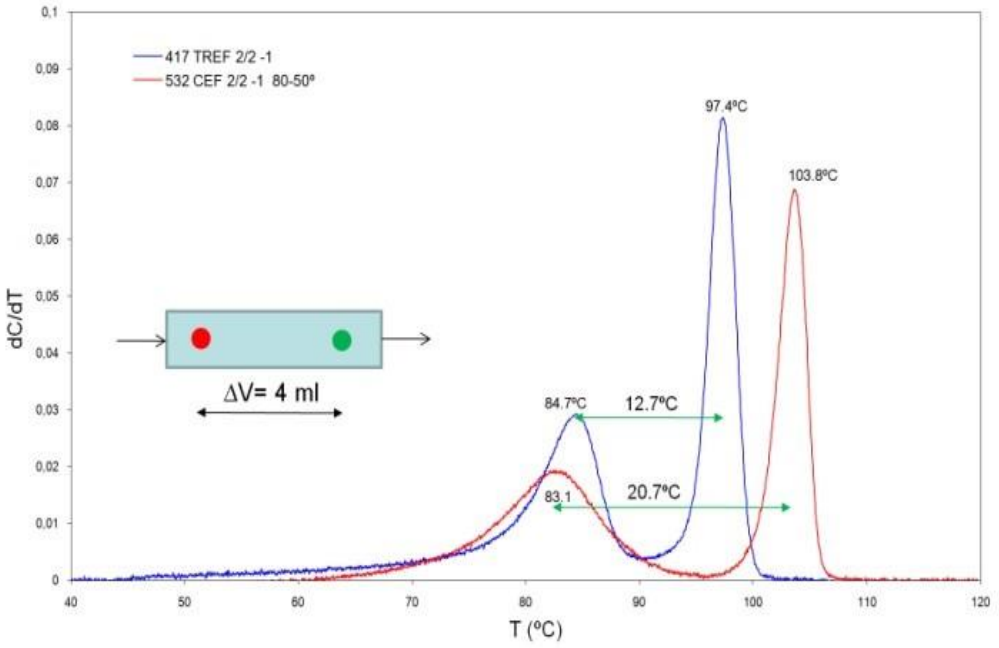

Figure 2.4 CEF and TREF analysis of a 50/50 blend of ethylene-octene copolymers (SSC-1and SSC-2) under similar analytical conditions.[36]

2.3.1.1 Differential scanning calorimetry (DSC)

DSC allows the determination of melting and crystallization temperatures, along with the corresponding enthalpy and entropy changes.[38] In the DSC technique, the principle of thermal analysis depends on detecting the fluctuations in the enthalpy content of a sample with temperature change.[39] The sample and the reference are exposed to the same temperature profile which is maintained throughout the analysis. When the temperature is increased, the

sample undergoes changes in physical or chemical state, e.g., melting, crystallization, phase transition or decomposition that are accompanied by a change in enthalpy. When the temperature of a polyolefin melt is decreased slowly, crystallization occurs. In the DSC experiment, the rate of heat flow to the pan with the sample is compared to an empty pan (reference) which is simultaneously heated and cooled at the same rate. The sample changes, associated with the evolution or absorption of heat, induce a change in the differential heat flow documented as a peak.

Branching affects the crystallization of polymers. Studies have shown that the thermal behaviour of a polyolefin is mainly influenced by SCB structure. The different SCB contents form lamellae with varying thicknesses and a lower SCB content results in a thicker lamella.[21,40] Long chain branching influences the formation of crystallites. Liang et *al.*[41] concluded that the LCB structure can function as a nucleating agent to promote crystal nucleation, decreasing spherulite size. It easily diffuses into the crystal lattice to form crystal nucleus. This makes it difficult for the formed nucleus to dissipate under the thermal motion due to the entanglement of LCB. Long chain branched polyethylene (LCBPE) is expected to have a higher crystallinity compared to LDPE.

DSC is more sensitive to short chain branches than long chain branches. The technique measures the comonomer distribution in branched polyethylene, however, if combined with FTIR, information on the copolymer type and α-olefin content can be provided. Its disadvantage is that it is less accurate for lower crystallinity fractions and completely insensitive to amorphous components.[42,43]

2.3.1.2 Successive self-nucleation and annealing (SSA)

SSA was designed to analyze the chain structures (branches, comonomers, stereo defects, and crosslinks) of crystallizing polymers based on the self-nucleation and annealing steps.[44] SSA employs a stepwise cooling of the sample after heating to a low temperature, resulting in self-nucleation of the polymer.[45] This is advantageous as it reduces measurement time, offers molecular segregation and enhanced resolution, hence, improving molecular structural information. Fig. 2.5 shows a DSC thermogram of two polymers before and after performing SSA as applied by Li *et al.*[46] Müller *et al.* showed the microstructural difference of the isotactic sequence length and distribution of homo- and co-polypropylene samples. [47]

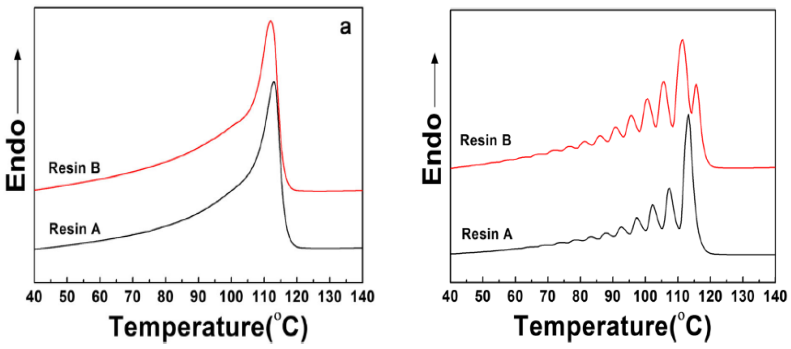

Figure 2.5 DSC heating curves (10 °C/min) of two LDPE resins (a) and their heating scans after SSA thermal fractionation. (a) before and (b) after SSA fractionation.

Furthermore, Bungu *et al.*[48,49] conducted SSA on TREF and MMF fractions of PE and concluded that the number of peaks increase when TREF temperatures decrease due to amorphous components and SCBs. For MMF fractions the thermograms broaden as the number of peaks and molar mass increases. This means that at high molar mass the polymer structure is more complex due to the influence of MM and branching. The same MMF trend is expected for the LDPEs in the current study.

2.3.1.3 Solution crystallization by laser light scattering (SCALLS)

SCALLS has been reviewed to be one of the newest fractionation techniques for semi-crystalline polymers. This technique involves the analysis of the turbidity of a polymer solution.[50,51]

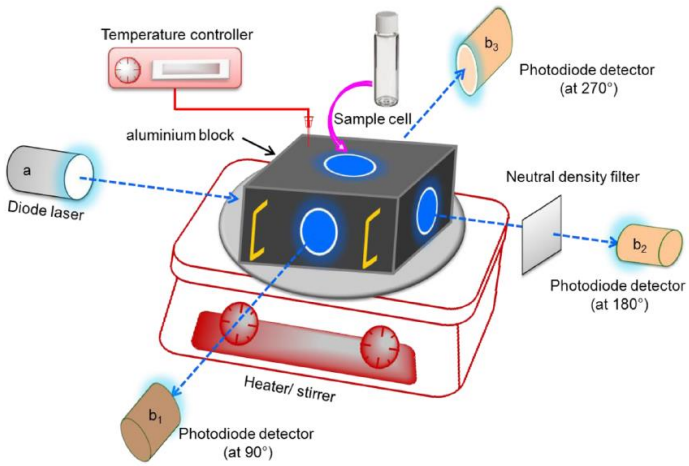

Figure 2.6 Diagrammatic representation of the SCALLS instrument.[52]

This is accomplished by measuring the strength of the laser light passing through a polymer solution. Crystals formed redissolve at respective temperatures during the cooling and heating runs, respectively.[52] Fig. 2.6 shows a diagrammatic presentation of the SCALLS instrument. The crystallization and dissolution of the polymers are greatly influenced by the type of solvent used.[52,53] Cheruthazhekatt *et al*.[52] investigated the solution crystallization and dissolution of PE and PP in various solvents by using SCALLS. This instrument allowed a fast detection of PE/iPP blend components.

2.3.2 Spectroscopic techniques

2.3.2.1 Carbon-thirteen nuclear magnetic resonance spectroscopy

Carbon-thirteen nuclear magnetic resonance spectroscopy (^{13}C-NMR) is used to determine and quantify a branched sample's branch types and branching content..[54] During NMR analysis (Fig. 2.7), the dissolved sample is placed in a magnetic field and subjected to a radiofrequency resulting in nuclei excitation which relaxes at rates dictated by the magnetic environment in the sample. This spin relaxation is recorded as free induction decay (FID) and is converted to a frequency domain by Fourier transformation.

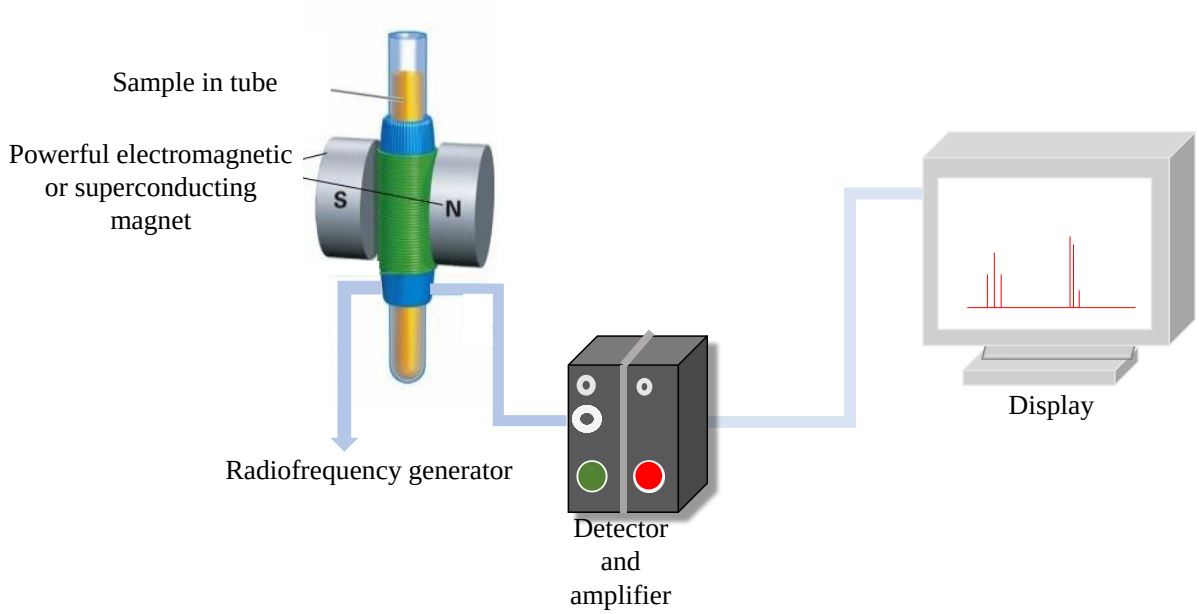

Figure 2.7 Schematic diagram of nuclear magnetic resonance spectrophotometer.

^{13}C-NMR is a direct method of LCB measurement, it gives complementary information about the number of branches, although it does not differentiate between alkyl branches and branches

with six or more carbon atoms.[55-58] Bovey *et al*.[59] studied short chain and long chain branching in LDPE, they were able to identify ethyl, butyl, amyl, hexyl and longer branches. The observations confirmed previous findings that butyl branches are the most predominant and propyl branches are rare.[60,61] Side chains longer than amyl branches resonating at 32.23 ppm have received special consideration being hypothesized that they represent very long branches.[54] Shroff *et al.* used six resins with similar MWs and MWDs, the number of long-chain branches that were determined by NMR revealed a random scatter.[58]

It was evident that NMR could not detect any LCB PEs that were synthesized by modification of linear PEs by peroxides due to their complex branches even though the rheological behaviour had changed.[58,62,63] As much as this is a good analytical technique, it has its limitations.

First, there exist a possibility of intermediate-length branches (hexyl, heptyl, octyl, etc.); which might cause errors in the estimation of LCBs by the C-3 (third carbon from the branch end) resonance at 32.2 ppm because LCBs cannot differentiated with the intermediate-length branches in the C-3 resonance. Secondly, problems are encountered in quantitative analysis when small peaks are compared with a large main peak. Thirdly, there is interference by low MM impurities. Some limitations include low sensitivity, acquisition scans can be increased but this is time-dependent in the low micromolar to the high nanomolar range[64] and the short chain branches tend to interfere with the acquisition.[65] Unlike SEC which gives the distribution in molar mass, average chemical compositions can be provided by FTIR and NMR but without distributions.[66] Coupling ^{13}C-NMR with GPC and DSC can help provide better information on LCB.

2.3.2.2 Fourier transform infrared spectroscopy

Fourier transform infrared spectroscopy (FTIR) is often used to identify functionalized organic compounds due to its ease of use, speediness, and inexpensive nature. It is the most traditional method used for the determination of crystallinity, composition, tacticity as well as the conformation of polymeric materials. The branching content and crystallinity of polyethylene are easily identifiable with this technique. The IR radiation is passed through the analyte during analysis, and the portion of the absorbed light is quantified either as transmittance or absorbance. FTIR allows a quick, simple and reliable analysis of the chemical composition in polyolefins. More quantitative evidence on the branch lengths has come from studies of the

infrared spectrum between 720 and 790 cm^{-1} making it possible to distinguish the type of branching in a polymer.[67]

From a survey of the spectra of low molecular weight liquid hydrocarbons it was shown that ethyl, propyl, butyl, and amyl branches are associated with absorption bands at about 770,740, 730, and 725 cm^{-1}.[46] For PE resins, the region 1050 to 1175 cm^{-1} bands are mostly caused by the amorphous phase involving methylene twisting. The pair of bands near 720 cm^{-1} is taken as the standard to know about the crystallinity of a known sample. Only one band is obtained in this region for amorphous PE, whereas a crystalline PE shows perfectly split bands. A measure of the relative intensities of the 720 cm^{-1} to 730 cm^{-1} bands can be used to rank the relative crystallinity of PE samples.[41] A significant amount of work has been done on polyolefins using FTIR.[68-70]

2.3.3 Chromatographic techniques

Chromatographic techniques allow for the separation of molecules regarding size, topology and chemical composition. This is the most widespread method to study the properties of polyolefins in solution.[71] It is mainly based on high temperatures ranging between 130 – 160 °C using particular solvents such as 1,2,4-trichlorobenzene (TCB), 1,2-dichlorobenzene (ODCB) and 1-decanol.

2.3.3.1 High-temperature size exclusion chromatography with triple and quadruple detection

The technique of gel permeation chromatography (GPC)/size exclusion chromatography (SEC) at elevated temperatures is fast and very reliable for the measurement of molar masses of polyolefins. A typical SEC column contains silica or polymer particles that have known porosities allowing the polymer molecules to get separated according to their hydrodynamic volume (V_h) in solution. Penetration into the stationary phase pores is dependent on the *Vh* of the macromolecules. The migration of the macromolecules through the stationary phase pores leads to separation with the largest molecules being eluted first as shown in Fig. 2.8. The proper choice of a stationary phase, pore size, and particle size among other factors is important for the success of the separation.[72]

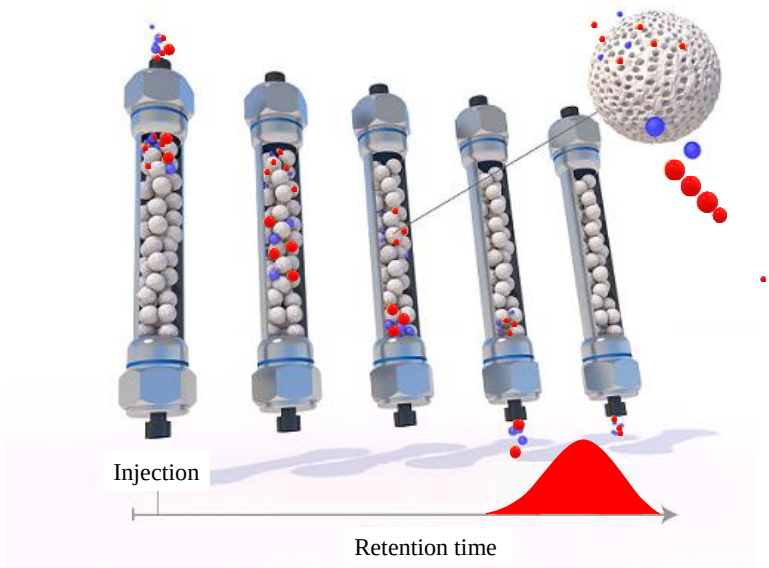

Figure 2.8 Schematic depiction of the separation in size exclusion chromatography.

The addition of different detectors to the separation device enhances the capabilities of this technique. Fig. 2.9 shows a schematic illustration of HT-SEC with a quadruple detector system. HT-SEC with multiangle laser light scattering (MALLS) has been used for detecting the degree of long chain branching by comparison of the hydrodynamic radius in solution to a linear reference.[73] It is challenging to determine the degree of branching when the sample has a low molar mass. The MALLS detector measures the lights scattered by a sample at many angles and creates a Debye plot. The modelling of the angular dependence of a sample scattering by the Debye plot models determines the M_w and radius of gyration (R_g) at every data slice in the chromatogram. Two types of scatterers are involved, (1) The isotropic scatterers (smaller than 10 – 15 nm in radius) will scatter light evenly in all directions, meaning only the M_W will be measured, (2) Anisotropic scatterers (samples more than 10– 15 nm in radius) will scatter more light in the forward direction hence allowing both M_w and R_g to be measured. A conformation plot can be generated which allows any structural differences in the samples to be measured.[74]

The combination of SEC-MALLS (providing absolute M_w) and shear rheological measurements can be considered to be the most sensitive way of detecting even very small amounts of long chain branches[75]. Such measurements demonstrate that branching is more pronounced at higher molar masses. Typical SEC detectors are MALLS, dynamic light scattering (DLS), viscometry (Visco), dRI, and UV.[2,60,76] In multidetector SEC, branching is quantified by investigating changes in molecular size or intrinsic viscosity as a function of

molar mass. Branching calculations are carried out on either the radius of gyration (measured or calculated) or the intrinsic viscosity (measured or calculated).

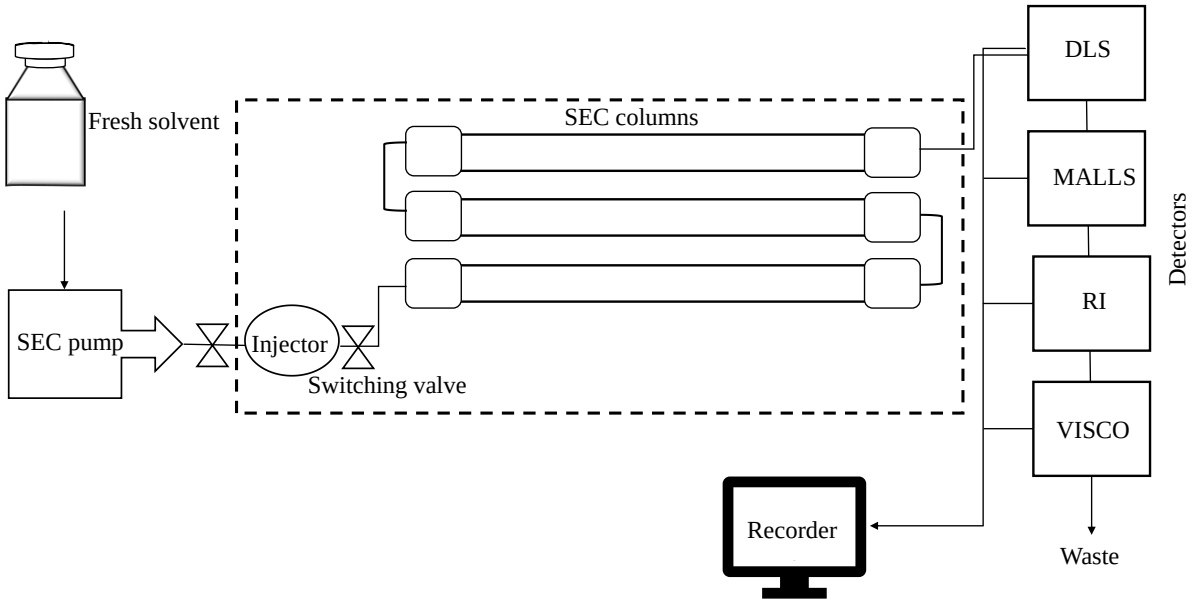

Figure 2.9 Schematic illustration of HT-SEC with quadruple detection.

Using the double-logarithmic plot of MM vs R_g or MM vs intrinsic viscosity $[\eta]$ an estimation of the conformation of these macromolecules can be made. This relationship is based on the following power law equations:

$$R_g = K \cdot M^{\nu} \tag{2.2}$$

$$[\eta] = K \cdot M^{\alpha} \tag{2.3}$$

Where exponents α and ν depend on the conformation of the macromolecules and the solvent quality. Branching density is determined by quoting the contraction factor, g, which is a measure of the degree of branching. It is defined as the ratio of the mean-square radius of gyration of a branched macromolecule to its linear counterpart at given MM. LCB reduces the molecular size of a long chain branched polymer resulting in a lower radius of gyration and hydrodynamic radius in solution.[77] Contraction factors are determined from the Mark-Houwink-Sakurada plot or conformation plot using the following relationships,

$$g = \frac{[R_G^2]B}{[R_G^2]L} \tag{2.4}$$

$$g' = \frac{[\eta]_B}{[\eta]_L} \tag{2.5}$$

$$g' = g^{\varepsilon} \tag{2.6}$$

where R_g is the radius of gyration, $[\eta]$ is intrinsic viscosity, ε is a constant, and the subscripts B and L denote branched and linear species, respectively.[78] The two contraction factors g and g' have advantages and drawbacks. The contraction factor g is only accurate for macromolecules that have a high MM whilst the contraction factor, g', can be determined in an unlimited range of molar masses. The radius of gyration can be calculated from the composition of a macromolecule, whereas the intrinsic viscosity cannot be predicted for complex structures like branched ones.[65,79]

The contraction factors are related by Eq. (2.6) where ε is an exponential factor (drainage factor) with a magnitude influenced by the type of polymer, type of LCB and the solvent quality.[60] Yu *et al*. analyzed long chain branching in polyethylene and concluded that the LCB detection limit was found to be MM dependent.[60] Therefore, as the MM decreases, the LCB detection level becomes increasingly poor. Furthermore, studies have shown that ε values ranging from 0.5 to 2.0 are seen in LDPEs and strongly depend on polymer MM.[77,80] Typical values are $0 \leq g, g' \leq 1$. With increasing number of branches, the deviation from the linear molecule increases and, thus, the higher the polymer coil contraction. Short-chain branches, such as ethyl, butyl, or hexyl branches, do not significantly influence the resin's melt rheology, but its R_g–MM relationship.

The hydrodynamic volume can remarkably vary with the branches' number, lengths, and positions in polymer chains. In this regard, chains with different molar mass (linear and branched molecules) can co-elute although they have differences in branching structures .[73] Chemically different polymers may co-elute if they have the same hydrodynamic size in solution.[81] Strongly branched macromolecules are delayed in elution from the SEC column and correspond to their number of branch-points (number of chain ends).[82]

Plüschke *et al*. presented a study using a high temperature SEC system with quadruple detection containing MALLS, DLS, VISCO and dRI as an efficient method to explore the size, molar mass, branching, solution characteristics and molecular density of PE.[83] However,

triple/quadruple detection SEC is cannot categorize samples into linear, low LCB (typically 0.1 LCB/1000CH_2), and high LCB (typically 1LCB/1000CH_2).[41]

2.3.3.2 Interaction chromatography

Interaction chromatography (IC) separates molecules according to chemical composition, tacticity, functionality, and topology using enthalpic forces. The separation is based on two mechanisms depending on the experimental conditions: either by adsorption-desorption or precipitation-redissolution. The type of separation is dependent on the choice of the stationary phase, the mobile phase, and the temperature.[34]

Porous graphitic carbon (PGC) is the most used stationary phase for the interaction chromatography of polyolefins and has high mechanical and thermal stability.[84] The flat layers of graphite enable strong interactions with the polymer molecules, and separation is highly dependent on the molecular surface of the polymer adsorbed on the graphite surface.[85] Silica-based stationary phases are also used; these provide separations that are based on the polarity of the macromolecules.[82] Various experimental conditions are applied to improve resolution, e.g. applying solvent gradient or temperature gradient IC, which enhance the thermodynamic interactions between eluent and substrate.

In temperature gradient interaction chromatography (TGIC), a temperature gradient is used with an isocratic mobile phase. The separation principle for polyethylene is similar to that in HT-SGIC. Here, the temperature gradient weakens the van der Waals forces of interaction between the analyte and the PGC stationary phase. Suitable solvents for polyolefins such as TCB and ODCB are used for HT-TGIC. Eluent composition is kept constant, and the interaction strength is enhanced by changing the operating temperature. The key advantage of TGIC is the possibility of detector coupling with MALLS, IR or viscometry.[86,87]

For solvent gradient interaction chromatography (SGIC), the dissolved analyte is injected in a poor solvent that promotes adsorption onto the stationary phase surface. A good solvent is then introduced gradually which allows the analyte to desorb. This is the most applied HT-IC technique, and it separates macromolecules at a constant temperature using the mechanism of adsorption/desorption. Interactions are influenced by differences in the number and type of functional groups, side chains, branches, and the molecular backbone.[41,88]

High-temperature two-dimensional liquid chromatography

The most important microstructural parameters of polyolefins are CCD and MMD. A direct correlation of these two can be achieved through cross-fractionation techniques. The complexity of polyolefins can be resolved by combining different methods in a way that maximizes the separation. Hyphenating two chromatographic modes with the first separation step distinguishing the polymer according to chemical composition and the second according to molar mass or vice versa depending on preference has been thoroughly researched.[89-91] MMD is easily acquired via HT-SEC whilst CCD is acquired via chromatography or crystallization-based techniques. High-temperature two-dimensional liquid chromatography (HT-2D-LC) (Fig. 2.10) usually employs HT-IC separations in the first and HT-SEC separations in the second dimensions. This allows easy management of the HT-SEC dimension regarding speed to accommodate fraction collection from the first dimension. When HT-IC is in the second dimension, speeding up separations gets challenging due to high backpressures and the need to apply solvent gradients.

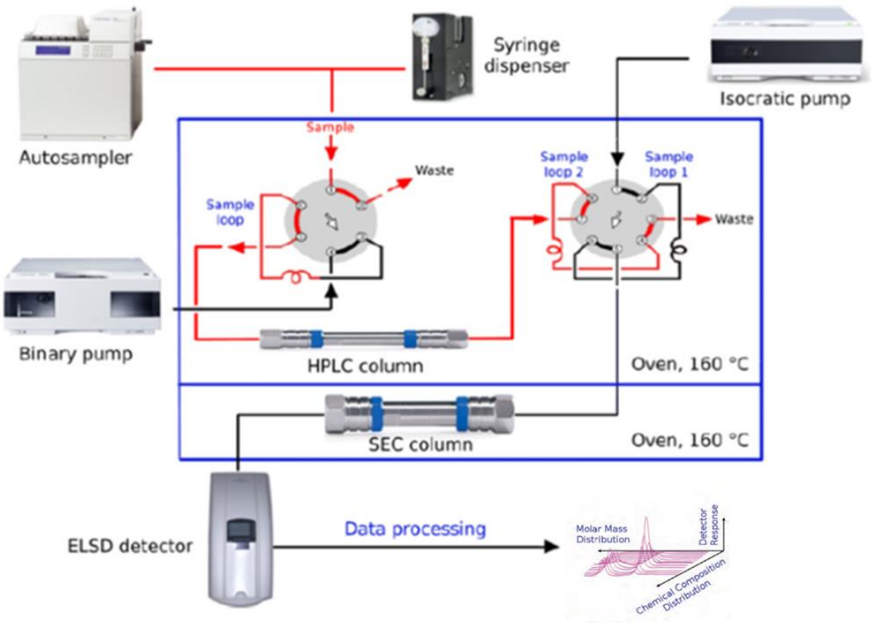

Figure 2.10 Setup for HT-2D-LC.[92]

IC×SEC or SEC×IC have their advantages and disadvantages though IC×SEC is more advantageous because besides IC being less sensitive to molar mass reverberation, SEC permits the use of multiple detectors.[66,91,93-95] 2D-LC is the most capable technique to investigate the correlation between chemical composition and molar mass of a complex sample like LDPE.

2.4 Preparative fractionation

Polyolefins usually have broad molar mass and chemical composition distributions and to narrow these down, preparative fractionation is used. The objectives of preparative fractionation are to prepare fractions narrow in composition.

2.4.1 Preparative temperature rising elution fractionation

The preparative temperature rising elution fractionation (p-TREF) technique is recognized as one of the oldest and most important polyolefin fractionation technique. p-TREF is regularly used to fractionate polyolefins into groups of similar crystallizabilities which correspond to similar chemical compositions.[72,96] Firstly, the polymer sample is dissolved in a thermodynamically stable solvent (TCB or xylene) at high temperatures of 130 – 140 °C. The crystallization step follows whereby the polymer solution is cooled on a support (sand, glass beads) at a programmed slow and constant cooling rate (CR) of 1 – 2 °C hr^{-1} from about 130 °C to ambient temperature.[97] By doing so, polymer chains crystallize on the support in an orderly manner from higher to lower crystallizabilities as schematically illustrated in Fig. 2.11.

The last step is elution where a pre-heated solvent is used to wash the crystallized polyolefin by transferring it into a TREF column that is equipped with programmable temperature. The elution involves the pumping of the solvent (xylene) into the column and then increasing the temperature of the column in a programmed temperature sequence. The collected fractions at each temperature are prepared for further analyses using offline techniques to find chemical composition, branching, and molar mass information[72]. The limitations of p-TREF are its inability to fractionate amorphous samples (>8-10% comonomer content), co-crystallization, as well as having long fractionation times.[45]

Studies have revealed that the crystallinity of ethylene copolymers is mainly based on the short chain branching content.[45] Xue *et al.*[98] used p-TREF to fractionate one poly(1-butene) copolymer and concluded that with increasing elution temperature the ethylene content decreased whilst isotacticity increased. Bungu et al.[18] used the same technique on LDPE and concluded that as TREF elution temperatures increase, non-crystallizable components decrease and the fractions have broader crystallization patterns which are indicative of broad branching distributions.

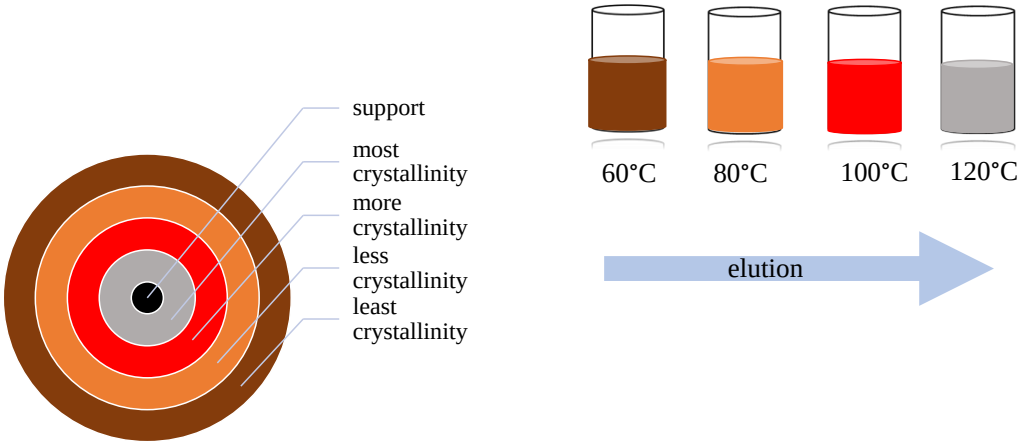

Figure 2.11 Schematic view on an inert support coated with different crystalline fractions of a polyolefin. After the TREF cooling process, fractions are eluted in order of increasing crystallinity.

2.4.2 Preparative molar mass fractionation

Preparative molar mass fractionation (p-MMF) is a technique that fractionates polyolefin samples according to their molar masses primarily based on their solubility in a given solvent system. To achieve this, a polyolefin sample is dissolved in a good solvent e.g., TCB, ODCB, or xylene at high temperatures between 130 – 150 °C.

Two approaches are utilized.

1. Upon complete polymer dissolution, aliquots of a non-solvent are slowly added into the polymer solution until the polymer precipitates out of the solution. After the first fraction is isolated, more non-solvent is added to the solution in incremental steps until all the polyolefin fractions precipitate out of the solution. The least soluble, high molar mass macromolecules precipitate first at minimal non-solvent amounts. In contrast, the lowest molar mass material precipitates at large amounts of non-solvent.[18] This fractionation technique produces fractions with narrow molar mass distributions but broad branching dispersities.
2. Alternatively, upon complete polymer dissolution, MMF is performed by phase distribution chromatography. A column is packed with inert glass beads (particle size

of 100-200μm) or sand coated with the source polymer. An eluent is used to flash the column, gradually changing its composition from a poor to a good solvent. In this case, MM increases with the order of the collected fractions.[22]

The fractionation is typically independent of the chemical composition or crystallinity of the polymer. The obtained fractions are analyzed further using various techniques to obtain meaningful information. Significant research has been done using this technique.[37,99,100]

Except for these fractionation approaches, the preparative polymer fractionation may be carried out by utilizing routine techniques such as IC, SEC, field-flow fractionation (FFF).[101,102] These are furnished with a exceptional preparative separation device like a column or channel. These techniques separate macromolecules or particles dissolved in a suitable solvent. After separation, the size, molar mass and/molecular structure of the molecules can be characterized using different detection technologies.

2.5 Mechanical analysis

Mechanical properties determine the end-use applications of a polymer.[103] They are determined by examining how soft or hard a material is, how much it can be stretched before it breaks, how much it can be bent and its behaviour when a repeated load is applied.[104] It is of importance to understand the microstructural properties of a polymer as they influence its end-use.

2.5.1 Tensile strength

Tensile strength is stress measured as force per area and is one of polymers' most adapted mechanical tests.[105] The stress-strain or tensile test involves pulling a sample of a fixed cross-section area with a tonometer by gradually increasing the force until it breaks. Measurements are done in repetition to determine an average value. This is done because polymers have a diverse and complex structure that can lead to inhomogeneity in mechanical properties. When carrying out the test on different sample types, different pulling rates are used, and they differ between 1 and 500 mm/min. Fig. 2.12 shows a typical stress-strain curve of a semicrystalline polymeric material. Most polymers that are not cross-linked like HDPE, LDPE, and LLDPE will neck during a stress-strain test.[106]

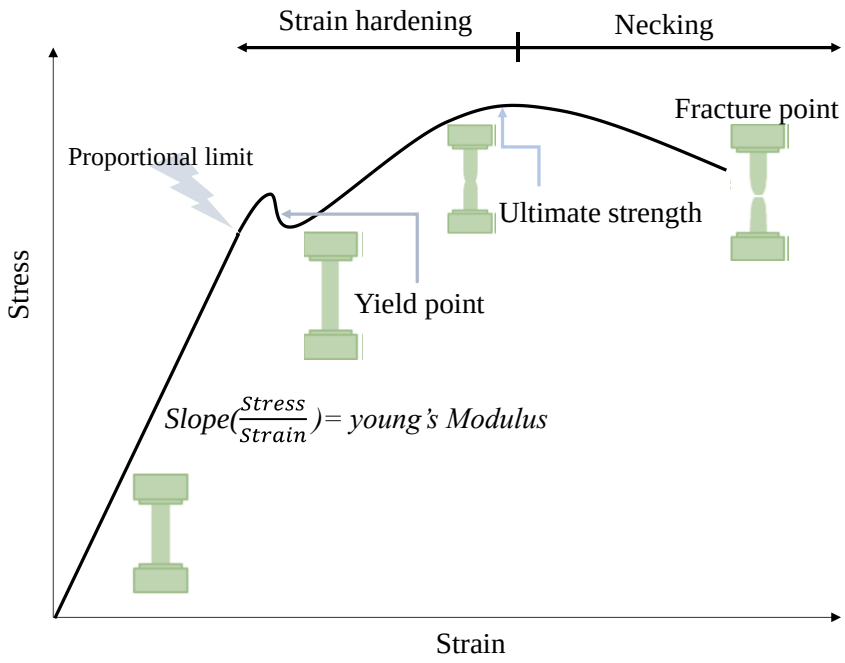

Figure 2.12 Typical diagrammatic presentation of a stress-strain curve of a semicrystalline polymeric material.

2.5.2 Young's modulus

Youngs's modulus is measured as the ratio of stress to strain and is also called tensile modulus or modulus of elasticity. Young's modulus measures the stiffness or rigidity of a material.[107] This means materials exhibiting high Young's modulus are rigid. When a material like polyethylene is subjected to external stress, it deforms before the yield point and is mostly recoverable when the external stress is withdrawn. The value is calculated from the initial slope in the stress-strain curve (Eq. 2.7). The hardness of LDPE is directly related to its tensile modulus and in most cases, the molar mass has a small influence due to branching which affects crystallinity.[108]

$$E \equiv \frac{tensile\ stress}{extensional\ strain} = \frac{\sigma}{\varepsilon} = \frac{F/A_o}{\Delta L/L} = \frac{FL_o}{A_o \Delta L} \qquad (2.7)$$

Where:

$E = Young's\ modulus$

$F = Force\ exerted\ on\ an\ object$

$A_o = Original\ cross{-}sectional\ area\ through\ which\ the\ force\ is\ applied$

$\Delta L = Amount\ by\ which\ the\ length\ changes$

$L_{\circ} = Original\ length\ of\ the\ object$

2.6 References

(1) Yan, D.; Wang, W.-J.; Zhu, S. *Polymer* **1999**, *40*, 1737–1744.

(2) Wang, W.-J.; Kharchenko, S.; Migler, K.; Zhu, S. *Polymer* **2004**, *45*, 6495–6505.

(3) v. Pechmann, H. *Ber. Dtsch. Chem. Ges.* **1898**, *31*, 2640–2646.

(4) Seymour, R. B. *J. Macromol. Sci. Part A Pure Appl. Chem.* **1989**, *26*, 1023–1032.

(5) Sauter, D. W.; Taoufik, M.; Boisson, C. *Polymers* **2017**, *9*, 185.

(6) Hogan, J. *J. Polym. Sci., Part A: Polym. Chem.* **1970**, *8*, 2637–2652.

(7) McDaniel, M.; Rohlfing, D.; Benham, E. *Polym. React. Eng.* **2003**, *11*, 101–132.

(8) Kaminsky, W. *Catal. Today* **2000**, *62*, 23–34.

(9) Imhoff, D. W.; Simeral, L. S.; Sangokoya, S. A.; Peel, J. H. *Organometallics* **1998**, *17*, 1941–1945.

(10) Malpass, D. B. *Introduction to Industrial Polyethylene: Properties, Catalysts, and Processes*; John Wiley & Sons: New Jersey, 2010, p 156.

(11) Ndiripo, A. *Comparative study on the molecular structure of ethylene/1-octene, ethylene/1-heptene and ethylene/1-pentene copolymers using advanced analytical methods*. MSc thesis, Stellenbosch University Stellenbosch, 2015.

(12) Roedel, M. *J. Am. Chem. Soc.* **1953**, *75*, 6110–6112.

(13) Boye, S.; Komber, H.; Friedel, P.; Lederer, A. *Polymer* **2010**, *51*, 4110–4120.

(14) Hadjichristidis, N.; Xenidou, M.; Iatrou, H.; Pitsikalis, M.; Poulos, Y.; Avgeropoulos, A.; Sioula, S.; Paraskeva, S.; Velis, G.; Lohse, D. J. *Macromolecules* **2000**, *33*, 2424–2436.

(15) Xie, L.; Liang, X.; Huang, H.; Yang, L.; Zhang, F.; Li, X.; Luo, Z. *RSC Adv.* **2019**, *9*, 1123–1133.

(16) Peacock, A. *Handbook of Polyethylene: Structures: Properties, and Applications*; CRC Press: New York, 2000, p 544.

(17) Vasile, C.; Pascu, M.; Limited, R. T. *Practical Guide to Polyethylene*; iSmithers Rapra Publishing: Shrewsbury, 2005, p 176.

(18) Eselem Bungu, P.; Pasch, H. *Polym. Chem.* **2017**, *31*, 4565–4575.

(19) Hansen, E. W.; Kristiansen, P. E.; Pedersen, B. *J. Phys. Chem. B* **1998**, *102*, 5444–5450.

(20) Strobl, G.; Hagedorn, W. *J. Polym. Sci., Polym. Phys. Ed.* **1978**, *16*, 1181–1193.

(21) Mirabella, F. M.; Bafna, A. *J. Polym. Sci., Part B: Polym. Phys.* **2002**, *40*, 1637–1643.

(22) Lederer, A.; Voigt, D.; Clausnitzer, C.; Voit, B. *J. Chromatogr. A* **2002**, *976*, 171–179.

(23) Shafagh Dehghani, S. *Study of ethylene/propylene polymerization, using a 4th generation Ziegler-Natta catalyst: Effect of external donor and feed ratio on polymerization*. MSc, University of Waterloo, Waterloo, Canada, 2012.

(24) Wood-Adams, P. M.; Dealy, J. M.; Degroot, A. W.; Redwine, O. D. *Macromolecules* **2000**, *33*, 7489–7499.

(25) Teresa Rodríguez-Hernández, M.; Angulo-Sánchez, J.; Pérez-Chantaco, A. *J. Appl. Polym. Sci.* **2007**, *104*, 1572–1578.

(26) Kim, Y.-M.; Park, J.-K. *J. Appl. Polym. Sci.* **1996**, *61*, 2315–2324.

(27) Usami, T.; Gotoh, Y.; Takayama, S. *Macromolecules* **1986**, *19*, 2722–2726.

(28) Kumar, V.; Locker, C. R.; in't Veld, P. J.; Rutledge, G. C. *Macromolecules* **2017**, *50*, 1206–1214.

(29) Ginzburg, A.; Macko, T.; Dolle, V.; Brüll, R. *Eur. Polym. J.* **2011**, *47*, 319–329.

(30) Ndiripo, A.; Eselem Bungu, P. S.; Pasch, H. *Polym. Int.* **2019**, *68*, 206–217.

(31) Anantawaraskul, S.; Soares, J. B. P.; Wood-Adams, P. M. In *Polymer Analysis Polymer Theory*; Springer: New York, 2005, pp 1–54.

(32) Monrabal, B. *J. Appl. Polym. Sci.* **1994**, *52*, 491–499.

(33) Monrabal, B. *Macromol. Symp.* **1996**, *110*, 81–86.

(34) Pasch, H.; Malik, M. I. *Advanced separation techniques for polyolefins*; Springer: Switzerland, 2014.

(35) Pasch, H.; Malik, M. I.; Macko, T. *Adv. Polym. Sci.* **2013**, *251*, 77–140.

(36) Monrabal, B.; Romero, L.; Mayo, N.; Sancho-Tello, J. In *Macromol. Symp.*; Wiley Online Library, 2009, pp 14–24.

(37) Pasch, H.; Malik, M. I.; Macko, T. In *Polymer Composites – Polyolefin Fractionation – Polymeric Peptidomimetics – Collagens*, Abe, A.; Kausch, H.-H.; Möller, M.; Pasch, H., Eds.; Springer Berlin Heidelberg: Berlin, Heidelberg, 2013, pp 77–140.

(38) Schick, C. *Anal. Bioanal. Chem.* **2009**, *395*, 1589.

(39) Naidoo, P. *A comparative analysis of the chemical composition of linear low density polyethylene polymers synthesised with 1-hexene comonomer under different catalytic conditions*. MSc thesis, Stellenbosch University, Stellenbosch, 2013.

(40) Xue, Y.-H.; Bo, S.-Q.; Ji, X.-L. *Chin. J. Polym. Sci.* **2015**, *33*, 508–522.

(41) Liang, X.-k.; Luo, Z.; Yang, L.; Wei, J.-t.; Yuan, X.; Zheng, Q. *J. Polym. Eng.* **2018**, *38*, 7–17.

(42) Zhang, Q.; Chen, P.; Xie, X.; Cao, X. *J. Appl. Polym. Sci.* **2009**, *113*, 3027–3032.

(43) Brüll, R.; Pasch, H.; Raubenheimer, H. G.; Sanderson, R.; van Reenen, A. J.; Wahner, U. M. *Macromol. Chem. Phys.* **2001**, *202*, 1281–1288.

(44) Eselem Bungu, P.; Pflug, K.; Pasch, H. *Macromol. Chem. Phys.* **2020**, *221*, 2000095.

(45) Knooren, J. *Recent developments in polyolefin fractionations.* MSc thesis, University of Amsterdam, Amsterdam, 2013.

(46) Li, P.; Xue, Y.; Liu, W.; Sun, G.; Ji, X. *J. Polym. Res.* **2019**, *26*, 56.

(47) Müller, A.; Michell, R.; Pérez, R.; Lorenzo, A. *Eur. Polym. J.* **2015**, *65*, 132–154.

(48) Bungu, P. S. E.; Pflug, K.; Pasch, H. *Polym. Chem.* **2018**, *9*, 3142–3157.

(49) Bungu, P. S. E.; Pasch, H. *Polym. Chem.* **2019**, *10*, 2484–2494.

(50) van Reenen, A.; Brand, M.; Rohwer, E.; Walters, P. In *Macromol. Symp.*; Wiley Online Library, 2009, pp 25–32.

(51) Amer, I.; van Reenen, A.; Brand, M. *Polym. Int.* **2015**, *64*, 466–476.

(52) Cheruthazhekatt, S.; Robertson, D. D.; Brand, M.; van Reenen, A.; Pasch, H. *Anal. Chem.* **2013**, *85*, 7019–7023.

(53) Robertson, D. D.; Neppalli, R.; van Reenen, A. J. *Polym. Test.* **2014**, *40*, 79–87.

(54) Axelson, D.; Levy, G.; Mandelkern, L. *Macromolecules* **1979**, *12*, 41–52.

(55) Wang, W.-J.; Yan, D.; Zhu, S.; Hamielec, A. E. *Macromolecules* **1998**, *31*, 8677–8683.

(56) Malmberg, A.; Kokko, E.; Lehmus, P.; Löfgren, B.; Seppälä, J. V. *Macromolecules* **1998**, *31*, 8448–8454.

(57) Wang, W. j.; Yan, D.; Charpentier, P. A.; Zhu, S.; Hamielec, A. E.; Sayer, B. G. *Macromol. Chem. Phys.* **1998**, *199*, 2409–2416.

(58) Shroff, R.; Mavridis, H. *Macromolecules* **2001**, *34*, 7362–7367.

(59) Bovey, F.; Schilling, F.; McCrackin, F.; Wagner, H. *Macromolecules* **1976**, *9*, 76–80.

(60) Yu, Y.; DesLauriers, P. J.; Rohlfing, D. C. *Polymer* **2005**, *46*, 5165–5182.

(61) Eselem Bungu, P. S.; Zentel, K.; Hintenlang, S.; Busch, M.; Pasch, H. *ACS Appl. Polym. Mater.* **2020**, *2*, 5864–5877.

(62) Kuwabara, K.; Kaji, H.; Horii, F.; Bassett, D. C.; Olley, R. H. *Macromolecules* **1997**, *30*, 7516–7521.

(63) Read, D.; McLeish, T. *Macromolecules* **2001**, *34*, 1928–1945.

(64) Emwas, A.-H.; Roy, R.; McKay, R. T.; Tenori, L.; Saccenti, E.; Gowda, G.; Raftery, D.; Alahmari, F.; Jaremko, L.; Jaremko, M. *Metabolites* **2019**, *9*, 123.

(65) Liu, P.; Liu, W.; Wang, W. J.; Li, B. G.; Zhu, S. *Macromol. React. Eng.* **2017**, *11*, 1600012.

(66) Pasch, H. *Polym. Chem.* **2013**, *4*, 2628–2650.

(67) Harvey, M. C.; Ketley, A. D. *J. Appl. Polym. Sci.* **1961**, *5*, 247–250.

(68) Cheruthazhekatt, S.; Mayo, N.; Monrabal, B.; Pasch, H. *Macromol. Chem. Phys.* **2013**, *214*, 2165–2171.

(69) Jørgensen, J. K.; Larsen, A.; Helland, I. *e-Polymers* **2010**, *10*, 1596–1612.

(70) Prasad, A. *Polym. Eng. Sci.* **1998**, *38*, 1716–1728.

(71) Striegel, A.; Yau, W. W.; Kirkland, J. J.; Bly, D. D. *Modern size-exclusion liquid chromatography: Practice of gel permeation and gel filtration chromatography*, Second edition ed.; John Wiley & Sons: New Jersey, 2009, p 512.

(72) Sigwinta, M. *Ethylene-1-octene elastomers: Molecular structure characterization by advanced analytical methods*. MSc thesis, Cape Peninsula University of Technology, Cape Peninsula University of Technology, 2019.

(73) Gaborieau, M.; Castignolles, P. *Anal. Bioanal. Chem.* **2011**, *399*, 1413–1423.

(74) Podzimek, S. In *Light Scattering, Size Exclusion Chromatography and Asymmetric Flow Field Flow Fractionation: Powerful Tools for the Characterization of Polymers, Proteins and Nanoparticles*; John Wiley & Sons: New Jersey, 2011, pp 99–206.

(75) Stadler, F. J.; Piel, C.; Kaminsky, W.; Münstedt, H. In *Macromol. Symp.*; Wiley Online Library, 2006, pp 209–218.

(76) Malik, M. I.; Pasch, H. *Prog. Polym. Sci.* **2014**, *39*, 87–123.

(77) Tackx, P.; Tacx, J. *Polymer* **1998**, *39*, 3109–3113.

(78) Shroff, R.; Mavridis, H. *Macromolecules* **1999**, *32*, 8454–8464.

(79) Kratochvíl, P.; Netopilík, M. *Eur. Polym. J.* **2014**, *51*, 177–181.

(80) Kuhn, R.; Krömer, H. *Colloid. Polym. Sci.* **1982**, *260*, 1083–1092.

(81) Macko, T.; Pasch, H. *Macromolecules* **2009**, *42*, 6063–6067.

(82) Netopilik, M.; Podzimek, S. *ACS omega* **2020**, *5*, 14254–14260.

(83) Plüschke, L.; Mundil, R.; Sokolohorskyj, A.; Merna, J.; Sommer, J.-U.; Lederer, A. *Anal. Chem.* **2018**, *90*, 6178–6186.

(84) Knox, J. H.; Kaur, B.; Millward, G. R. *J. Chromatogr. A* **1986**, *352*, 3–25.

(85) Monrabal, B. *Macromol. Symp.* **2015**, *356*, 147–166.

(86) Cong, R.; Degroot, W.; Parrott, A.; Yau, W.; Hazlitt, L.; Brown, R.; Miller, M.; Zhou, Z. *Macromolecules* **2011**, *44*, 3062–3072.

(87) Cong, R.; deGroot, A. W.; Parrott, A.; Yau, W.; Hazlitt, L.; Brown, R.; Cheatham, M.; Miller, M. D.; Zhou, Z. *Macromol. Symp.* **2012**, *312*, 108–114.

(88) Heinz, L.-C.; Pasch, H. *Polymer* **2005**, *46*, 12040–12045.

(89) Plüschke, L.; Ndiripo, A.; Mundil, R.; Merna, J.; Pasch, H.; Lederer, A. *Macromolecules* **2020**, *53*, 3765–3777.

(90) Macko, T.; Brüll, R.; Zhu, Y.; Wang, Y. *J. Sep. Sci.* **2010**, *33*, 3446–3454.

(91) Lee, D.; Miller, M. D.; Meunier, D. M.; Lyons, J. W.; Bonner, J. M.; Pell, R. J.; Shan, C. L. P.; Huang, T. *J. Chromatogr. A* **2011**, *1218*, 7173–7179.

(92) Ginzburg, A.; Macko, T.; Dolle, V.; Brüll, R. *Eur. Polym. J.* **2011**, *47*, 319–329.

(93) van der Horst, A.; Schoenmakers, P. J. *J. Chromatogr. A* **2003**, *1000*, 693–709.

(94) Im, K.; Park, H.-w.; Lee, S.; Chang, T. *J. Chromatogr. A* **2009**, *1216*, 4606–4610.

(95) Cheruthazhekatt, S.; Harding, G. W.; Pasch, H. *J. Chromatogr. A* **2013**, *1286*, 69–82.

(96) Cheruthazhekatt, S.; Pijpers, T. F.; Mathot, V. B.; Pasch, H. In *Macromol. Symp.*; Wiley Online Library, 2013, pp 22–29.

(97) Ndiripo, A. *High temperature multidimensional chromatography of complex and functionalized polyolefins*. Ph.D. thesis, Stellenbosch University, Stellenbosch, 2018.

(98) Xue, Y.; Liu, W.; Li, P.; Men, Y.; Bo, S.; Ji, X. *Ind. Eng. Chem. Res.* **2019**, *58*, 16869–16876.

(99) Eselem Bungu, P. S. *Development of a multiple fractionation protocol for the comprehensive analysis of low density polyethylene*. Ph.D. thesis, Stellenbosch: Stellenbosch University, Stellenbosch, 2018.

(100) Ndiripo, A.; Eselem Bungu, P. S.; Pasch, H. *Polym. Int.* **2019**, *68*, 206–217.

(101) Messaud, F. A.; Sanderson, R. D.; Runyon, J. R.; Otte, T.; Pasch, H.; Williams, S. K. R. *Prog. Polym. Sci.* **2009**, *34*, 351–368.

(102) Cölfen, H.; Antonietti, M. In *New Developments in Polymer Analytics I*, M, S., Ed.; Springer Berlin Heidelberg: Berlin, Heidelberg, 2000, pp 67–187.

(103) Peacock, A. *Handbook of Polyethylene: Structures: Properties, and Applications*; CRC Press: New York, 2000, p 1–24.

(104) Amjadi, M.; Fatemi, A. *Polymers* **2020**, *12*, 1857.

(105) Robertson, R.; Paul, D. *J. Appl. Polym. Sci.* **1973**, *17*, 2579–2595.

(106) Swallowe, G. M. *Mechanical Properties and Testing of Polymers: An A-Z Reference*; Springer: London, 1999, p 302.

(107) Liang, J.-Z.; Ma, W.-Y. *J. Polym. Eng.* **2012**, *32*, 343–348.

(108) Islam, A.; Hussein, I. A. *J. Appl. Polym. Sci.* **2006**, *100*, 5019–5033.

Chapter 3 : Experimental details

This chapter provides detailed information on the samples, solvents, as well as procedures used. Some of the procedures utilized were adapted and modified from literature.

3.1 Materials

Laboratory synthesized polyethylene samples were kindly supplied by Borealis (Linz, Austria). Commercial low density polyethylene samples were obtained from different suppliers; LDPE 1 was obtained from Sigma-Aldrich, South Africa, LDPE 2 from Sabic (Saudi Arabia), and LDPE 3 from Sasol Polymers (Secunda, South Africa.). Ten linear polyethylene reference standards were obtained from PSS (Mainz, Germany). The molar mass (M_w) of the standards in g/mol are as follows: 282, 563, 2000, 16 000, 36 500, 60 000, 99 700, 181 000, 883 500 and 1 070 000.

3.1.1 Stabilizers

Stabilizers were used during p-MMF as well as in the analyses of LDPE samples in HT-SEC. IRgnarox 1010 (Ciba Speciality Chemicals, Switzerland) was used at 2 wt % during the dissolution of the p-MMF samples to prevent oxidative degradation during the fractionation process. 0.0125 wt/vol % butylated hydroxytoluene (BHT ≥ 99.0 %, Sigma-Aldrich) was added to the TCB mobile phase in HT-SEC.

3.1.2 Solvents

Xylene (99 %), ethyl cellosolve (2-ethoxyethanol) (≥ 99 %), 1,2,4-trichlorobenzene (≥ 99 %), 1,2-dichlorobenzene (>99%) and 1-dodecanol (>98.0%) were obtained from Sigma-Aldrich and used as received, 1,1,2,2-tetrachloroethane (Merck, South Africa> 99.5 %) was also utilized as an internal reference and a solvent for all solution ^{13}C-NMR analyses. 1,2,4-trichlorobenzene (TCB) Chromasolv® (Sigma-Aldrich, South Africa ≥99 %) was used as the mobile phase in HT-IC while TCB and 1,2-dichlorobenzene (ODCB) reagent plus ® grades (Sigma-Aldrich, South Africa ≥ 99 %) were utilized as the mobile phase in HT-SEC.

3.2 Chromatographic techniques

3.2.1 High-temperature size exclusion chromatography (SEC-IR)

The molar masses and dispersities of the samples were determined on a Polymer Char SGIC instrument (Valencia, Spain) equipped with an infrared detector (IR4). The samples (8 mg) were dissolved in 4 mL of TCB for 2 hr together with 0.025 % BHT that acted as a stabilizer to prevent sample decomposition/degradation. TCB with 0.0125 % BHT was used as the mobile phase at a flow rate of 1 mLmin^{-1}. Three 300 × 7.5 mm^2 PLgel Olexis columns (Agilent Technologies, UK) were used together with a 50 × 7.5 mm^2 PLgel Olexis guard column. 200 µL of each sample was injected. All experiments in HT-SEC were done at 150 °C. The chromatograph was calibrated using narrow polystyrene standards (Polymer Standards Service, Mainz, Germany).

3.2.2 High-temperature quadruple-detector size exclusion chromatography

High-temperature size exclusion chromatography with quadruple detection was performed with a PL-GPC 220 (Agilent Technologies, US) which has an online degasser, an online pre-injection filter, and two PLgel Olexis (Agilent Technologies, US) columns packed with 13 µm particle size of crosslinked polystyrene. Experiments were carried out at a flow rate of 1 mL min^{-1} and an operating temperature of 150 °C. 1,2,4-trichlorobenzene (TCB, Aldrich, DE) was used as a mobile phase. Samples were run in triplicate, which involved dissolving and injecting them separately. The samples were dissolved in TCB with concentrations between 3.5 – 4.0 mg mL^{-1} for 1 –3 hours depending on the nature of the sample. The injection volume was 200 µL. The SEC was coupled to four consecutive detectors: A DAWN Heleos-II 18-angle static light scattering photometer (MALLS, Wyatt Technology, US), DYNAPRO Nanostar (DLS, Wyatt Technology, US), a four-capillary viscometer (Agilent Technologies, US), and a differential refractometer (Agilent Technologies, US). For normalization of the MALLS photodiodes, interdetector delays as well as band broadening calculation, measurements of polystyrene-30 kg/mol (PSS, DE) with narrow molar mass distribution were performed. The raw data was processed and analyzed using the software ASTRA (Wyatt Technology, US).

3.2.3 High-temperature solvent gradient interaction chromatography

Interaction chromatography experiments were dome on a solvent gradient interaction chromatography (SGIC) built by polymer Char (Valencia, Spain). The instrument is equipped with an autosampler (a separate component connected to the injector via heated transfer line), two separate ovens, switching valves, and two pumps that are fitted with vacuum degassers (Agilent, Waldbronn, Germany). For solvent gradient elution in IC, a high-pressure binary gradient pump (Agilent, Waldbronn, Germany) was utilized. The evaporative light scattering detector (ELSD, model PL-ELS 1000, Polymer Laboratories, Church Stretton, England) was used with the following parameters: gas flow rate of 1.5 L/min, 160 ℃ nebulizer temperature, and an evaporative temperature of 270 ℃. A porous graphitic carbon column (Hypercarb ®, Thermo Scientific, Dreieich, Germany) with a size of 100 × 4.6 mm^2 packed with porous graphite particles which have an typical particle diameter of 5 μm (making a surface area of 120 m^2g^{-1}) and a pore size of 250 Å was used for all HT-HPLC experiments. The column was put in an oven and the temperature was maintained at 160 °C. The flow rate of the mobile phase during analysis was 0.5 $mLmin^{-1}$. To achieve separation, a linear gradient was applied from 100 % 1-dodecanol to 100 % TCB within 10 min after sample injection. These conditions were held for 20 min before re-establishing 1-decanol to 100 %. A second shallow gradient was applied in 30 min for better separation. For all HT-LC analyses, a concentration of 1 – 1.2 $mgmL^{-1}$ was used (approximately 4 mg in 4 mL of TCB) with 200 μL of each sample being injected.

3.2.4 High-temperature temperature gradient interaction chromatography

The first TGIC experiments were performed by using ODCB (1,2-dichlorobenzene) as the mobile phase. A 100 × 4.6 mm^2 Hypercarb® column was utilized as the stationary phase, a concentration of 1 – 1.2 $mgmL^{-1}$ was used (~4 mg in 4 mL of ODCB) with 200 μL of each sample being injected. The flow rate during the cooling step was set to 0.02 $mLmin^{-1}$ and 0.5 $mLmin^{-1}$ during the elution step. For this work, all elution volumes to start at 0 mL i.e., the volume during the crystallization stage of the TGIC experiment is omitted. Linear temperature gradients were applied in all cases (10 °C and 4 °C for cooling and heating, respectively). An infrared detector was used for detection and the branching distribution was calculated via dividing the methyl (CH_3-) absorbances by the methylene (-CH_2-) absorbances. The temperature and mobile phase flow profiles used in the present work are illustrated in Fig. 3.1.

The second TGIC was performed using the procedure above, but the stationary phase was plain silica, and the detector was ELSD.

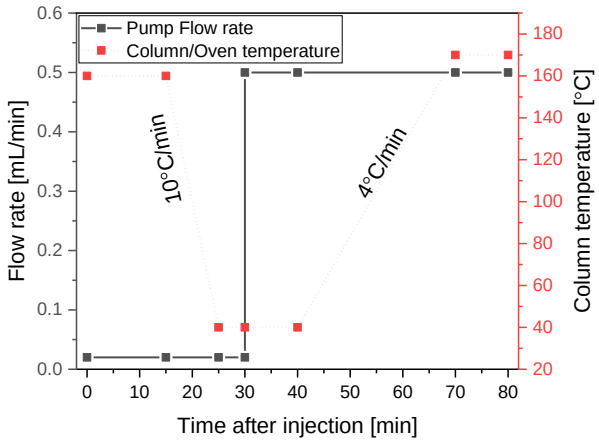

Figure 3.1 Temperature and flow profiles used in TGIC. The temperature profile is shown by the red line and the flow profile by the black line.

3.2.5 High-temperature two-dimensional liquid chromatography (HT-2D-LC)

HT-SGIC and HT-TGIC were coupled to HT-SEC with the aid of an electronically controlled eight-port valve system (VICI Valco Instruments, Houston, Texas, USA) equipped with two 100 µL sample loops. Injection in the 1st dimension (HT-SGIC and HT-TGIC) was done using a 200µL sample loop and the flow rate was 0.05mLmin^{-1}. A similar gradient as in the one-dimensional HT-SGIC and HT-TGIC analyses was used in the 1st dimension and three times the concentration of the sample was used (i.e., 3 mgmL^{-1}). A flow rate of 2.75 mLmin^{-1} was used in the 2nd dimension (HT-SEC), and ODCB was used as the mobile phase. In the 2nd dimension, a PL Rapide M (Agilent, U.K.) 100 × 10 mm^2 internal diameter column with a 10 µm particle diameter was used at 160 °C. The evaporative light scattering detector (ELSD) was used with the following parameters: gas flow rate of 1.5 L/min, 160 °C nebulizer temperature, and an evaporative temperature of 230 °C.

3.3 Carbon-13 nuclear magnetic resonance analysis (^{13}C-NMR)

The ^{13}C-NMR quantitative analyses of the samples and fractions were carried out using a 600 MHz Varian Unity Inova NMR spectrometer at a resonance frequency of 150 MHz. All samples (~60 mg) were dissolved in 0.6 mL deuterated 1,1,2,2-tetrachloroethane- d_2 (TCE-d2)

(95.5+ atom% D, Sigma-Aldrich) with chromium(lll) acetylacetonate as the paramagnetic relaxation agent (0.735 g in 25g of TCE-d2), making a sample concentration of ≈ 100 mg mL^{-1}. TCE-d_2 was also utilized as an internal reference (74.3 ppm). The samples were pre-dissolved in the NMR tube to get a homogenous solution at 130 °C and were analyzed overnight at 120 °C. The peaks associated with backbone carbons and branching carbons were integrated and the integrals of the peaks were used to determine the branching content per 1000 carbons (Br/1000C) using Equation 3.1 and 3.2

$$\frac{LCB}{1000_{carbons}} = \left[\left(\frac{I_{LCB}}{sum\ of\ integrals}\right) - \left(\frac{2}{PN \times 2}\right)\right] \times 1000 \quad 3.1$$

$$\frac{SCB}{1000_{carbons}} = \frac{I_{SCB}}{Sum\ of\ integrals} \times 1000 \quad 3.2$$

Where:

I = integral value

PN = $\frac{M_n}{28.05(Mw\ of\ ethene)}$

3.4 Differential scanning calorimetry

The bulk samples were analyzed using the NETZSCH DSC 214 POLYMA instrument (NETZSCH-Geraetebau GmbH-Selb, Germany) at a heating rate of 10 °C min^{-1} across a temperature range of 0 – 200 °C. An aluminum pan and lid creased and pressed were used as a reference and roughly 5 mg of each sample were used. The initial heating cycle was used to wipe out the thermal history of the sample, and the second heating and first crystallization cycles being used for quantitative and qualitative analysis.

3.5 Crystallization analysis fractionation

A commercial CRYSTAF apparatus Model 200 was utilized for crystallization analysis fractionation experiments. Approximately 20 mg of each sample was dissolved in 35 mL of TCB. Crystallization was done under constant agitation in stainless steel reactors which are fitted with automatic agitation and filtration devices. The samples were dissolved for 150 min. After dissolution, the temperature was reduced from 100 °C to approximately 30 °C at a rate

of 0.2 °C/min. The concentration of the solution was measured repeatedly using an infrared detector operating at a fixed wavelength of 3.5 μm.

3.6 Fourier-Transform infrared spectroscopy

Attenuated total reflectance (ATR) measurements of the bulk LDPEs and their p-MMF fractions were recorded on a thermo Nicolet iS10 spectrometer. Solid samples were measured in all the analyses with no preceding modifications. Spectra recorded from 4 000 to 650 cm^{-1} were obtained from a collection of 64 scans at a resolution of 4 cm^{-1} with automated background subtraction. Thermo Scientific OMNIC software (version 8.1) was used for data collection and processing.

3.7 Preparative molar mass fractionation

3.7.1 Preparative solvent gradient fractionation (p-SCF)

Xylene and ethyl cellosolve (2-ethoxyethanol) were used as the good and poor solvent, respectively. Approximately 5.0 g of polymer sample was weighed and dissolved at 130 °C in 100 mL of xylene stabilized with 2.0 wt. % Irganox 1010. After dissolution, the solution was titrated using a dropping funnel with an excess of ethyl cellosolve (500 mL) in two hours to produce a fine dispersion of polymer precipitate at a constant temperature. The polymer solution was then introduced into a column packed with sea sand (white quartz, Sigma-Aldrich, South Africa) at 130 °C. The column was left to equilibrate at 130 °C for a further 1 hr before being emptied to collect the first fraction. After that, a series of preheated solvent mixtures with varying amounts of xylene and ethyl cellosolve were added and emptied one at a time as shown in Table 3.1. A total of 0.75 hr was allocated to each step to minimize the kinetic effects of the dissolution process on the fractionation. The eluted solution was transferred to a flask and dried using a rotor vapor before precipitating the fractions in acetone. The obtained fractions were dried to a steady weight in a vacuum oven at room temperature. The full time required to complete one experiment was ~ 14 hr. Fig. 3.2 shows the p-MMF setup used.

Table 3.1 Solvent ratios used during fractionation.

Fraction	Xylene (mL)	Cellosolve (mL)
1	100	500
2	200	300
3	225	275
4	250	250
5	270	230
6	290	210
7	300	200
8	325	175
9	500	0

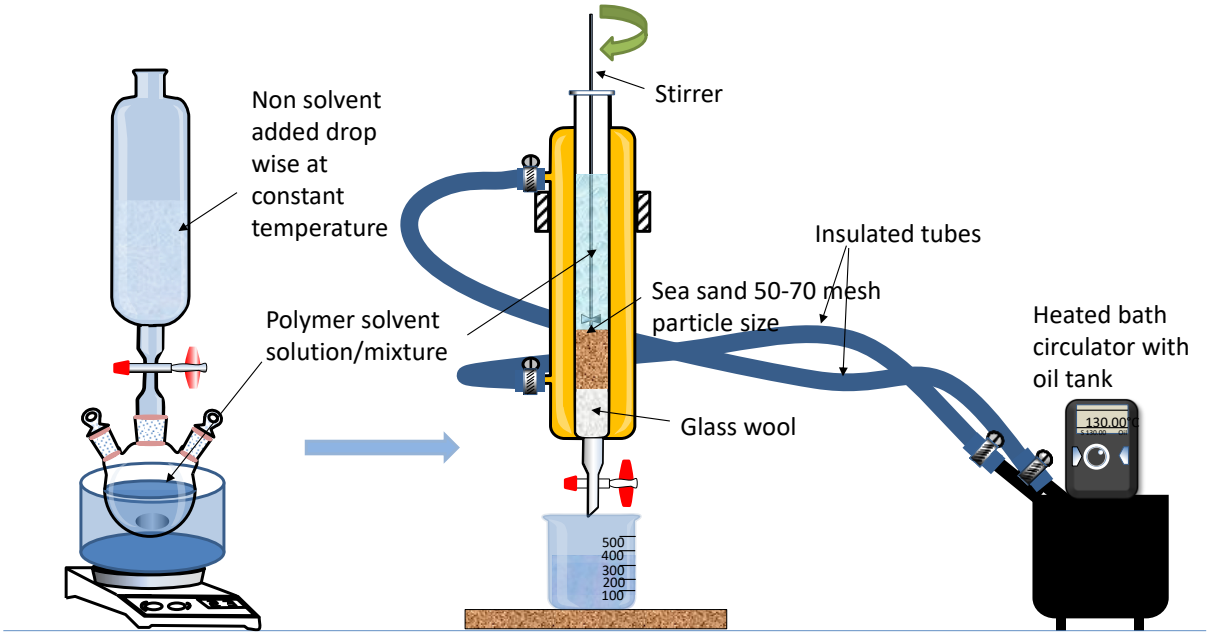

Figure 3.2 Preparative solvent gradient fractionation setup.

3.7.2 Preparative molar mass fractionation by precipitation

Preparative molar mass by precipitation was performed using a unique glass column, which was equipped with an oil inlet and outlet connecting the column to an external oil circulator. In the glass column, approximately 3.0 g of polymer was dissolved in 200 mL of ODCB in the presence of 2.0 wt. % Irganox 1010 (Ciba Speciality Chemicals, Switzerland) as a stabilizer. The sample dissolution completed at 130 °C under constant stirring. After that, 140 mL of 2-ethoxyethanol was added as a non-solvent into the polymer solution to give a non-

solvent/solvent ratio of 0.70. Then after 45 minutes, the temperature was dropped to 115 °C. The polymer solution was given a further 30 minutes to equilibrate at 115 °C. The precipitated fraction was collected as the first fraction. After complete isolation of the first fraction from the solution, 30 mL of 2-ethoxyethanol were added to make a non-solvent/solvent ratio of 0.85 and the fraction was collected. The polymer-solvent that remained in the solution was gathered as the third fraction (soluble fraction). All the accumulated fractions were washed in methanol and vacuum dried to a constant weight.

3.7.3 HT-TGIC preparative fractionation using a silica stationary phase

The HT-TGIC experiments were performed by using ODCB (1,2-dichlorobenzene) as the mobile phase and plain silica as the stationary phase. The ELSD detector was disconnected so as to collect fractions using elution volumes obtained from the previous HT-TGIC experiments. The flow rate during the cooling step was treated in a similar manner as described in Section 3.2.4. Linear temperature gradients were applied in all cases (10 ℃ and 4 °C for cooling and heating, respectively). The fractions collected were vacuum dried at high temperatures to a constant weight.

3.8 Mechanical properties

3.8.1 Molding of test specimens

Specimens for mechanical analyses were molded using a Thermo Scientific Haake Mini Jet II injection molding apparatus. The melt temperature was 190 °C with the mold temperature being kept at 60 °C for all samples and the pressure was maintained at 350 bars. After injection, the mold was opened, and the specimen was promptly cooled.

3.8.2 Tensile strength determination

Tensile properties of the injection-molded test samples were determined according to ASTM D 638 M standards. The specimens were 5.2 mm thick, 1.6 mm wide and had a 42 mm gauge length. All determinations were carried out beyond 24 hours of molding on a Lloyd Instruments LRX tensile testing apparatus. Young's modulus and tensile properties were gauged at an extension rate of 50 mm/min.[1,2]

3.9 Melt flow index

The melt flow index (MFI) was measured using the Ceast apparatus (Fig. 3.3). LDPE was processed at 190 °C. The weight used was 2.16 kg and the samples used ±5 g.

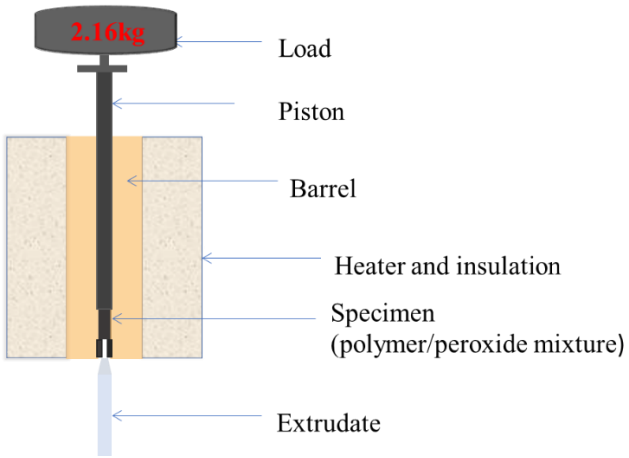

Figure 3.3 Melt flow index cross-section.

MFI was calculated using the formula:

$$({}^{600}/_{t}) \times weight\ of\ extrudate = g/10\,\text{min} \quad 190℃@2.16kg$$

3.10 References

(1) Ndiripo, A. *Comparative study on the molecular structure of ethylene/1-octene, ethylene/1-heptene and ethylene/1-pentene copolymers using advanced analytical methods*. MSc, Stellenbosch: Stellenbosch University2015.

(2) Liang, X.-k.; Luo, Z.; Yang, L.; Wei, J.-t.; Yuan, X.; Zheng, Q. *J. Polym. Eng.* **2018**, *38*, 7–17.

Chapter 4 : Results and discussion

Analysis of low density and long chain branched polyethylene (LDPE and LCBPE)

The present chapter discusses the analysis of branching in two sets of polyethylene samples using advanced fractionation techniques.

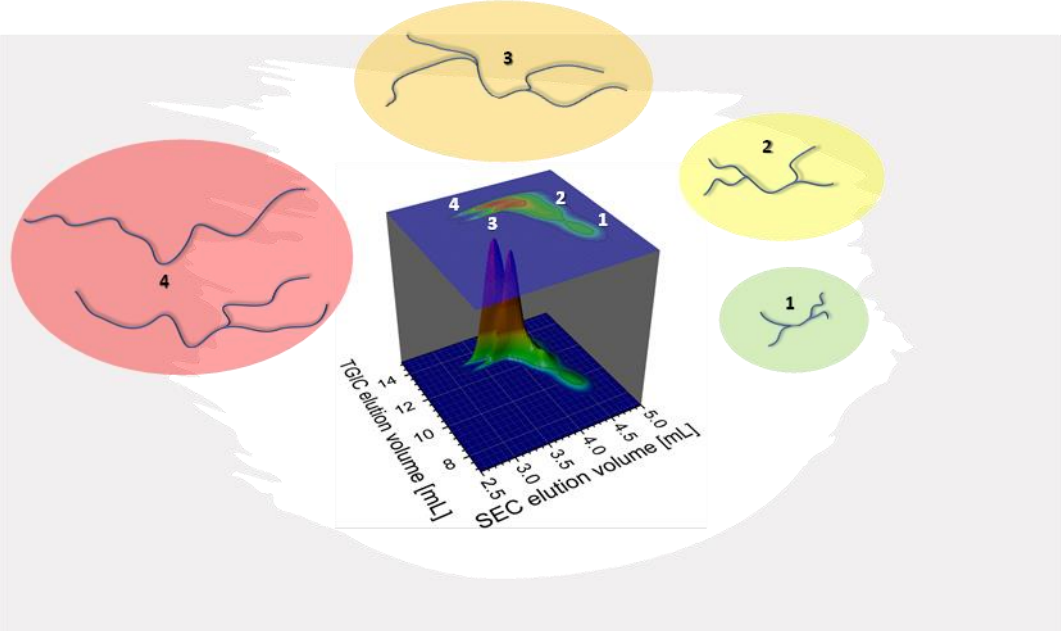

Fractionation of a polyethylene with long chain branches using high temperature two-dimensional liquid chromatography (HT-2D-LC). The first dimension separates the polymer according to chemical composition and the second dimension according to molar mass.

4.1 Introduction

The microstructural properties of polyethylene (PE) differ depending on the synthesis technique. Low density polyethylene (LDPE) comprises of both long and short chain branches with varying numbers, lengths, and branching densities. In this chapter, three commercial LDPEs and four laboratory synthesised long chain branched polyethylenes (LCBPE) with different numbers of long chain branches are analysed using a variety of advanced analytical techniques as described in Chapter 3. The commercial LDPEs contain short (SCBs) and long chain branches (LCBs) and the laboratory PEs contain only LCBs. A comparison of the two PE types shall help to understand the contributions LCB and SCB on the molecular properties and ultimately mechanical and physical properties.

Infrared (IR) spectroscopy has been widely used to qualitatively and quantitatively characterize polymers.[1] FTIR is one quick and efficient way of analysing the chemical composition and crystallinity of polyolefin resins. The compositional analysis of PE by FTIR is well documented in literature.[2,3] The FTIR spectra in Fig.4.1 show very similar attributes in the two sets of samples and both are typical of PE. Differences in the crystallinities of the two sample sets can be seen in the 1500 – 1420 cm^{-1} (CH_3 bending) and 750 – 700 cm^{-1} (deformation vibration in $(-CH_2)_n$) regions.[4] For the LDPE samples, a single broad peak is seen in the spectral region of 1500 – 1420 cm^{-1} while for the LCBPE, the shouldering/bending of the peak indicates the presence of long $-CH_2-$ sequences which increase from 027A to 043A. As the crystallinity of the PEs increase, the peaks tend to split.

The peak at 730.6 cm^{-1} is absent in the LDPE samples which indicates lower crystallinity.[1,3] On the other hand, the LCBPEs show increasing crystallinity from 027A to 043A. More subtle distinctions in the branching structures of the samples cannot be provided by FTIR, but by the more chemically sensitive carbon-thirteen nuclear magnetic resonance spectroscopy (^{13}C-NMR). Due to the nature of commercial LDPE production at high pressure, various branching structures with different lengths and frequencies are produced.

4.2 Spectroscopic analyses for average chemical composition

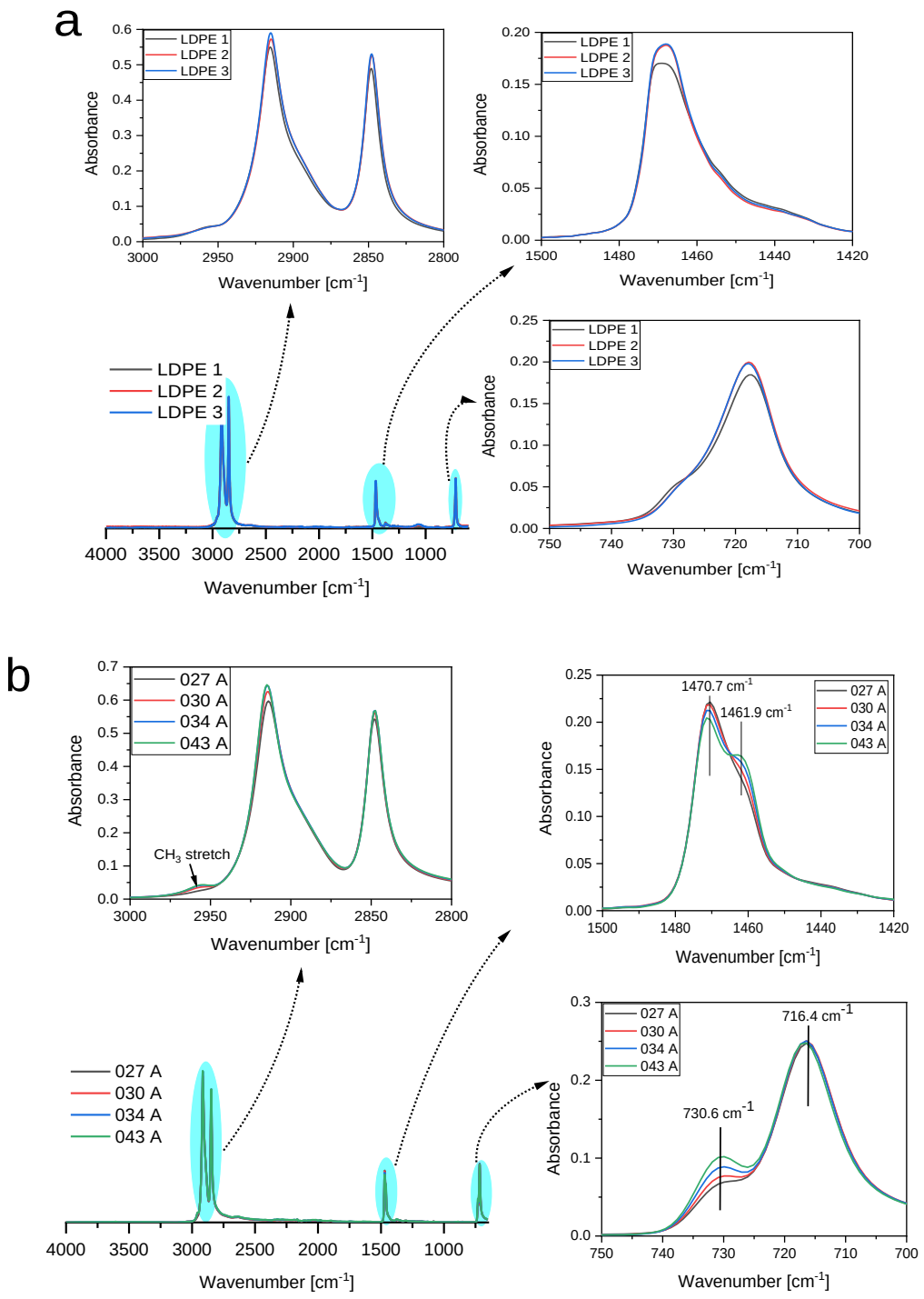

Figure 4.1 FTIR spectra of commercial LDPEs (a) and long chain branched PE (LCBPE) (b).

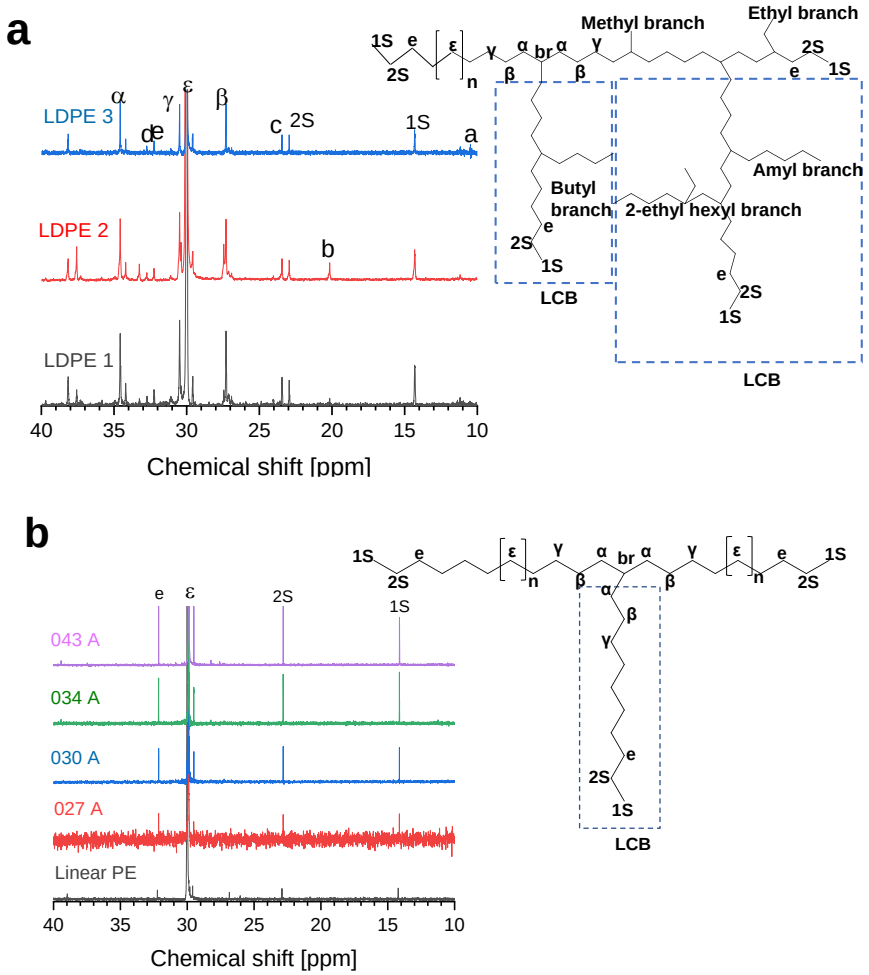

Figure 4.2 ^{13}C-NMR spectra of LDPEs (a) and LCBPEs (b).

^{13}C-NMR spectroscopy was used to determine and quantify the branch types and branching contents of the LDPEs and LCBPEs. The ^{13}C-NMR spectra are shown in Fig. 4.2 and the calculated branch contents are summarized in Table 4.1. The signals were assigned based on literature.[5-7] The spectra are typical of commercial LDPEs. Branches were named as xB_n where n and *x* are the length of the branch and carbon number, respectively. The peaks labelled α, β, γ, ε, and br constitute the backbone carbons. For LDPEs, resonance signals of specific carbons at **a** = 11.25 ($1B_2$), **b** = 20.17 ($2B_3$), **c** = 23.61 ($2B_4$), and **d** = 32.94 ($3B_5$) are seen, indicating that the resin has ethyl, methyl, butyl, and amyl branches.

The ethyl, methyl, butyl and amyl branches are referred to as SCBs as they have branches with less than five carbons. In addition, the resonance peak at **e** = 32.25 ($3B_{6-n}$) indicates the presence of LCB (n ≥6). The resolution in ^{13}C-NMR is inadequate to differentiate branches longer than five carbons. They are, therefore, identified in the spectrum by the -CH_2 carbon atom

designated as "e" resonating at 32.25 ppm. LDPE is observed to have both SCBs and LCBs whereas the long chain branched PE has LCBs only. The estimation of LCB content of the PEs was achieved by chain-end correction which is subtracting the number of the chain ends of the main chain as shown from the previous chapter using the third carbon from the chain end (**e** =32.25).

Table 4.1 Summary of branch types and Br/1000C in the LDPEs and long chain branched PEs. The branch contents were calculated from ^{13}C-NMR spectra.

	$2B_3$	**$1B_2$**	**$2B_4$**	**$3B_5$**	**$3B_{6-n}$**		
Sample name	Methyl	Ethyl	Butyl	Amyl	LCB	Total SCB	Total branches
LDPE 1	1.3	2.8	7.3	2.8	3.5	14.2	17.7
LDPE 2	4.8	0.9	4.8	1.2	1.4	11.7	13.1
LDPE 3	-	0.3	6.4	1.4	2.1	8.1	10.2
027 A	-	-	-	-	2.7	-	2.7
030 A	-	-	-	-	3.7	-	3.7
034 A	-	-	-	-	4.2	-	4.2
043 A	-	-	-	-	5.7	-	5.7
δ_{exp}	20.17	11.18	23.44	32.74	32.25		
δ_{lit}	20.30	11.25	23.61	32.61	32.18		

δ_{exp} = experimental chemical shift, δ_{lit} = chemical shift stated in literature.

Quantitative calculations according to Usami *et al.* were done to obtain the content of each branch type per thousand carbons (branch/1000C).[8] Butyl branches constitute the highest amount (7.3, 4.8 and 6.4/1000C for LDPE 1, 2 and 3, respectively). The long chain branches were 3.5, 1.4 and 2.1/1000C for LDPE 1, 2 and 3, respectively. On the other hand, the LCBPEs only show the presence of long chain branches which increase from 027A – 043A.

LCB is known to influence the polymer processibility.[9] In this regard, the relationship between LCB and melt flow index (MFI) is illustrated in Fig. 4.3. For the LDPEs, the long chain branching is low and does not appear to significantly influence the MFI; this is probably due to the presence of SCB. SCB is more effective in reducing polyolefin crystallinity. On the other hand, LCBPEs show a pronounced increase in MFI with increase in LCB. MFI is influenced by molar mass, however, we can also see the contributions of LCB. ^{13}C-NMR just tells us if

the branches are shorter or longer than C_5. To influence MFI, the branches must be significantly longer than C_5 or C_{10}. This means that LCBPEs have long chain branches longer than C_{50}.

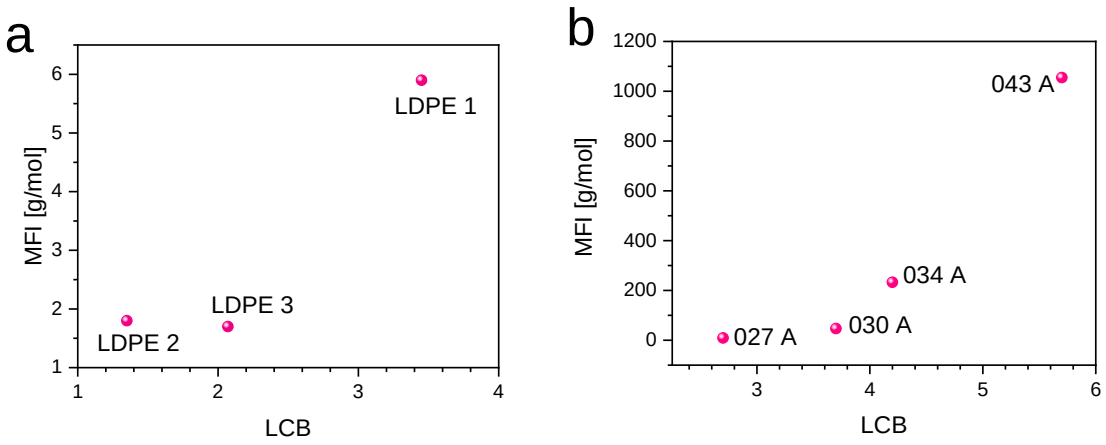

Figure 4.3 Plots of melt flow index as a function of long chain branching (^{13}C-NMR) for LDPEs (a) and LCBPEs (b).

The LCBPEs have true long branches which influence the crystal arrangements of the macromolecules giving them a rather compact structure. The physical and mechanical properties of polyethylene are reliant on the type and quantity of branches (refer to Appendix B for the physical properties of LDPEs).

4.3 Molar mass analyses

The mechanical properties of LDPE are highly influenced by the average molar mass (M_w) whereas the molar mass distribution (MMD) is responsible for rheological properties. A rundown of the molar masses and dispersities of the LDPEs and LCBPEs is given in Table 4.2. In the present study, two HT-SEC systems were used for molar mass analyses. Infrared detection with CH_3- and -CH_2- sensors was used to determine the average number of branches as a function of molar mass for both sets of PEs as illustrated in Fig. 4.4 a and 4.4 b. The LDPEs have similar molar mass distributions, except for the LDPE 1 which has a high molar mass tail. On the other hand, the LCBPEs show increasing molar masses as the LCB decreases, see Fig. 4.4 b. Contributions of LCB may very well play a role in the observed shift in the MMDs since PE coils become more compact with increasing LCB content.

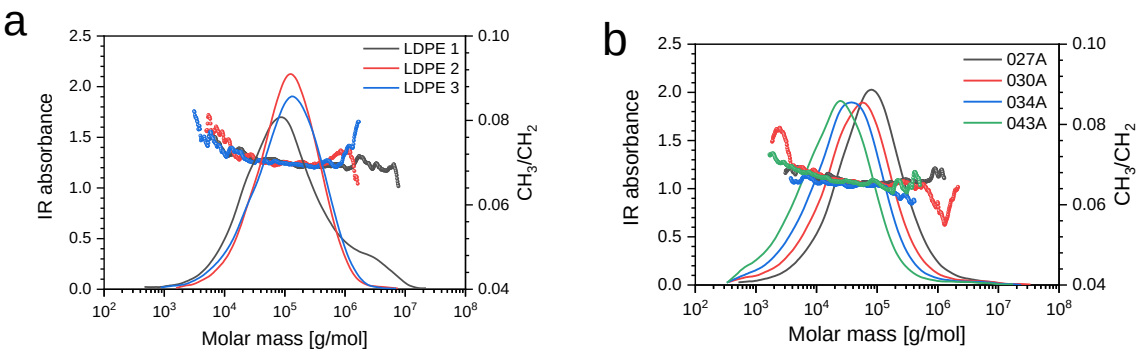

Figure 4.4 Molar mass distribution profiles obtained from HT-SEC-IR and number of branches as a function of molar mass obtained by dividing the methyl (CH_3-) absorbances by the methylene (-CH_2-) absorbances.

Table 4.2 A summary of LDPEs and LCBPEs molar mass, thermal and melt flow properties.

Sample	MFI [g/10min]	M_n[a] [kg/mol]	M_p[a] [kg/mol]	M_w[a] [kg/mol]	Đ[a]
LDPE 1	5.9	29.2	89.6	485.8	16.6
LDPE 2	1.8	49.4	124.1	215.2	4.4
LDPE 3	1.7	39.2	153.1	226.2	5.8
027A	9.3	24.5	78.7	222.0	9.1
030A	47.0	13.6	58.9	191.1	14.1
034A	232.9	9.5	41.5	99.0	10.4
043A	1054.9	7.0	25.1	84.2	12.0

[a] as determined from HT-SEC-IR

High-temperature quadruple-detector size exclusion chromatography (HT-SEC-d4) with a concentration detector (RI) and two molar mass sensitive detectors (MALLS and Vis) was utilized for LCB characterization of the bulk samples. This system provides comprehensive qualitative and quantitative information by presenting LCB (instead of total branches) as a function of molar mass.

A better understanding of the molecular shape of polymers can be obtained from the radius of gyration (R_g) as obtained by light scattering detection. The physical relationship between polymer size and molar mass is afforded by the power law:

$$R_g = K \cdot M^v \tag{4.1}$$

$$R_g = 0.029 \cdot M^{0.57} \tag{4.2}$$

For linear PE molecules in a thermodynamically good solvent, the typical intercept *(K)* and gradient (v) values of 0.029 and 0.57, respectively, were used.[10] There is a relationship between polymer dimensions and molar mass, and this can be obtained for each sample. The power law exponent *v* is sensitive to the scaling properties of the macromolecule which yield information regarding the solution properties of the polymer.

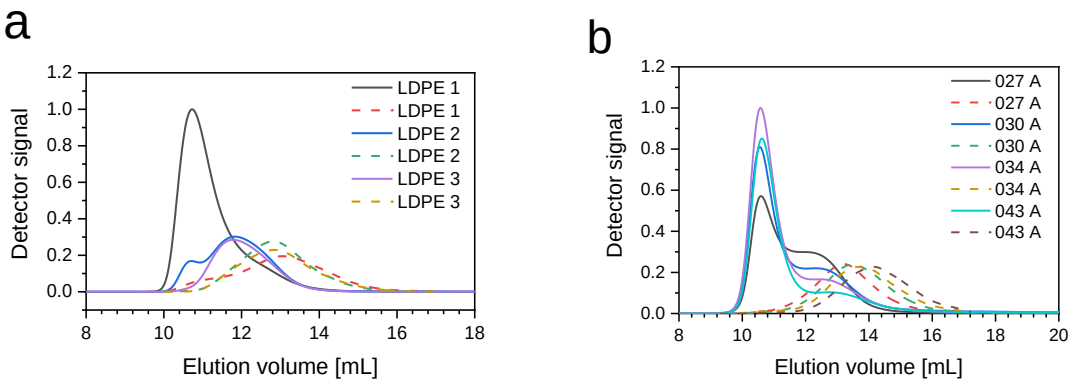

Figure 4.5 HT-SEC-d4 chromatograms of LDPEs (a) and long chain branched PEs (b) as detected by RI and 90° MALLS (dotted lines) detectors.

To retrieve the scaling exponent, a plot of radius and molar mass information in a double-logarithmic fashion was produced and the slope of the linear curve determined. The conformation plots of R_g vs. molar mass comparing the branched PE resins to a perfect linear PE of similar molar mass is presented in Fig. 4.6. For a branched polymer, the molecular size is affected by molar mass and the degree of LCB, which is identified by the deviation of the conformation plot of branched molecules from their linear equivalent. Different characteristic polymer architectures have been reported in literature, e.g., hard sphere (ν = 0.33), randomly hyperbranched structures (ν = 0.3−0.5) and linear coil (ν = 0.58).[11,12] Based on the obtained ν values, the conformation plots of the LDPEs are deviating away from the linear plot with the increase in the molar mass. The *v* values increase from 0.32 to 0.39 and 0.48 for LDPE 1, LDPE 2 and LDPE 3, respectively. Although the *v* values represent the averages of the bulk samples,

the LDPEs have components with different scaling exponents which implies complex branching architectures.

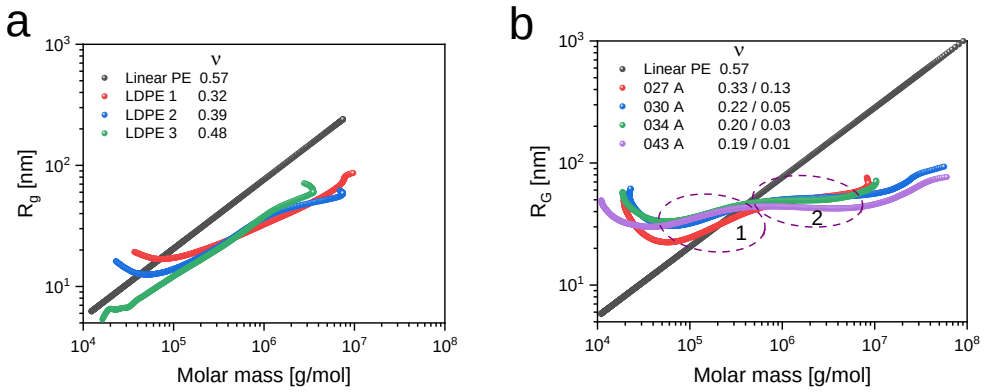

Figure 4.6 Conformation plots of LDPEs (a) and LCBPEs (b) obtained from HT-SEC-d4.

The conformation plots of LCBPEs show a rather distinct trend. The plots are divided into two molar mass segments as highlighted by the circular boxes labelled 1 and 2 for the low (1), and high (2) molar mass regions, see Fig. 4.6 b. At the low molar mass end of segment 1, *v* values are higher indicating less branching as compared to the higher molar mass fraction 2 that shows more branching. The conformation plots of the LCBPEs continuously deviate away from linearity as the molar mass increases (segment 2). LCBPEs clearly show the influence of LCB as seen in the deviation from the linear reference in the order 043 A > 034A > 030 A > 027 A.

More information about molar mass dependencies is given by Mark-Houwink-Sakurada (MHS) plots. Similar to R_g, intrinsic viscosity $[\eta]$ is related to molar mass by a power law:

$$[\eta] = K \cdot M^{\alpha} \tag{4.3}$$

$$[\eta] = 0.053 \cdot M^{0.703} \tag{4.4}$$

For linear macromolecules in a thermodynamically good solvent, the characteristic intercept *(K)* and the gradient (α) values of 0.053 and 0.703, respectively, were applied.[10]

The values of the exponent α depend on topological properties, e.g. 0 for a hard sphere, 0.3-0.5 for worm-like hyperbranched structures and 0.5 – 0.8 for random coils of linear macromolecules.[13] The MHS plots of the samples are presented in Fig. 4.7. The slopes and

intercepts of the curves depend on the branching density. Similar to the conformation plots, the MHS plots are divided into two molar mass segments as illustrated by the rectangular boxes labelled 1 and 2, corresponding to the low (1), and high 2) molar mass regions. For the LDPEs, in the low molar mass region (1) the plots show a linear relationship with a slope that is close to the linear reference mainly owing to the SCB structures in the resins.

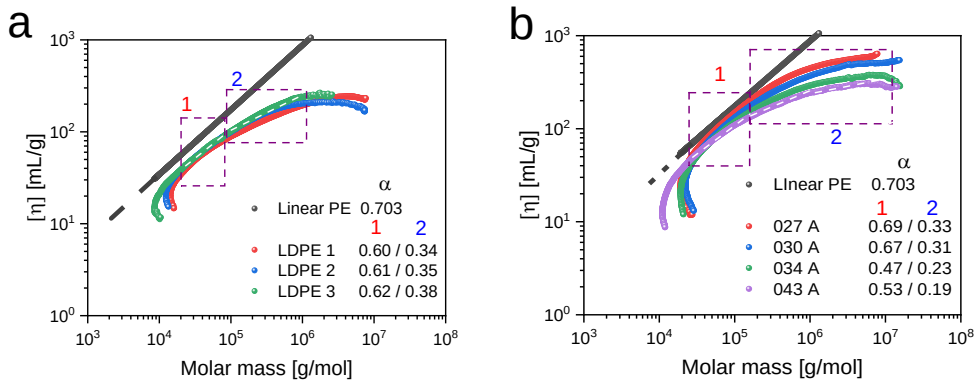

Figure 4.7 MHS plots of LDPEs (a) and LCBPEs (b) obtained from HT-SEC-d4. The values of α in the rectangle boxes are given in the bottom right of each figure.

The slopes decrease (segment 2) with increasing molar mass, showing relatively low slopes with α = 0.34, 0.35 and 0.38 for LDPE 1, LDPE 2 and LDPE 3, respectively. The slopes deviate from linear behaviour which is a clear indication of the contribution of LCBs. As mentioned before, these values reflect the influence of LCB on the hydrodynamic size. This behaviour is typical of LDPEs.[14] For the LDPEs, it is evident that LCB increases with molar mass as would be expected. The behaviour of the LCBPEs points to distinct structural differences compared to the LDPEs. The first segments of the curves in the lower mass range are very close to the linear plot. This indicates a very low degree of branching. If any, there might be small amounts of short chain branches which could not be detected by ^{13}C-NMR.

As the molar mass increases (segment 2), a strong deviation from linearity is observed which shows the presence of high LCB contents in the high molar mass region. The slopes of the MHS plots of LCBPEs at high molar mass decrease to α = 0.33, 0.31, 0.23 and 0.19 for 027 A, 030 A, 034 A and 043 A, respectively. This indicates a structural transition to high degrees of LCB and very “compact” molecular topologies.

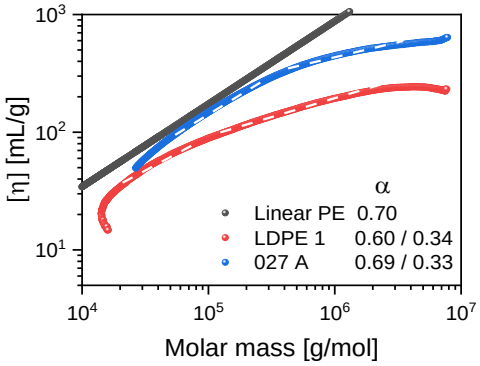

Figure 4.8 Comparison of MHS plots of LDPE 1 and 027 A obtained from HT-SEC-d4.

Fig. 4.8 shows a comparison of an LDPE and a LCBPE. The slope of LDPE is significantly lower in comparison to linear PE due to SCBs. The intrinsic viscosity of LCBPE at high molar mass region is lower than that of LDPE due to a high degree of LCB. At high molar mass range, the polymers have a further reduction of $[\eta]$ most likely due to intramolecular entanglement or interpenetration of the polymer chains.[13,15] Plots of both set of samples deviate from the linear relationship and scaling exponents shift towards smaller values, which indicates contraction of the coils in solution at high molar mass.[16] This contraction is a typical feature of LCB in polymer molecules. This is seen for all samples in the present study.

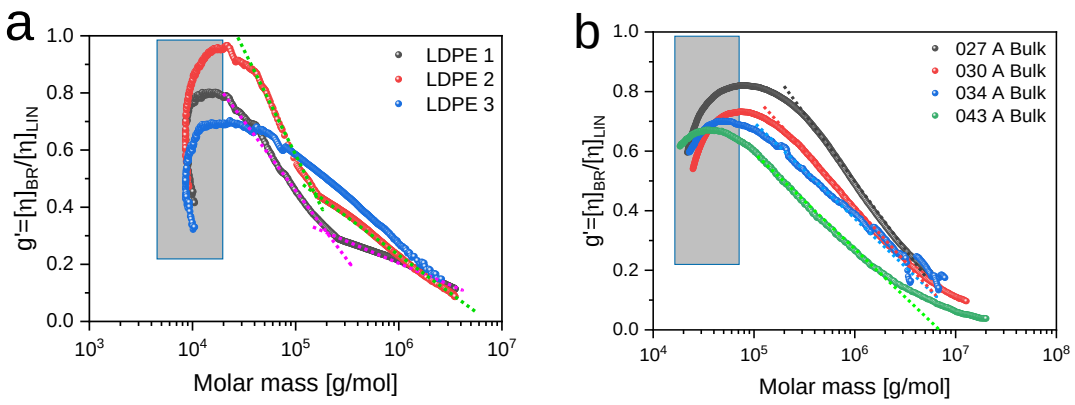

Figure 4.9 Molar mass dependences of the contraction factor *g'* of the bulk samples; LDPEs (a) and long chain branched PEs as obtained by HT-SEC-d4 (b). The shaded regions indicate molar mass ranges where the viscometer does not give reliable data. The dotted line in the figures show the slopes in the respective regions.

Further evaluation of branching was done by calculating the contraction factors as discussed in Section 2.3.3. Contraction factors quantify the size reduction of a branched molecule compared

to its linear analogue hence evaluating the branching density. The molar mass dependences of *g'* of all PE samples are given in Fig. 4.9. On both sets of samples, there is high error in the low molar mass region as indicated by a rectangular box due to the insensitivity of the detectors to low molar mass.[13]

The determined quantity of the level of branching centered on the concept of the contraction factor *g'* significantly confirms the dissimilar branching densities of the samples. The descending order of *g'* for LDPE 1 and LDPE 2 is similar, this could indicate similar branching behaviour. LDPE 3 displays a different branching behaviour at high molar mass regions as g' is greater than the other LDPEs. 027 A , 030 A and 043 A display a similar branching behaviour which is different from 034 A. Branching ratio determined at a given molar mass gives an average for all molecules having this molar mass.[17] However, the molecules may have different degrees of branching at the same molar mass, this is seen for 034 A at high molar mass regions.

Chain branching directly affects the polymer melt and viscosity properties in solution by promoting molecular entanglements and/or reducing the radii of gyration, this in turn modifies the flow characteristics and hence MFI.[18]

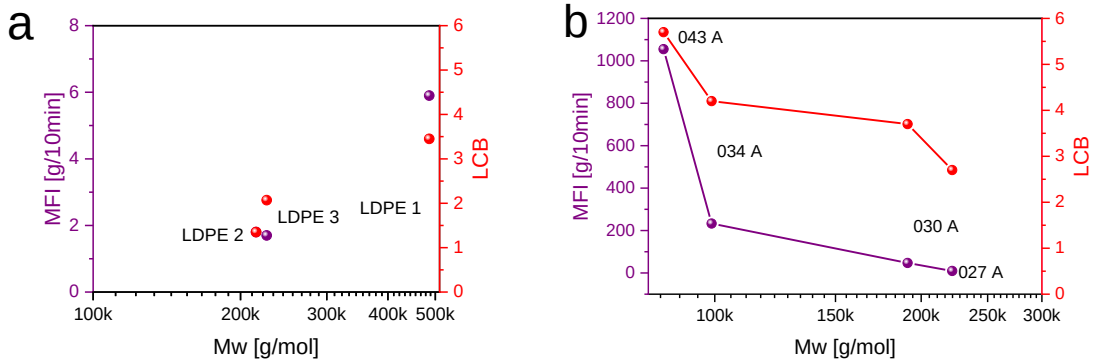

Figure 4.10 MFI as a function of molar mass for LDPEs (a) and LCBPEs (b). The right y-axis shows the correlation LCB content.

The leading effect of branching (SCB and LCB) is the decrease of the molecular size (R_g) and hydrodynamic volume due to the formation of more compact macromolecules.[18-20] In the present study, it is evident that LCBPEs are most affected as they only have LCB, this in turn reveals the effect these branches have on the structure and size of the molecules. To further elucidate this, the molar mass-melt flow index relationship was plotted to understand the effect

molar mass has on MFI of these resins (Fig. 4.10 a-b). Rodríguez-Hernández *et al.* found that for low density polymers, branching and polydispersity increase with molar mass.[18]

It has been found that more accurate predictions can be made by considering the effect of the whole MMD instead of average values like M_w.[21] LDPEs and LCBPEs in this regard show a trend (Fig. 4.10). The MFI of LDPEs increased with increase in molar mass whereas LCBPEs show a decrease in MFI with increase in molar mass (Fig. 4.10 b). This indicates that the number of LCBs in LDPEs is too low to have an impact on the MFI of the materials while SCBs may also impact the melt flow properties. For LCBPEs, MFI is dependent on the number of LCBs and molar mass.

Table 4.3 Summary of LDPEs and LCBPEs thermal properties.

	T_c[a] (°C)	T_c[b] (°C)	T_m[a] (°C)	ΔH_m[a] (J/g)	X_c[a,c] (%)
LDPE 1	90.7	55.8	107.8	123.5	42.2
LDPE 2	93.5	59.6	110.6	138.3	47.2
LDPE 3	95.6	62.5	112.6	143.0	48.8
027A	120.6	87.2	131.4	242.9	82.9
030A	120.1	87.0	130.7	252.1	86.0
034A	119.5	86.7	129.5	257.3	87.8
043 A	118.6	86.3	128.8	260.7	89.0

[a] as determined from DSC, [b] as determined from CRYSTAF

[c] $X_c = (\Delta H_m / \Delta H_{m\theta} \times 100\ \%)$, $\Delta H_{m\theta} = 293$ J/g.[22]

The thermal properties (Table 4.3) of polyolefins can provide insight and complementary information on the microstructure. DSC analyses of the bulk resins were conducted using the method described in Chapter 3 and the thermal behaviour of both sets of samples is illustrated in Figs. 4.11 and 4.12. The first heating cycle of the experiment was used to remove the thermal history of the polyethylene resins and therefore, not used for any quantitative or qualitative work. The LDPEs have low melting and crystallization temperatures (T_m and T_c, respectively) as well as crystallinities as can be seen in Fig. 4.11. This trend is expected due to the presence of short chain branches.

Branches bulkier than methyl groups cannot be integrated into the PE crystal lattice hence cannot be adequately undercooled and, therefore, will not crystallize. The presence of SCBs

interferes with the kinetics of crystallization and they have a stronger influence on the polymer crystallinity than molar mass.[23] LDPE 1 has the lowest crystallinity and the highest SCB content as it contains a high number of short branches as seen from ^{13}C-NMR. The contributions of SCB are more pronounced in these resins than those of LCBs. LCBs, due to their low concentration, seem to have little or no influence on the crystallinity of the LDPEs and the effect of molar mass on their thermal properties is not significant.

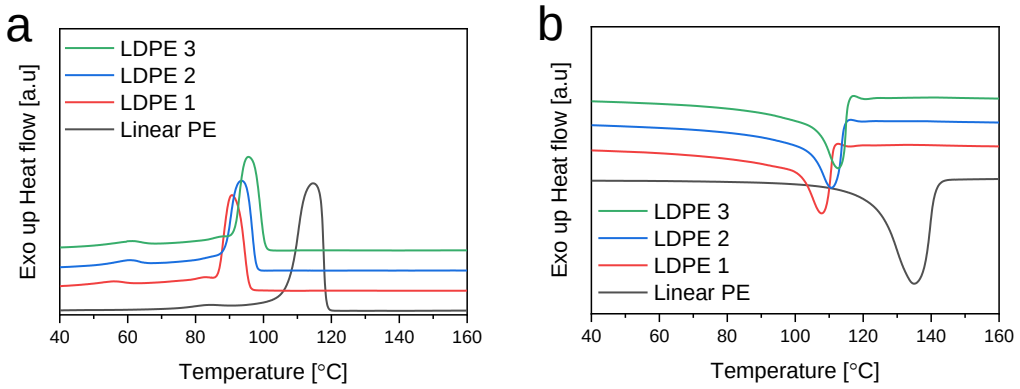

Figure 4.11 DSC 1st crystallization curves (a) and 2nd melting curves (b) of LDPE 1, 2, 3 and linear PE. The first heating cycle was used to erase the thermal history.

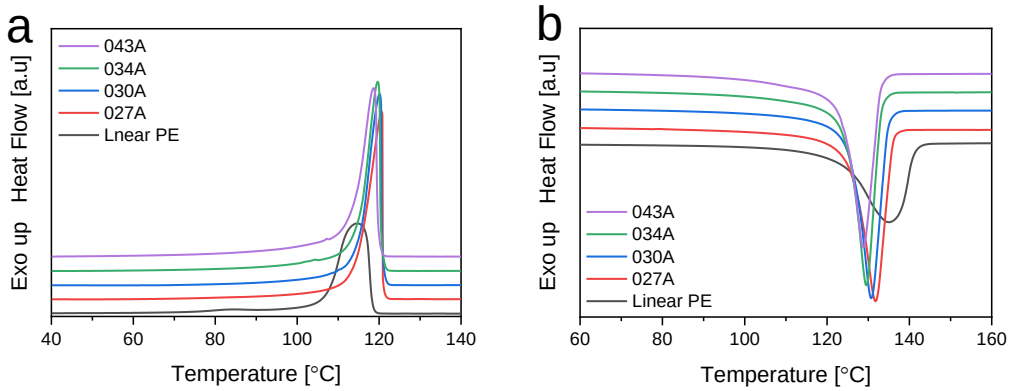

Figure 4.12 DSC 1st crystallization curves (a) and 2nd melting curves (b) of long chain branched polyethylenes and linear PE. The first heating cycle was used to erase the thermal history.

LCBPEs have higher T_m and T_c and the enthalpies are also higher as compared to the LDPEs, see Table 4.3 and Fig. 4.12. This indicates larger folded chain groups as compared to those in the LDPEs. It is easy to deduce the contributions of SCB since short branches do not fold into organised structures (lamella). LCBPEs show increased crystallinity (X_c) with an increase in

LCB, i.e., from 027 A to 043 A. Although T_m and T_c decrease with increasing LCB, the changes are rather small. The trends in T_m, T_c and X_c are summarised in Table 4.3 and Fig. 4.13.

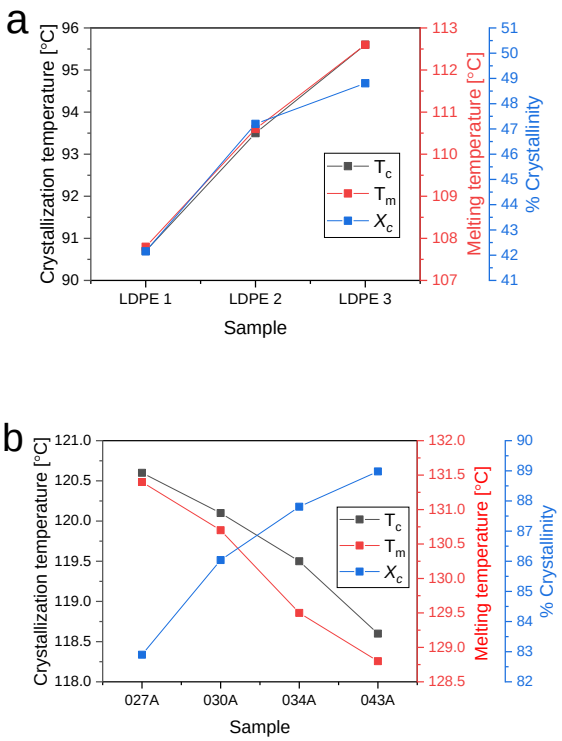

Figure 4.13 Plots showing the 1st crystallization temperature (T_c), 2nd melting temperature (T_m) and calculated crystallinity (X_c) for LDPE (a) and long chain branched polyethylene (b).

It can be noted from Figs. 4.13 a and 4.13 b that there is a direct relationship between T_c, T_m and X_c of the LDPEs whereas an inverse relationship is observed for LCBPEs. It must be noted that the figures only illustrate the samples' relationships to the mentioned physical properties also presented in Table 4.3. This is due to the presence of both SCB and LCB in LDPEs but contributions of LCB in LCBPEs can be evaluated. ^{13}C-NMR spectroscopy is considered to be a method useful for LCB determination in polyethylene. However, the technique is not useful in distinguishing between the LCBs as it is with SCBs although some of the branches can be quantified.

Here, we will assume that the LCBs are quite long as also deduced from HT-SEC-d4 where significant influences on [η] were observed. It is logical to assume that these long chain branches form small crystallites which have less errors than a longer unbranched chain would.

It is well known that the melting temperature of a polyethylene is less influenced by molar masses above ~ 10 kg/mol. Work by Parvez and coworkers[24] also studied polyethylenes with ~0.6 – 1.1 LCB branches although their samples did not exclusively have LCB like in the case of the LCBPEs used in the present study. Fig. 4.14 attempts to illustrate LCB side chain crystallization which leads to smaller lamella with higher crystallinity. The resultant decrease in T_m may not be significant if the LCB branches are long.

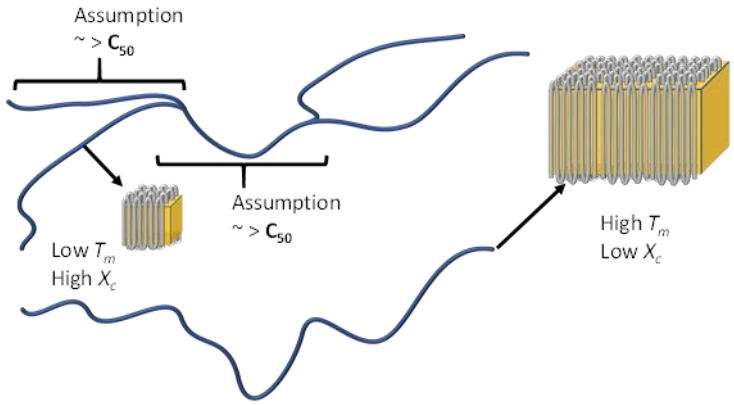

Figure 4.14 Relationship between chain branch length and lamella size.

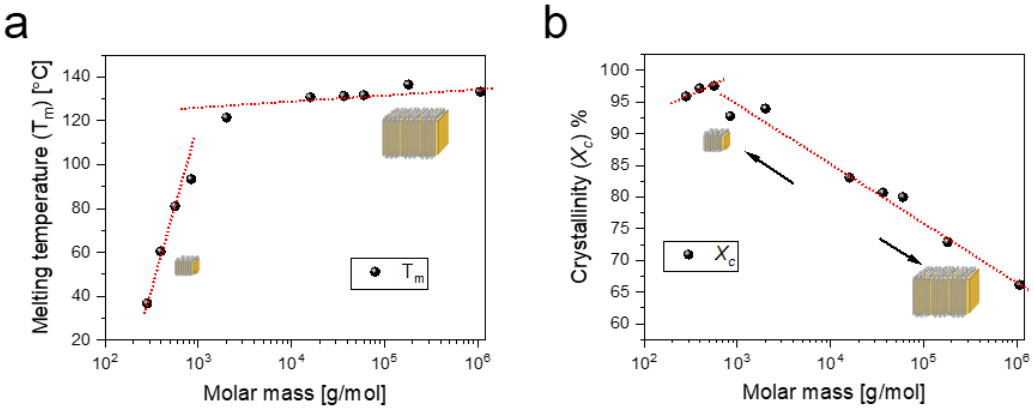

Figure 4.15 Melting temperature, T_m (a) and crystallinity, X_c (b) of narrowly distributed linear PE standards as a function of molar mass. The dotted red lines indicate the respective trends.

To understand the contributions of chain length to T_m and X_c, ten linear PE standards with varying molar masses were analysed using DSC. Fig.4.15 shows the relationship between molar mass and crystallinity plots. The initial increase in T_m seen in Fig. 4.15a is attributed to an increase in the lamella thickness as the molar mass increases. Consequently, more energy is required to break the forces holding the chains together. For high molar mass PEs, the increase

is not significant most probably due to the formation of more lamella after a critical size is reached. Furthermore, larger lamella are much more prone to errors in arrangement within their structures leading to a decrease in the crystallinity as shown in Fig. 4.15b. Chain entanglement in the linear macromolecule can result in lower T_c in comparison to its long chain branched counterpart of the same M_w and therefore the disentanglement of a branched polymer is easier compared to a linear polymer under the same conditions.[25]

DSC suffers from two challenges: (1) Some polyethylene fractions can be amorphous and do not show peaks, (2) pronounced co-crystallization and chain entanglement always complicates the fractionation of multiple component polyolefins. Contributions of molar mass are also challenging to pinpoint in DSC. To overcome these two key challenges, solution-based techniques have been developed where chain entanglement is not pronounced as in CRYSTAF.

4.3 Chemical composition distribution analyses

The branched PEs were further analysed by crystallization analysis fractionation (CRYSTAF) to understand their crystallization behaviour in solution. As shown in Fig. 4.16 a, the crystallization behaviour of LDPE in solution is mainly influenced by SCBs which vary amongst the resins.

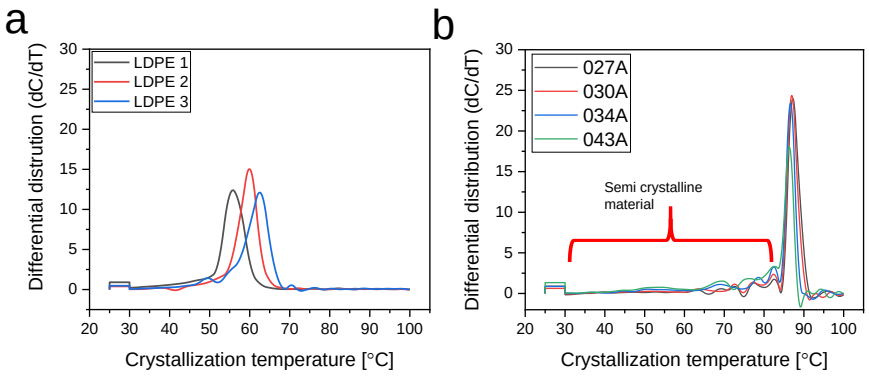

Figure 4.16 CRYSTAF crystallization curves of LDPEs (a) and LCBPEs (b) obtained from a TCB solution.

It was observed that the crystallization properties of LCBPEs are also influenced by molar mass (Fig 4.16 b). As the molar masses of the samples increase, their melting and crystallization temperatures increase. In solution, the differences in the crystallization temperatures are rather small. Very small quantities of soluble material and semi-crystalline material are seen for the LCBPE samples. The amount of semi-crystalline material appears to increase as the molar mass

decreases. However, this is not very significant, see Fig. 4.16 b. The melting and crystallization temperatures obtained from DSC as well as those from CRYSTAF show a dependence on molar mass and branching for LCBPEs as seen in Figs. 4.17.

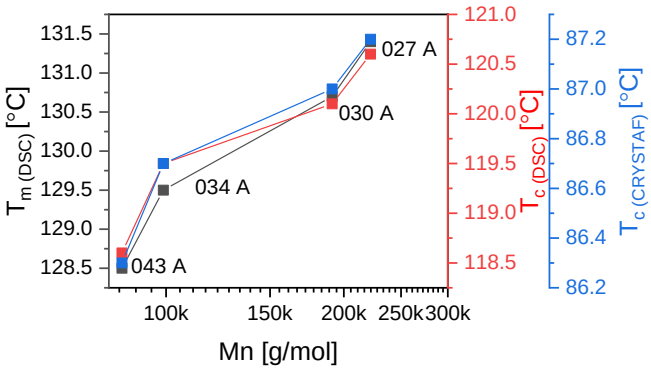

Figure 4.17 DSC melting and crystallization temperature ($T_{m\ DSC}$, $T_{c\ DSC}$), respectively, and CRYSTAF crystallization temperature ($T_{c\ CRYSTAF}$) as a function of sample peak molar mass for LCBPEs.

High temperature interaction chromatography (HT-IC) offers an alternative mechanism of separation. Here, unique stationary phases allow for adsorption/desorption and crystallization/redissolution interactions of analytes in the presence of a mobile phase flow. HT-IC typically uses porous graphitic carbon (PGC) marketed under the trade name Hypercarb®, a unique stationary phase for the separation of polyolefins. HT-IC applications for polyolefins by using solvent gradient techniques have been reviewed in recent puplications.[26-28] The packing structure of the material in Hypercarb® is known to be composed of hexagonally arranged flat sheets of carbon atoms with no micropores.[29] The principles of interaction of nonpolar molecules (polyethylenes) on these flat graphene structures are governed by van der Waals forces. The interaction strength depends on the available contact surface area (methylene sequence length) the molecules interact with the adsorbent surface.

To achieve separation, solvent or temperature gradients (SGIC and TGIC), respectively, can be used as modes of HT-IC to control the adsorption.[30] HT-SGIC was used to analyse both sets of samples. Fig. 4.18 shows the elution behaviour of the LDPEs using a linear gradient from 100 % 1-dodecanol to 100 % TCB applying a shallow 30-minute gradient for better separation (*1-dodecanol→TCB*$_{30\ min}$).

A PGC column length of 300 mm was used for all experiments. A linear PE with a molar mass of 73 kg/mol was used as a reference. All three LDPEs elute in a multimodal manner below 13.0 mL with a smaller early eluting peak (labelled 1) and a larger later eluting peak (labelled 2). The linear reference elutes between 13.0 and 14.0 mL. The distinct multimodal elution patterns obtained indicate that the separation is influenced by molar mass and/or branching heterogeneity. The first eluting peak can be designated to SCB-rich components while the late eluting peak is assigned to fractions with low branching contents. This implies that the LDPEs have very little to no linear non-branched components that would behave like the PE reference. The multimodal elution pattern implies heterogeneity in the branching distribution or molar mass influences. As expected, the LDPEs elute in the order of decreasing SCB content: LDPE 1→LDPE 2→LDPE 3 with total branching of 14.2, 11.7 and 8.1 per 1000C, respectively.

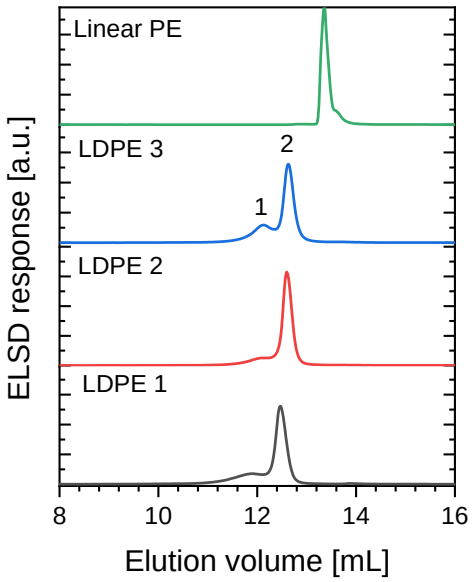

Figure 4.18 Elugrams of the LDPEs obtained by HT-SGIC using a 1-dodecanol→TCB_{30min} solvent gradient with PGC (Hypercarb® 300 × 4.6 mm^2) as the stationary phase at 160 °C. The ELSD was used as the detector with the following conditions: nebuliser = 160 °C; evaporator = 270 °C; high grade nitrogen gas flow = 1.5 L/min.

Similar analyses of the LCBPEs are shown in Fig. 4.19. Here, the PEs elute in broad multimodal peaks, which are in the same region as the linear PE reference. For sample 027 A, peak 2 is the largest, while peaks 1 and 3 are rather small. As the LCB increases, peaks 1 and 3 increase in relative area.

The increase in peak 1 can be due to an increase in low molar mass components while an increase in peak 3 might be due to an increase in long chain branched chains. At long chain lengths, long branches are expected to contribute to stronger retention of PE assuming that the PE macromolecule is fully extended on the PGC surface. All these events are at the expense of peak 2, which can be linear PE. Since 027 A has the lowest LCB, it has the longest undisturbed linear backbone and, accordingly, its elution behaviour resembles the linear reference. Peak 1 can be attributed to low molar mass components that result in weaker interactions.

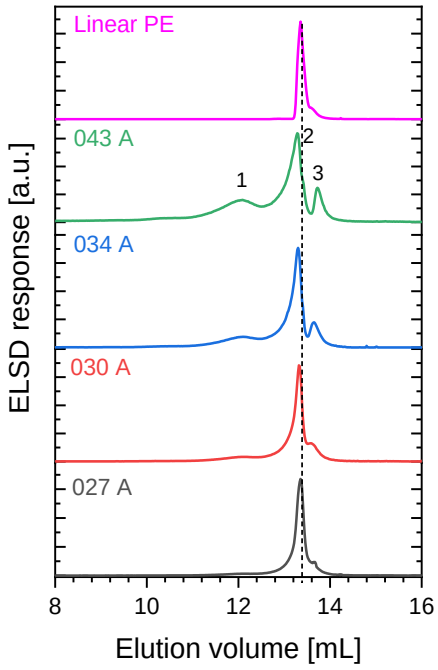

Figure 4.19 Elugrams of LCBPEs obtained from SGIC using a 1-dodecanol→TCB_{30min} solvent gradient with PGC (Hypercarb® 300 × 4.6 mm^2) as the stationary phase at 160 °C.

To further understand the structural behaviour of these resins, HT-TGIC was employed. Separate sets of experiments were used to identify the best one. In the first set, the three LDPEs were analysed using PGC as the stationary phase and ODCB as the mobile phase; the elugrams are shown in Fig. 4.20 a. The eluting peaks of all samples were broad i.e., from ~ 12.0 mL to 20.0 mL. Small differences in the elution behaviour are apparent e.g., the marginal increase in the peak elution volumes of the LDPEs from LDPE 1 – LDPE 3. Interactive forces result in high peak elution volumes when PGC is used although the Hypercarb column length is shorter than the silica one that is used in Fig. 4.20 b. The interactive force on PGC is stronger and may perform well under SGIC conditions rather than TGIC. In TGIC, the crystallization and

redissolution processes coupled with a dynamic mobile phase flow allow for the distinction of differently branched samples.

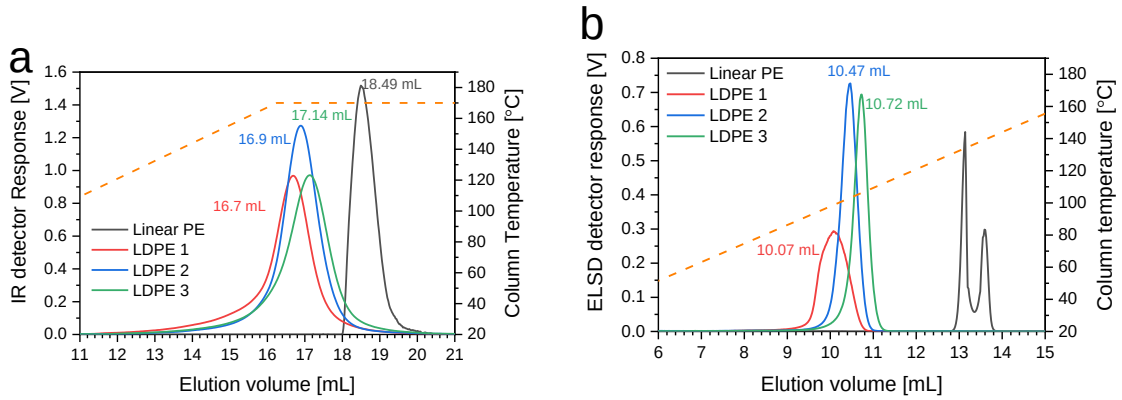

Figure 4.20 TGIC elugrams of the LDPEs on 100 × 4.6 mm^2 PGC in comparison to a linear PE standard (a) and 250 × 4.6 mm^2 silica (b). Similar temperature profiles and mobile phase flow were used for both sets of experiments. The IR detector was used with PGC and the ELSD with the silica stationary phase. ODCB was used as the mobile phase.

In another set of experiments, silica was employed as the stationary phase with the knowledge that it is a non-adsorptive stationary phase. In the past, silica and other weakly adsorbing stationary phases have been tried with solvent gradient methods for the separation of polyethylene and polypropylene blends.[31] Macko *et al*. have shown that modified silica gel is a stable stationary phase for high-temperature separations.[32] Fig. 4.20 b shows the elution behaviour of the three LDPEs on silica with ODCB as the mobile phase. The elution order also corresponds to that revealed by findings in DSC, see earlier discussion. The linear PE standard elutes in a bimodal behaviour when silica is used as the stationary phase. Such behaviour has not been reported in literature yet.

The LCBPEs were analysed using similar techniques, the results are illustrated in Fig. 4.21. A linear PE was also used as a reference. From Fig. 4.21 a, it can be observed that on Hypercarb, linear PE and the LCBPEs have the same elution volume which is an indication of similar adsorption and desorption behaviour. However, the tailing of the LCBPEs is more pronounced as LCB content increases. When silica is used (Fig. 21 b), the samples have broad elution profiles that reflect the increasingly complex compositions. Four broad elution peaks can be identified, with an elution behaviour that slightly differs from HT-SGIC. An expanded plot is shown in Fig. 4.21 c. Peak 1 and 2 can be tentatively assigned to material with low molar mass that increases as the overall molar mass of the sample decreases. Peak 3 can be assigned to

linear PE and peak 4 to PE chains with LCB. Linear PE forms larger crystallites which require slightly higher temperature to redissolve and elute as compared to peaks 1 and 2. On the other hand, we speculate that LCB may contribute to the formation of more compact crystallites upon crystallization from solution. Long chain branches can crystallise on their own allowing for compact and differently oriented crystallites. Crystal structure analyses of these fractions is recommended for future work. In addition, the increase in the peak area appears to be inversely proportional to the area of peak 4, which contrasts HT-SGIC findings.

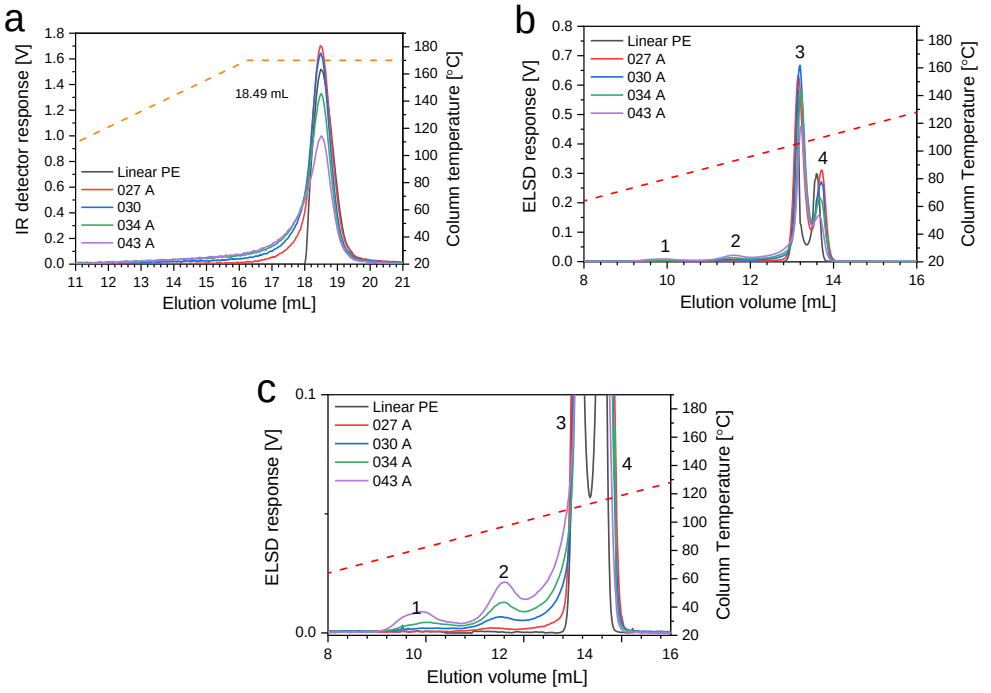

Figure 4.21 TGIC elugrams of LCBPEs on 100 × 4.6 mm^2 PGC (a), 250 × 4.6 mm^2 silica (b) and expanded plot of b (c)Similar temperature profiles and mobile phase flow were used for both sets of experiments. The IR detector was used with PGC and the ELSD with the silica stationary phase. ODCB was used as the mobile phase.

The strength of the interaction of molecules increases with increasing methylene sequence length. The behaviour observed for linear PE and LCBPEs indicates that the attractive interactions between the stationary phase and the samples depend on the type of column packing and on the mobile phase.[33] The bimodality of linear PE could have been due to the solvent used, different fractions with high molar mass and flow rate. Therefore, this behaviour of linear PE could not be seen in the conformation plots and there is no literature reporting this yet.

Fractionation of the bulk samples can help concentrate the smaller components for analyses with other techniques, e.g., DSC or FTIR. This can be achieved by collecting the eluent and drying the fractions. Furthermore, preparative fractionation using established methods such as molar mass fractionation can yield larger quantities of fractions for a comprehensive analysis protocol. Coupling of the 1D analytical protocols discussed thus far with fast HT-SEC in HT-2D-LC will confirm the relative molar masses of the fractions.

4.4 HT-2D-LC analysis

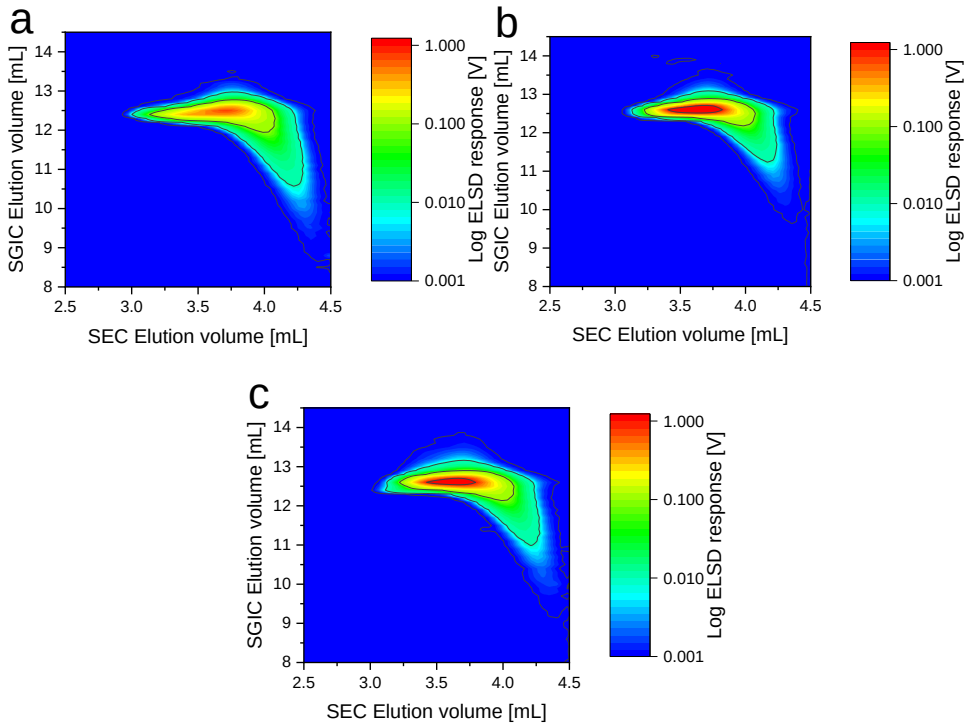

Figure 4.22 SGIC×SEC contour plots of LDPE 1(a), LDPE 2 (b) and LDPE 3 (c) obtained with a 300 × 4.6 mm PGC column in the 1st dimension and a 100 × 7.5 mm PL Rapide column in the 2nd dimension. A 1-dodecanol→TCB $_{300min}$ gradient was used in the 1st dimension at a flow rate of 0.05 mL. ODCB was used in the 2nd dimension at a flow rate of 2.75 mL/min.

To gain more information on the dependence of chemical composition (CC) on molar mass (MM), HT-2D-LC was carried out on all the bulk samples. The 1st dimension separates polyolefins according to their chemical composition, and the 2nd dimension distinguishes polyolefins regarding their molar mass.

HT-SGIC was coupled to HT-SEC and the contour plots are shown in Figs. 4.22 a – 4.22 c for LDPE 1-LDPE 3, respectively, and Figs. 4.23 a – 4.23 d for samples 027 A – 043 A

respectively. It is evident that the low molar mass tailing increases in a similar manner as observed in 1D analyses.

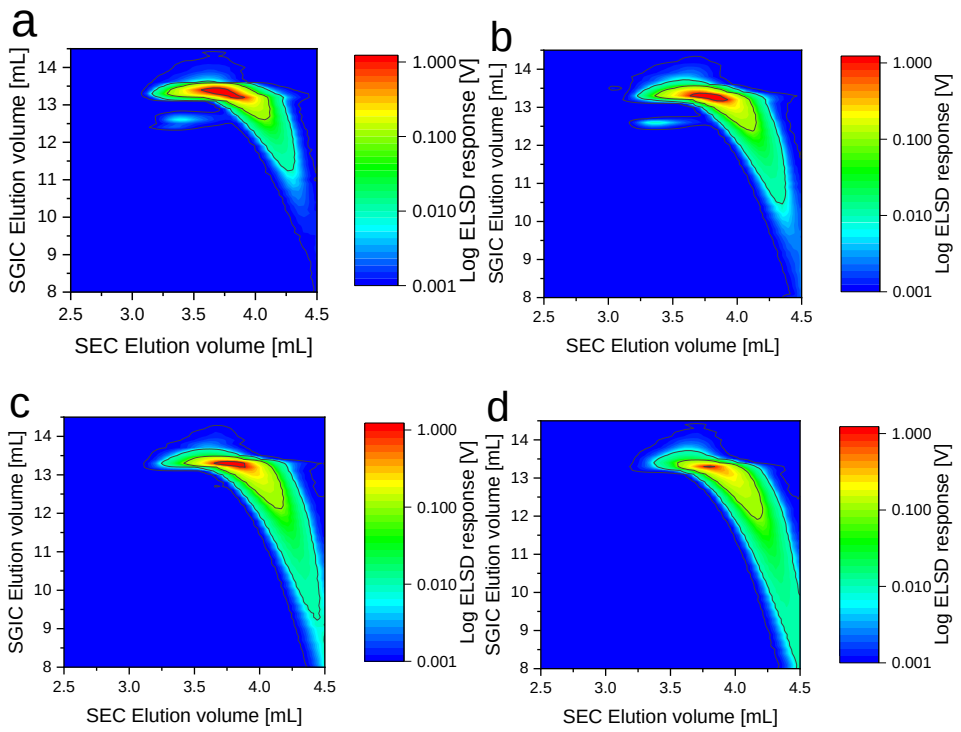

Figure 4.23 SGIC×SEC contour plots of long chain branched PEs 027 A (a), 030 A (b), 034 A (c) and 043 A (d) obtained with a 300 × 4.6 mm PGC column in the 1st dimension and a 100 × 7.5 mm PL Rapide column in the 2nd dimension. A 1-dodecanol→TCB $_{300min}$ gradient was used in the 1st dimension at a flow rate of 0.05 mL. ODCB was used in the 2nd dimension at a flow rate of 2.75 mL/min.

It was observed that the separation of the 1st dimension in the 2D analyses is not as efficient at low flow rates that are used i.e., 0.05 mL/min vs 0.5 mL/min in the 1D analyses. Probably when desorption takes place, linear and long chain branched chains mix, decreasing the resolution. This challenge is also observed with other PE materials.[34] The limits for 2nd dimension in the plots was set to cut at 4.5 mL to exclude the solvent detection as gradient increases.

To solve this challenge, TGIC was used in the 1st dimension as previously discussed. It was thought that at low flow rates and an adsorptive force in the 1st dimension perhaps using a non-interactive stationary phase can enable the undisturbed crystallization and redissolution of the PE chains. Contour plots of the LDPEs and a linear PE reference are shown in Figs. 4.24. The samples show interesting multimodal elution patterns which are also seen in the 1D analyses.

Unlike with SGIC in the 1st dimension, the resolution was preserved in the 2D analyses despite low flow rate.

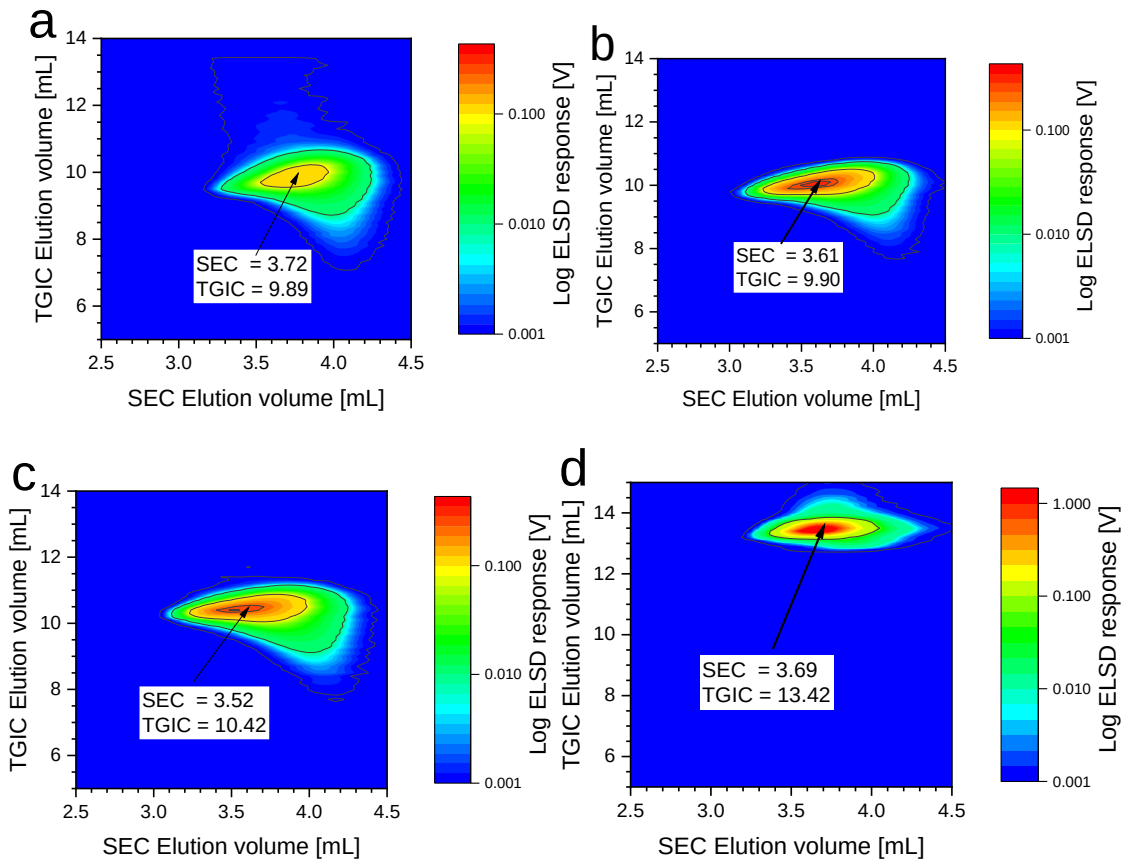

Figure 4.24 TGIC×SEC contour plots of LDPE 1 (a), LDPE 2 (b) LDPE 3 (c) and Linear PE (d) obtained with a 250 × 4.6 mm silica column in the 1st dimension and a 100 × 7.5 mm PL Rapide column in the 2nd dimension. A 0.4 °C/min temperature gradient was used in the 1st dimension with a ODCB flow rate of 0.05 mL. ODCB was also used in the 2nd dimension at a flow rate of 2.75 mL/min.

For the LDPEs, a higher molar mass component is seen which elutes earlier. The intensity of this component decreases from LDPE 1 to LDPE 3, respectively, as branching also decreases. For LCBPEs the peak eluting at 13.1 mL was assigned to the linear PE component within the samples. This peak increases as seen in the contour plots which corresponds to the increase in the LCB branches. The tailing observed in the low molar mass region at ~ 4.5 mL in the SEC dimension increases with a decrease in the molar mass of the samples.

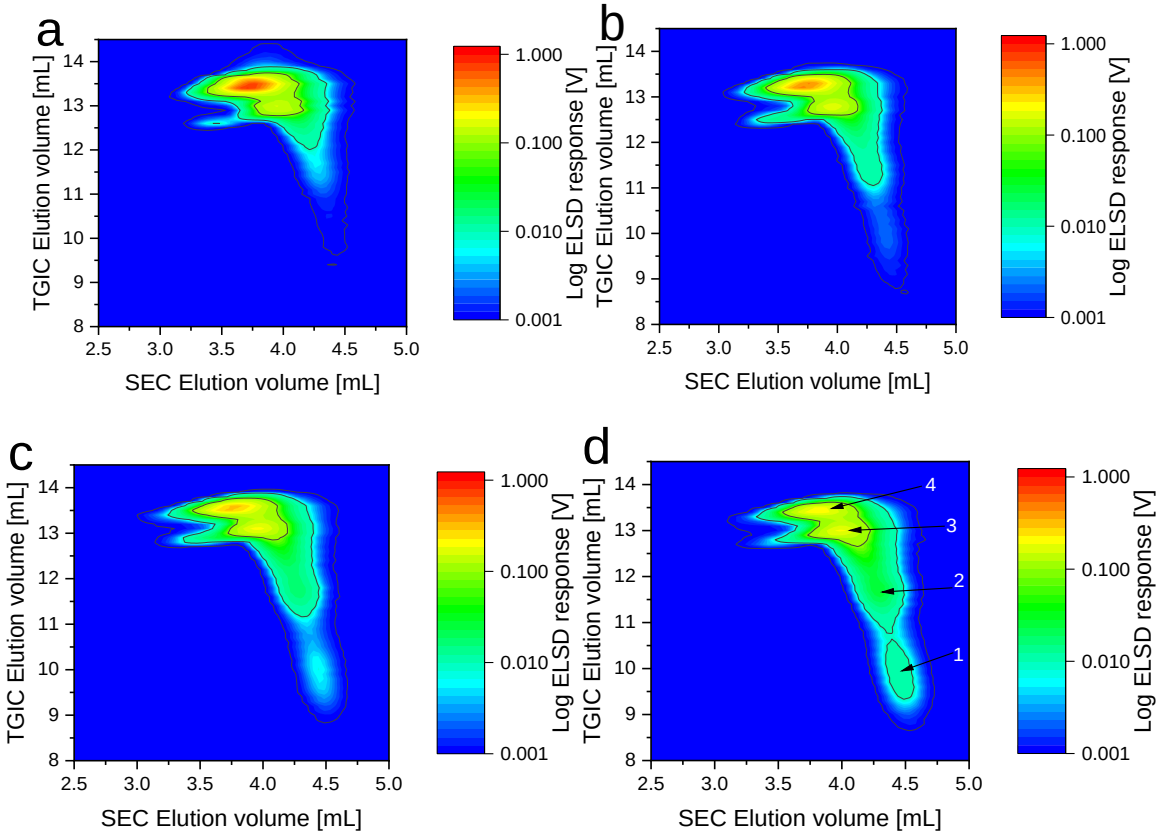

Figure 4.25 TGIC×SEC contour plots of long chain branched PEs 027 A (a), 030 A (b) 034 A (c) and 043 A (d) obtained with a 250 × 4.6 mm silica column in the 1st dimension and a 100 × 7.5 mm PL Rapide column in the 2nd dimension. A 0.4 °C/min temperature gradient was used in the 1st dimension with a ODCB flow rate of 0.05 mL. ODCB was also used in the 2nd dimension at a flow rate of 2.75 mL/min.

The 2D separation of the LCBPEs reveals their molar mass and chemical composition dependence as shown in Fig. 4.25. These resins contain components that are highly retained in the 1st dimension compared to the LDPEs indicating macromolecules with rather long undisturbed ethylene sequences. The amount of the early eluting fractions (labelled as 1 from Fig. 4.25 d) in the 1st dimension increases from (a) to (d), i.e., from low to high LCB which also correlates to decrease in molar mass. The samples eluted in two main fractions which showed bimodality seen in the 1st dimension. Their quantities somehow increase with decrease in molar mass and increase in branching. Long branches in polyethylene form much more organized crystallites that somehow behave like linear chains. The HT-2D-LC findings show the influence of MM and branching on the elution behaviour of these resins.

Sample 043 A shows more interesting results as already indicated from Figs. 4.25 d. Four peaks can be identified in the contour plot. The retention of these peaks is dependent on molar mass

and the pronounced tailing is due to increase in long chain branching. Peaks 1 and 2 can be assigned long chain branched low molar mass components which are retained to a lower extent in the 1st dimension and longer in the 2nd dimension. Peak 3 can be assigned to PE chains with LCB as the intensity of this peak increases from 027 A to 043 A (Figs. 4.25 a-d). Peak 4 can be assigned to linear PE as it is comparable to the behaviour of linear PE observed in Fig 4.24d.

4.6 Conclusions

In the present chapter, two sets of polyethylene have been analyzed using various advanced analytical techniques. The first set comprises three low density polyethylenes (LDPE) and the second set comprised laboratory-synthesized polyethylenes with long chain branching (LCBPE).

The analysis of the LDPE samples with spectroscopic methods revealed that their average chemical compositions comprise complex branching structures and low crystallinity. High resolution ^{13}C-NMR enabled the identification and quantification of the diverse branches such as methyl, ethyl, butyl, amyl and long chain branches (LCB). LDPE 1 was found to have the highest amount of short chain branches (SCB) and LDPE 2 and 3 differed in the LCB contents, with LDPE 3 having more LCBs. On the other hand, LCBPEs showed high crystallinity from FTIR, while ^{13}C-NMR confirmed the absence of SCBs and presence of LCB. However, the length of the LCBs cannot be revealed using ^{13}C-NMR. Differences in crystallinity seen by FTIR analyses were confirmed by the calculated enthalpies in DSC for the respective samples.

A quadruple HT-SEC system was used to study the behaviour of the resins in solution. LDPEs were observed to have both SCB and LCB as the conformation and Mark-Houwink-Sakurada (MHS) plots showed a typical deviation from linear PE behaviour. LCBPEs had high LCB densities in the high molar mass range, which confirmed an increase in LCB with molar mass. In the low molar mass range, the plots resembled the behaviour of linear PE. Similarly, contraction factors (g') were below 1. Again, ^{13}C-NMR showed increasing LCB contents with an increase in crystallinity for the LCBPEs. It was observed that LCBPEs had mostly LCBs compared to the LDPEs, which had more SCBs than LCBs. Therefore, in the presence of SCBs, LCBs do not significantly alter PE crystallinity but can significantly increase crystallinity at the expense of melting and crystallization temperature (T_m and T_c, respectively).

Chemical composition analyses in the presence and absence of a stationary phase were utilized for chemical composition distribution analyses (CCD). Crystallization analyses fractionation (CRYSTAF) revealed evident differences between the three LDPEs, which was in agreement with DSC analyses. LCBPEs, on the other hand, had narrow high crystalline peaks. The lack of semi-crystalline and soluble material was attributed to the lack of SCBs. Interaction chromatography at high temperature (HT-IC) analyses were conducted using HT-SGIC firstly and then HT-TGIC.

In HT-SGIC, two distinct fractions were observed to elute for LDPEs; the first fraction (low eluting peak) was assigned to low molar mass highly branched material while the second (late eluting peak) was assigned to low SCB content material. Here, the contributions of LCB to retention were obscured by the presence of SCBs. LCBPEs produced three eluting peaks; the third eluting peak had a retention volume (V_r) similar to PE homopolymer, indicating a long undisturbed ethylene sequence. The low eluting peaks were assigned to low molar masses of LCBPE with decreased interaction with the porous graphitic carbon (PGC) stationary phase. HT-TGIC on PGC did not show significant differences between the three LDPE samples and produced broad elugrams, therefore, non-interactive stationary phase silica was used. Distinct elution behaviours of the three LDPE samples were observed. In addition, several peaks could also be resolved and assigned to different LCB contents for the LCBPEs. HT-2D-LC was ultimately utilized to confirm the molar masses of eluting components of the samples; molar mass plays a role in elution behaviour of LDPEs and LCBPEs. LCB influences elution in both HT-SGIC and HT-TGIC.

Melt flow index (MFI) measurements were conducted on all samples, and it was observed that LCB and molar mass influence the flow behaviour of the resin. The presence of LCBs has two effects: (1) it allows for the formation of smaller compact crystallites/spherulites which have low viscosities in the melt, and (2) LCB increases crystallinity but at the expense of melt temperature, which improves processing while maintaining other important physical attributes. Mechanical strength and Young's moduli of the LDPE samples could be linked to crystallinity and total branching differences. The contributions of SCB overshadow those of LCB but when SCB is comparable, more LCBs result in higher tensile strength.

To understand the microstructure of the samples in great detail, appropriate fractionation tools shall be applied to narrow down the molar mass or chemical composition distributions.

Subsequent analyses of the fractions shall be conducted with regard to molar mass and branching.

4.7 References

(1) Zhang, Q.; Chen, P.; Xie, X.; Cao, X. *J. Appl. Polym. Sci.* **2009**, *113*, 3027–3032.

(2) Gulmine, J. V.; Akcelrud, L. *Polym. Test.* **2006**, *25*, 932–942.

(3) Gulmine, J. V.; Janissek, P. R.; Heise, H. M.; Akcelrud, L. *Polym. Test.* **2002**, *21*, 557–563.

(4) DesLauriers, P. J.; Rohlfing, D. C.; Hsieh, E. T. *Polymer* **2002**, *43*, 159–170.

(5) Xue, Y.-H.; Bo, S.-Q.; Ji, X.-L. *Chin. J. Polym. Sci.* **2015**, *33*, 508–522.

(6) Eselem Bungu, P.; Pasch, H. *Polym. Chem.* **2017**, *31*, 4565–4575.

(7) Hay, J.; Mills, P.; Ognjanovic, R. *Polymer* **1986**, *27*, 677–680.

(8) Usami, T.; Takayama, S. *Macromolecules* **1984**, *17*, 1756–1761.

(9) Yan, D.; Wang, W.-J.; Zhu, S. *Polymer* **1999**, *40*, 1737–1744.

(10) Wang, W.-J.; Kharchenko, S.; Migler, K.; Zhu, S. *Polymer* **2004**, *45*, 6495–6505.

(11) Plüschke, L.; Ndiripo, A.; Mundil, R.; Merna, J.; Pasch, H.; Lederer, A. *Macromolecules* **2020**, *53*, 3765–3777.

(12) Boye, S.; Komber, H.; Friedel, P.; Lederer, A. *Polymer* **2010**, *51*, 4110–4120.

(13) Plüschke, L.; Mundil, R.; Sokolohorskyj, A.; Merna, J.; Sommer, J.-U.; Lederer, A. *Anal. Chem.* **2018**, *90*, 6178–6186.

(14) Bungu, P. E.; Pasch, H. *Polym. Chem.* **2018**, *9*, 1116–1131.

(15) Lu, W.; Mays, J. In *Molecular Characterization of Polymers*; Elsevier: Amsterdam, 2021, pp 281–304.

(16) Xue, Y.; Bo, S.; Ji, X. *J. Polym. Res.* **2015**, *22*, 160.

(17) Podzimek, S. In *Light Scattering, Size Exclusion Chromatography and Asymmetric Flow Field Flow Fractionation: Powerful Tools for the Characterization of Polymers, Proteins and Nanoparticles*; John Wiley & Sons: New Jersey, 2011, pp 99–206.

(18) Teresa Rodríguez-Hernández, M.; Angulo-Sánchez, J.; Pérez-Chantaco, A. *J. Appl. Polym. Sci.* **2007**, *104*, 1572–1578.

(19) Brun, Y.; Gorenstein, M.; Hay, N. *J. Liq. Chrom. & Rel. Technol.* **2000**, *23*, 2615–2639.

(20) Bueche, F. *J. Chem. Phys.* **1964**, *40*, 484–487.

(21) Zahedi, M.; Ahmadi, M.; Nekoomanesh, M. *J. Appl. Polym. Sci.* **2008**, *108*, 3565–3571.

(22) Mirabella, F. M.; Bafna, A. *J. Polym. Sci., Part B: Polym. Phys.* **2002**, *40*, 1637–1643.

(23) Krishnaswamy, R. K.; Yang, Q.; Fernandez-Ballester, L.; Kornfield, J. A. *Macromolecules* **2008**, *41*, 1693–1704.

(24) Parvez, M.; Rahaman, M.; Soares, J.; Hussein, I.; Suleiman, M. *Polym. Sci. Ser. B* **2014**, *56*, 707–720.

(25) Dartora, P. C.; Santana, R. M. C.; Moreira, A. C. F. *Polímeros* **2015**, *25*, 531–539.

(26) Macko, T.; Brüll, R.; Zhu, Y.; Wang, Y. *J. Sep. Sci.* **2010**, *33*, 3446–3454.

(27) Meunier, D. M.; Wade, J. H.; Janco, M.; Cong, R.; Gao, W.; Li, Y.; Mekap, D.; Wang, G. *Anal. Chem.* **2020**, *93*, 273–294.

(28) Kot, D.; Macko, T.; Arndt, J.-H.; Brüll, R. *J. Chromatogr. A* **2019**, *1606*, 360038.

(29) Monrabal, B.; Mayo, N.; Cong, R. *Macromol. Symp.* **2012**, *312*, 115–129.

(30) Prabhu, K.; Brüll, R.; Macko, T.; Remerie, K.; Tacx, J.; Garg, P.; Ginzburg, A. *J. Chromatogr. A* **2015**, *1419*, 67–80.

(31) Heinz, L.-C.; Pasch, H. *Polymer* **2005**, *46*, 12040–12045.

(32) Macko, T.; Pasch, H.; Kazakevich, Y.; Fadeev, A. *J. Chromatogr. A* **2003**, *988*, 69–76.

(33) Macko, T.; Pasch, H.; Milonjic, S.; Hiller, W. *Chromatographia* **2006**, *64*, 183–190.

(34) Sigwinta, M.; Ndiripo, A.; Wewers, F.; Pasch, H. *Polym. Int.* **2020**, *69*, 291–300.

Chapter 5 : Results and discussion

Preparative molar mass fractionation (p-MMF) of bulk resins and analysis of p-MMF fractions

The present chapter discusses the preparative molar mass fractionation of the two sets of branched polyethylenes using advanced analytical techniques.

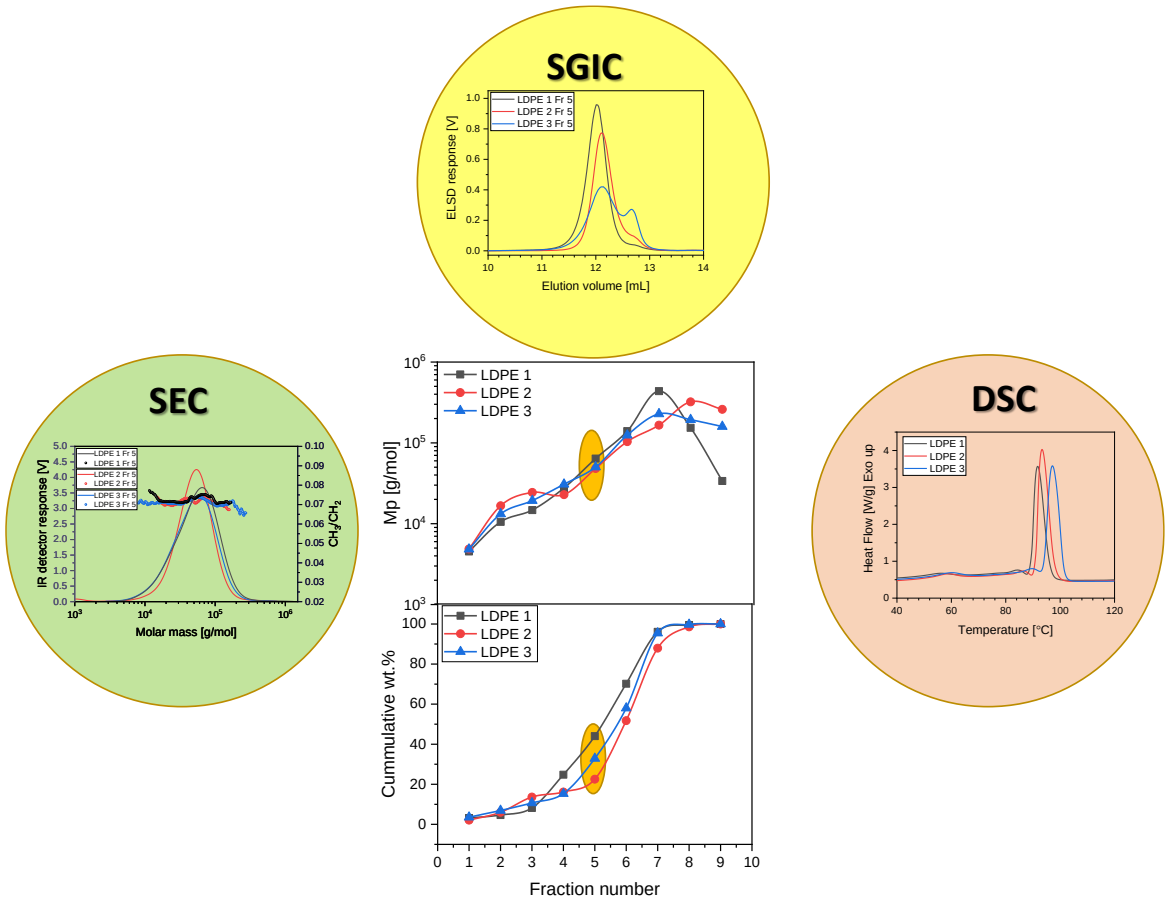

Summary of the analysis of p-MMF Fractions 5 of LDPEs by SEC, SGIC and DSC. Distinct differences are observed which reveal why the bulk samples have varying physical and mechanical properties.

5.1 Introduction

Although bulk analysis might provide some qualitative branching and molar mass information, conclusive information on all molecular characteristics is challenging to obtain. Preparative temperature rising elution fractionation (p-TREF) has been utilized in the past fractionating polyolefins according to crystallizability, which is a function of chemical composition and/or branching. In the absence of pronounced chemical composition heterogeneity such as in homopolymers, p-TREF becomes less interesting in obtaining useful fractions for further analyses, as crystallizability does not primarily depend on molar mass. Preparative molar mass fractionation (p-MMF) is a commonly used fractionation technique for semi-crystalline polyolefins. It produces fractions with narrow MMDs irrespective of branching or chemical composition and is especially suitable for homopolymers where chemical composition does not influence solubility properties. Different polyolefins such as linear low density polyethylene (LLDPE)[1,2] and low density polyethylene (LDPE)[3,4] have been fractionated through this technique. Previous studies have shown that fractionation by the degree of branching and by molar mass has enabled polyolefins to be comprehensively characterized.[5] Bulk analysis often does not address contributions of smaller components to the overall properties of the polymer. Therefore, to elucidate the molecular heterogeneity of LDPEs and long chain branched polyethylenes (LCBPEs), these bulk resins were fractionated by p-MMF.

5.2 Fractionation of bulk samples

Three LDPE samples and four LCBPEs with varying branching contents were fractionated using p-MMF. Fig 5.1 shows the plots of fractions recovered in weight percentage. Two different methods of p-MMF were applied for the two sets of polyolefins. Preparative solvent gradient fractionation (p-SGF) was applied for LDPEs and p-MMF by precipitation was applied on the LCBPEs. The main difference between the two techniques is that the precipitation method allows for handling smaller sample sizes of less than 1 g. Since the LCBPEs were small in quantity, p-MMF by precipitation was chosen for fractionation. Samples with high crystallinities are more challenging to fractionate using p-SGF due to their poor solubility, see the technical procedure in the Experimental Chapter.

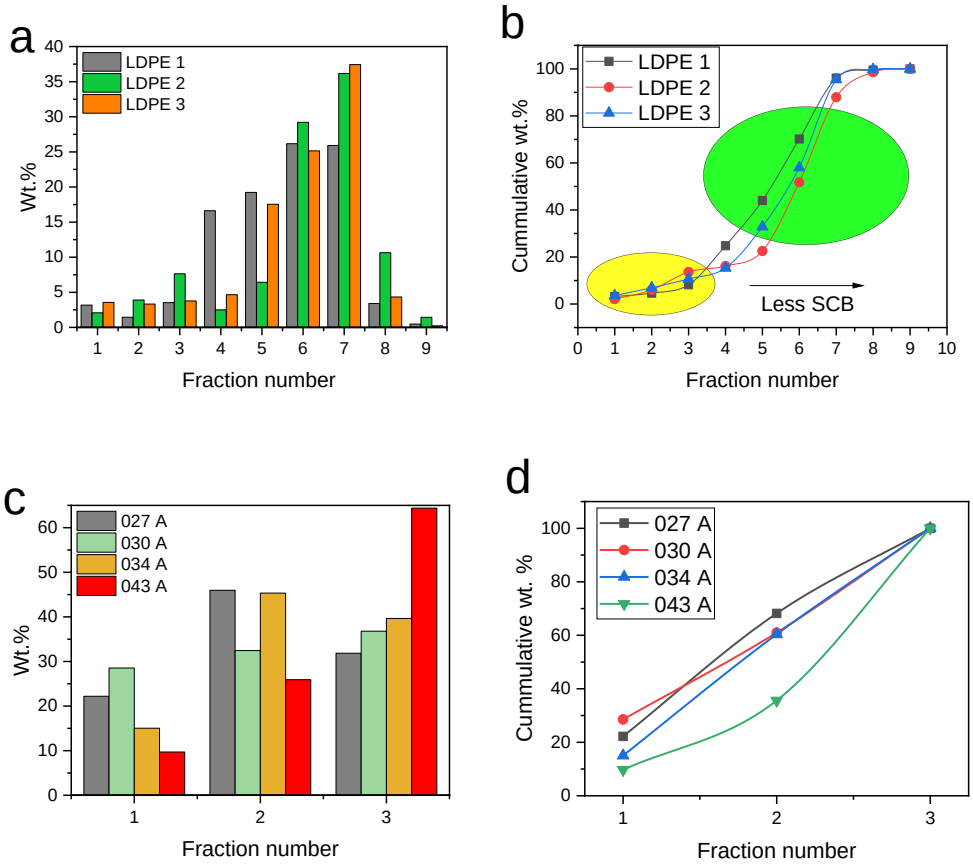

Figure 5.1 Plots showing p-MMF fraction quantities obtained from LDPEs in (a) and the cumulative weight fraction as a function of fraction number in (b). Similar plots for LCBPEs are shown in (c) and (d), respectively.

Both techniques are based on the solubility of the polyolefin in a solvent/non-solvent mixture. Fractions were collected by instantaneously increasing the solvent and decreasing the non-solvent (p-SGF) in the mixture or vice versa (p-MMF by precipitation). LDPE fractions collected from the three samples provided nine molar mass fractions. The order of fractionation for p-SCF is from low molar mass to high molar mass, this is vice versa for p-MMF. The main difference in the p-MMF fractions of the LDPE samples is observed in Fr. 4 (Fig. 5.1 a), which constitute about 16.2, 2.5 and 4.7 wt.% of LDPE 1, LDPE 2 and LDPE 3, respectively. Fr. 4 to 8 form the majority components which proves that the bulk samples comprise mostly of high molar mass components. Fig. 5.1 b shows the cumulative weight percentage as a function of the fraction number. The

differences in the plots can be tentatively interpreted as a result of differences in SCB and LCB with SCB playing a major role in the redissolution of the LDPE chains during p-SGF.

LCBPE fractions collected from the four samples provided three molar mass fractions. The main differences in the p-MMF fractions of the LCBPEs are observed in Fr. 3 (Fig. 5.1 c), which constitute about 31.8, 37.5, 39.6 and 61.4 wt.% of 027 A, 030 A, 034 A and 043 A, respectively. Fr. 2 and 3 form the majority components but interestingly, for 043 A fraction 3 which constitutes 61.4 wt.% forms the majority component. The cumulative profiles of the samples are shown in Fig. 5.1 d.

As can be observed, for all samples a trend to higher molar masses with increasing fraction number is observed (Fig. 5.2 a) till Fr. 7, then a drop in peak molar mass (M_p) from Fr. 8 to Fr. 9 is seen. This verifies the high selectivity of p-MMF regarding molar mass fractionation. The drop in M_p can be explained probably by the presence of chains with predominantly high LCB content as well as some component with highly linear chains. Fig. 5.2 b clearly shows the differences in the peak molar masses of the three fractions obtained for each sample indicating successful p-MMF.

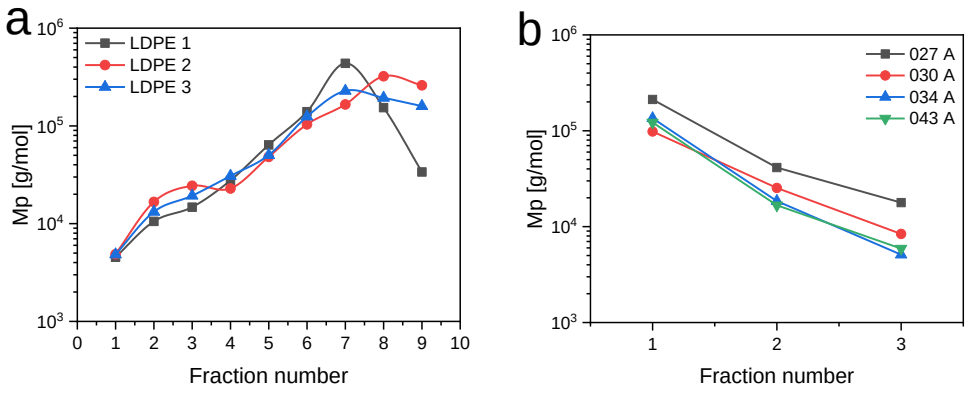

Figure 5.2 Molar masses of LDPE fractions (a) and LCBPEs (b).

LDPE fractions are expected to increase in molar mass from Fr 1 to Fr 8 whereas LCBPE fractions are expected to decrease in molar mass from Fr 1 to Fr 3 according to the techniques used. Preparative MMF delivers a much-needed way of fractionating polyolefin samples by producing homogenous molar mass fractions with broad branching distributions. Fractions can be collected

and analyzed to acquire comprehensive information regarding the microstructure of these samples.[3] After the LDPE and LCBPE bulk samples were fractionated, their fractions were analyzed using several techniques as will be discussed in the subsequent sections.

5.3 LDPE and LCBPE fraction analyses

5.3.1 Molar mass analyses

HT-SEC-IR and HT-SEC-d4 experiments were conducted on the fractions. Figs. 5.3 and 5.4 show the molar mass distributions of the p-MMF fractions and the respective bulk samples. Analyses of the p-MMF fractions revealed unimodal distributions in MMD which indicates homogeneity except for Fr. 7 and Fr. 8 of LDPE 1. The LDPE fractions show increasing molar masses as the good solvent (xylene) is increased. LCBPEs were fractionated using molar mass fractionation by precipitation and the molar masses of the fractions decreased with an increase in the non-solvent. The molar mass distributions of the LDPE sample fractions follow the same trend though distinct differences are seen for the high molar mass fractions (compare Figs. 5.3 a-c). LCBPE fractions also follow similar trends with a distinct difference in Fr. 3.

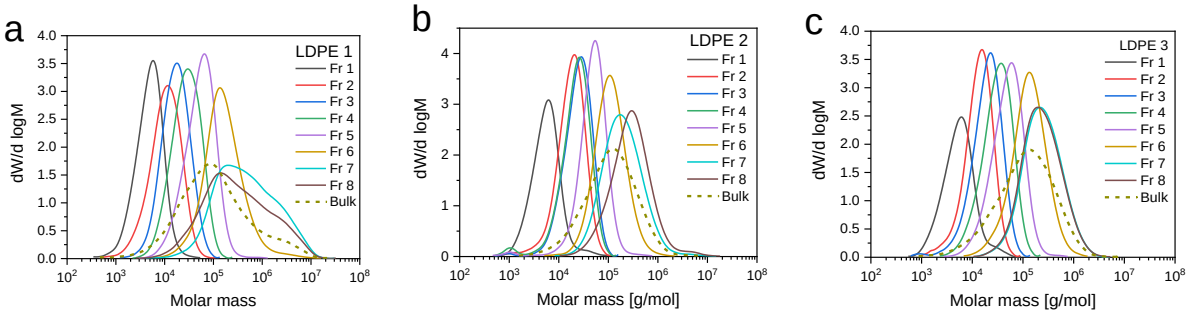

Figure 5.3 Molar mass distribution profiles of p-MMF fractions of the three LDPEs obtained by HT-SEC-IR. The fractions of LDPE 1, LDPE 2 and LDPE 3 are shown in a-c, respectively. The branching information is not included to allow for clarity.

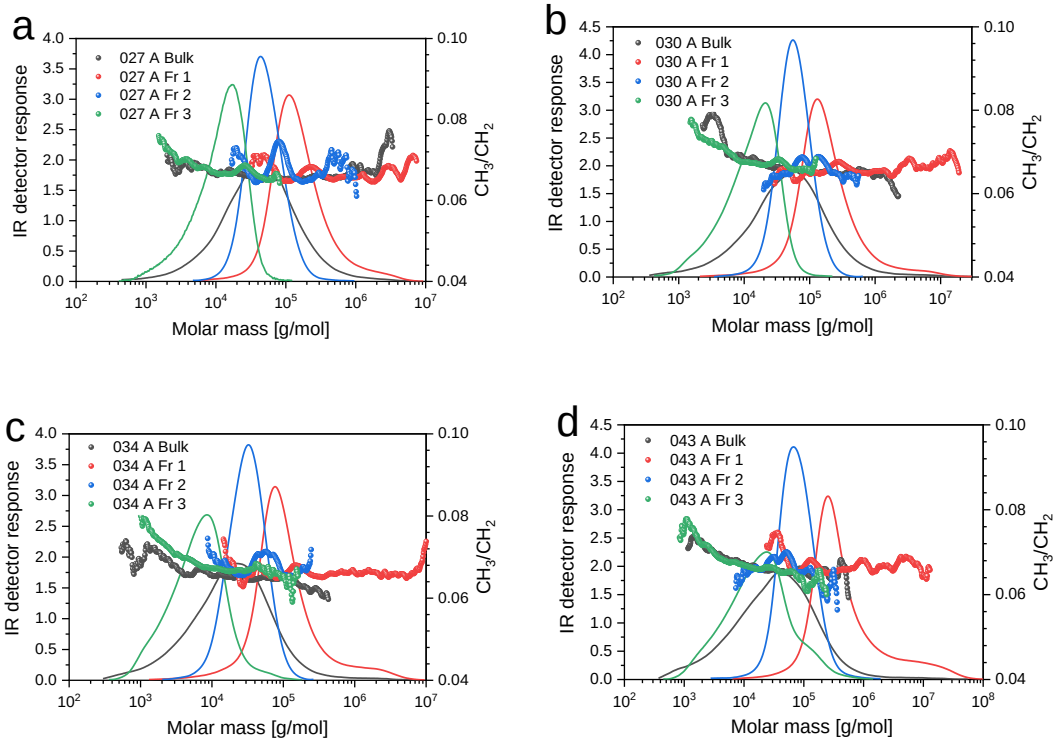

Figure 5.4 Molar mass distribution profiles and total branching as a function of molar mass of p-MMF fractions of the four LCBPEs as obtained by HT-SEC-IR. The fractions of 027 A, 030 A, 034 A and 043 A are shown in a-d, respectively.

All LDPE fractions are narrowly distributed from Fr. 1 to Fr. 5 exhibiting increasing M_p. The fractions become broader with an increase in molar mass for Fr. 6 to 8 hence exhibiting broader molar mass dispersity which indicates a notable heterogeneity. Molar mass dispersities ranging between 1.2 and 9.3 were recorded for the LDPE fractions. This is indicative of significant molar mass heterogeneities in some fractions as Fr. 6 and 7 make up most of the sample components for the LDPEs. These fractions with broad dispersities are expected to have high LCB contents.

A different trend is seen for LCBPEs. All fractions are broadly distributed except for Fr. 2 in all the samples. The fronting of the molar mass distributions of Fr. 3 for all the samples is due to the concentration of smaller molecules that were previously not seen in the bulk samples. This low molar mass front increases dispersity factors M_w/M_n.

Table 5.1 Summary of p-MMF fraction properties of LDPE 1, LDPE 2 and LDPE 3.

Fraction	Recovery wt.%	M_n[a] [kg/mol]	M_p[a] [kg/mol]	M_w[a] [kg/mol]	Đ
		LDPE 1			
Fr 1	3.2	3.8	5.8	5.9	1.6
Fr 2	1.4	7.5	11.4	13.1	1.7
Fr 3	3.5	13.3	18.4	20.7	1.6
Fr 4	16.6	21.5	28.6	34.3	1.6
Fr 5	19.2	39.9	67.2	69.0	1.7
Fr 6	26.1	104.9	144.4	291.7	2.8
Fr7	25.9	188.0	386.4	1152.0	6.1
Fr 8	3.4	105.0	158.6	975.2	9.3
Fr 9	0.5	--			
		LDPE 2			
Fr 1	2.1	4.5	6.3	7.2	1.6
Fr 2	3.9	12.6	20.5	21.1	1.7
Fr 3	7.6	17.4	27.9	28.9	1.7
Fr 4	2.5	13.2	26.4	26.4	2.0
Fr 5	6.42	26.8	52.5	59.6	2.2
Fr 6	29.2	81.7	108.4	144.1	1.8
Fr7	36.2	128.6	193.6	317.1	2.5
Fr 8	10.6	180.6	323.2	478.5	2.6
Fr 9	1.3	--			
		LDPE 3			
Fr 1	3.6	4.2	6.2	7.1	1.7
Fr 2	3.3	7.6	15.4	15.5	2.0
Fr 3	3.8	13.4	22.6	23.4	1.7
Fr 4	4.70	23.5	36.8	37.9	1.6
Fr 5	17.5	37.0	58.9	62.9	1.7
Fr 6	25.1	91.3	133.7	176.7	1.9
Fr7	37.4	161.9	233.0	349.2	2.2
Fr 8	4.3	156.1	237.1	342.7	2.2
Fr 9	0.2	--			

[a] determined by HT-SEC-IR

The high molar mass fractions (Fr. 1) exhibit broad molar mass dispersities of 3.2, 4.5, 5.7 and 5.8 for 027 A, 030 A, 034 A and 043 A, respectively, suggesting significant molar mass heterogeneities in these fractions as seen from Figs. 5.4 a-c. Again, due to the concentration of chains previously not detected at the bulk level, pronounced tailing can be seen at the high molar mass end in Fig. 5.4 especially in 5.4 c and 5.4 d. A sharp decrease in polydispersity of fractions

compared to their bulk samples was observed, this signifies a successful separation of the polymer chains based on their molar mass. It is known that LDPEs are characterized by a high content of SCBs and LCBs resulting from the free radical polymerization processes during synthesis. On the other hand, LCBPEs were lab synthesized to produce only LCB and no SCB. Therefore, the molecular structures and topology of the two sets of samples differ significantly.

Table 5.2 Summary of p-MMF fractions of LCBPE 027 A, 030 A, 034 A and 043 A as determined by HT-SEC-IR.

Fractions	**NS/SR[a] [mL]**	**Recovery Wt.%**	**M_n[b] [kg/mol]**	**M_p[b] [kg/mol]**	**M_w[b] [kg/mol]**	**Đ**
			027 A			
Fr 1	0.70	22.2	194.7	238.5	620.9	3.2
Fr 2	0.85	46.0	71.3	79.6	113.1	1.6
Fr 3	soluble	31.7	10.6	27.4	24.5	2.3
			030 A			
Fr 1	0.70	29.2	98.5	134.1	438.4	4.5
Fr 2	0.85	32.2	47.0	56.5	68.0	1.4
Fr 3	soluble	37.5	7.5	20.5	18.0	2.4
			034 A			
Fr 1	0.70	15.1	100.0	155.8	567.3	5.7
Fr 2	0.85	44.3	41.0	58.3	65.1	1.6
Fr 3	soluble	39.6	5.7	13.5	15.0	2.6
			043 A			
Fr 1	0.70	9.7	123.8	128.5	712.1	5.8
Fr 2	0.85	25.7	34.0	36.9	52.3	1.5
Fr 3	soluble	61.4	6.0	14.1	21.4	3.6

[a] denotes non-solvent/solvent ratio, [b] determined by HT-SEC-IR.

HT-SEC-d4 was used to study the molecular conformation of each fraction. To obtain more insight into the microstructure, the radius of gyration (R_g) was determined as a function of the molar mass (measured using MALLS). The results were compared with a linear reference. R_g and intrinsic viscosity [η] are influenced by molar mass and molecular topology (branching).[6] A summary of α values obtained from Figs. 5.5 a-c and Figs. 5.6 a-d show the scaling relationship between R_g and M_w for each fraction.

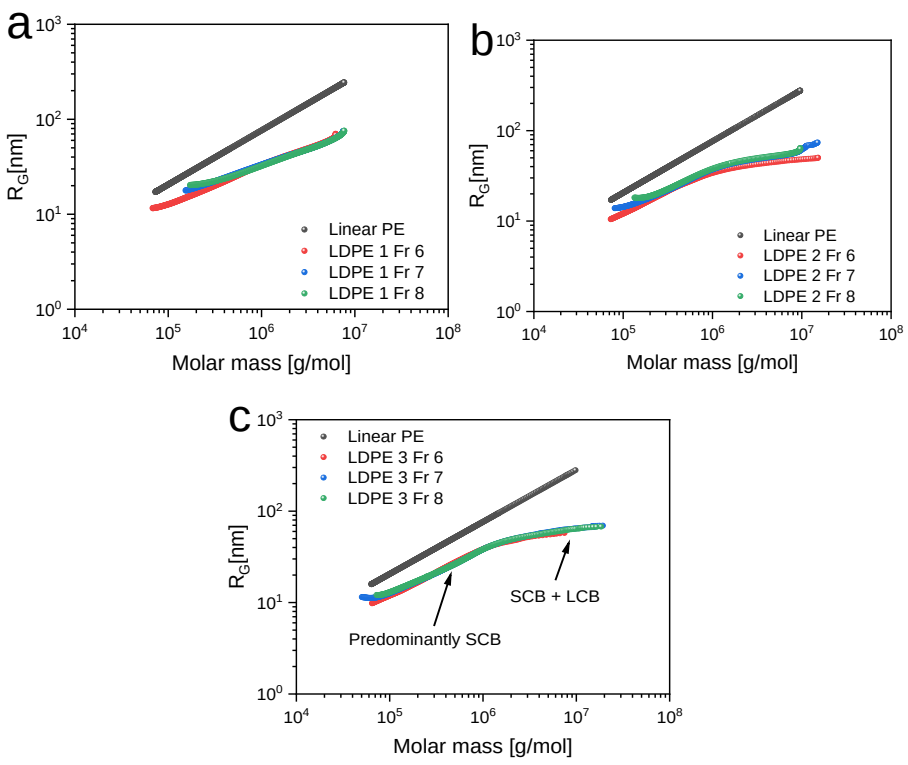

Figure 5.5 Variation of the radius of gyration with molar mass of p-MMF fractions of LDPE 1, LDPE 2 and LDPE 3. The arrows in (c) indicate the differences in the slopes of LDPE 3 fractions which differ from LDPE 1 fractions in (a).

Yu *et al.*[7] concluded that as molar mass decreases, the LCB detection level becomes increasingly poor. It is well known that the amount of scattered light of a macromolecule is correlated to the molar mass of the polymer in solution.[8] MALLS can measure molar masses from below 1 kDa up to ~1 GDa, but is limited to determining R_g above ~10 – 20 nm (corresponding to a molar mass of ~ 10^5 g/mol for typical polymers).[9-12] Thus the accuracy of the radius of gyration, obtained in the region of low molar masses, begins to deteriorate rapidly and is unreliable. This is seen for the LDPE Fr. 1 to 5. In the present study, some of the R_g values were below 10 nm hence the data obtained were unreliable. Table 5.3 summarises the values obtained of R_g and [η] slopes, v and α, respectively.

In Fig. 5.5 a-c, the R_g values of the LDPE sample fractions gradually decrease with the increase in molar mass. Resolution increases with an increase in molar mass, which is evident from Fr 6 to 8. As molar mass increases, the slope deviates from linearity which is evidence of LCBs.[13] The plots

of Fr. 6 to 8 of the LDPEs lie lower than the linear PE indicating SCBs and continuously deviate from linearity which is a clear indication of LCB.

Table 5.3 Summary of R_g and $[\eta]$ slopes of p-MMF fractions of LDPEs.

	$R_g = K \cdot M^{\nu}$: **ν values** Linear PE = 0.57			$[\eta] = K \cdot M^{\alpha}$: ***α values*** Linear PE = 0.703		
Fraction	LDPE 1	LDPE 2	LDPE 3	LDPE 1	LDPE 2	LDPE 3
1	--	--	--	--	--	--
2	--	--	--	--	--	--
3	--	--	--	0.57	0.57	0.55
4	--	--	--	0.62	0.59	0.63
5	--	--	--	0.54 / 0.30	0.59	0.59 / 0.47
6	0.40	0.48 / 0.19	0.51 / 0.17	0.27	0.54	0.61 / 0.40
7	0.34	0.42 / 0.19	0.47 / 0.22	0.30	0.43 / 0.06	0.47 / 0.16
8	0.33	0.43 / 0.17	0.47 / 0.18	0.29	0.43 / 0.03	0.40 / 0.15

Table 5.4 Summary of R_g and $[\eta]$ slopes of p-MMF fractions of LCBPEs.

	$R_g = K \cdot M^{\nu}$: **ν values** Linear PE = 0.57				$[\eta] = K \cdot M^{\alpha}$: ***α values*** Linear PE = 0.703			
Fraction	027 A	030 A	0.34 A	043 A	027 A	030 A	034 A	043 A
Fr 1	0.32/ 0.11	0.23 / 0.07	0.06	0.07	0.38/ 0.15	0.67/ 0.39	0.31	0.32/ 0.04
Fr 2	0.12	0.59 / 0.08	0.52 / 0.18	0.55/ 0.15	0.64/ 0.09	0.39/ 0.09	0.60/ 0.12	0.54/ 0.11
Fr 3	0.45/ 0.14	--	--	--	0.68/ 0.32	0.62/ 0.48	0.75/ 0.41	0.68/ 0.35

The influence of LCB on R_g is much more pronounced in the fractions of LCBPEs, see Fig. 5.6 and Table 5.4. The upbending in the conformation plots is often characterised by the co-elution or anchoring effect in SEC. It is encountered when the long side branches of a high molar mass molecule penetrate the pores of the stationary phase, causing a delay. This forces the molecules to elute late (at higher elution volumes), corresponding to the low molar mass region.[9,14] 027 A fractions keep deviating from linearity but are not displaced from the linear reference plot, a sign that they contain LCB and no SCB, refer to Fig. 5.6 a. The low molar mass plots (Fr 3) give poor resolution and could not be recorded except for Fr 3 of 027 A which had a R_g above 10 nm. In the high molar mass region, a sharp deviation from linearity is observed and is an effect of LCB. This

proves that the material properties of polyethylene are sensitive to the degree of branching and the type of branching.[15]

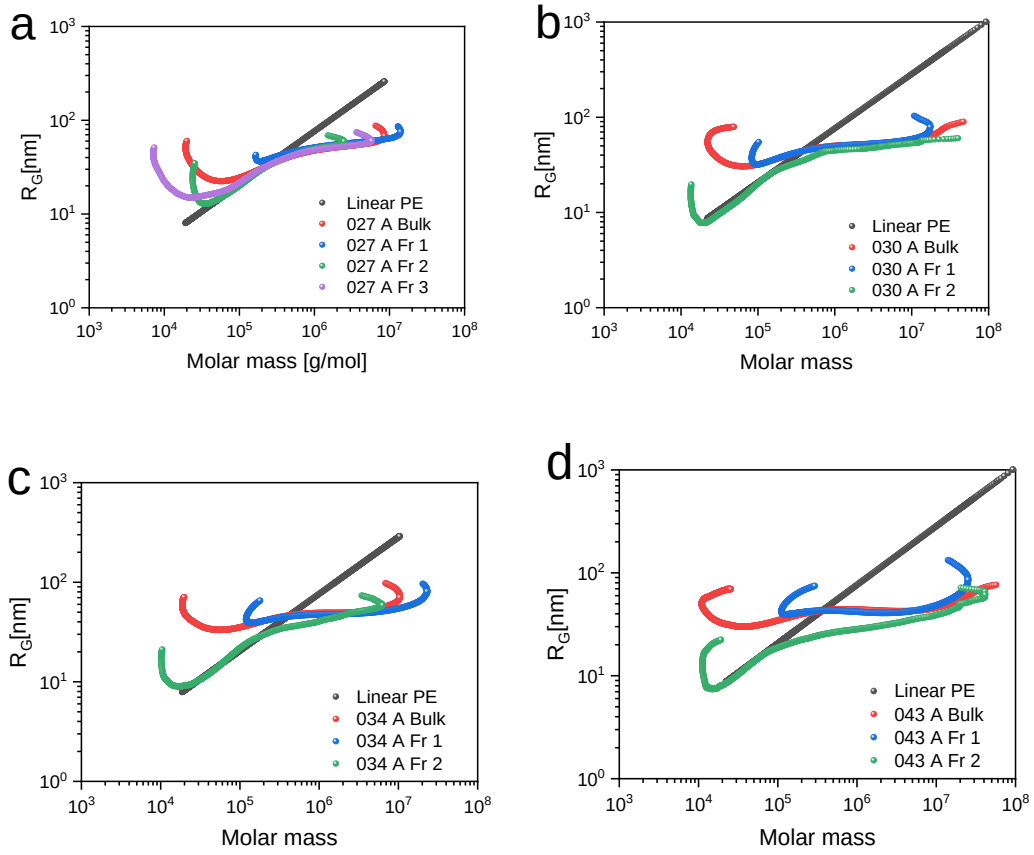

Figure 5.6 Variation of the radius of gyration with molar mass for p-MMF fractions of 027 A (a), 030 A (b), 034 A (c) and 043 A (d).

Plots of $[\eta]$ as a function of molar mass also known as Mark-Houwink-Sakurada plots (MHS) are perhaps the reliable standard in polymer branching analyses. The behaviour of the fractions was studied to understand the branching behaviour in a dilute solution. Branching differences were illustrated by comparing the solution properties of the branched polyethylene sample with a linear equivalent. It was observed that just like the R_g (conformation plots), for LDPE fractions at low molar mass the resolution was poor and provided unreliable data. Viscosity detection is more sensitive to low molar mass polymer chains as compared to MALLS for determining the presence of LCB.[2] However, the very low molar mass fractions provide unreliable data due to the

shortcomings of viscometry and light scattering detectors and thus cannot be used for MHS plots; for this reason Fr 1 and 2 of LDPEs were omitted from the plots in Fig. 5.7.

At low molar masses, SCBs are seen as the plots lie lower but parallel to the linear reference. As the fraction number increases with increase in MM, the plots deviate further from the linear reference an indication of LCBs. Similar branch distributions in the LDPE fractions can be attributed to similar synthesis conditions for the LDPE samples.

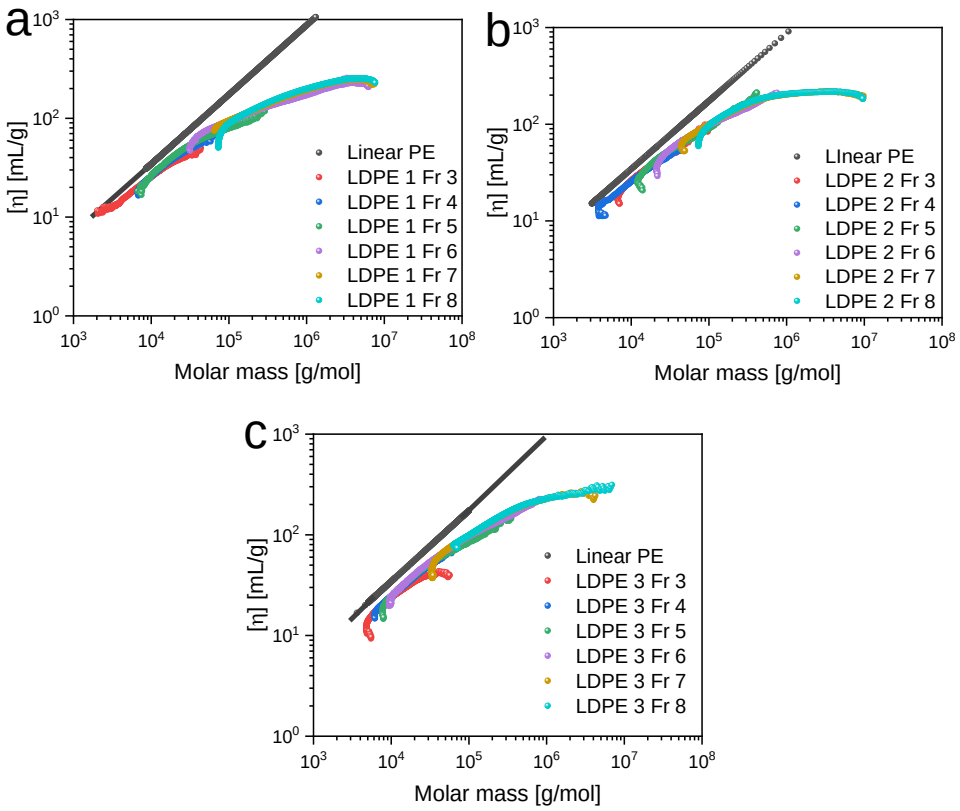

Figure 5.7 MHS plots of p-MMF fractions of LDPE 1 (a), LDPE 2 (b)and LDPE 3 (c) obtained from HT-SEC-d4.

High molar mass fractions have a high degree of long chain branching with Fr 7 and 8 having branch distributions that are almost identical. The MHS plots (Fig. 5.8) of the LCBPE fractions were compared to their equivalent linear reference as well as their respective bulk samples. The fractions and the bulk samples show significantly different behaviour from the LDPEs. As expected, [η] increases with decreasing branching density.

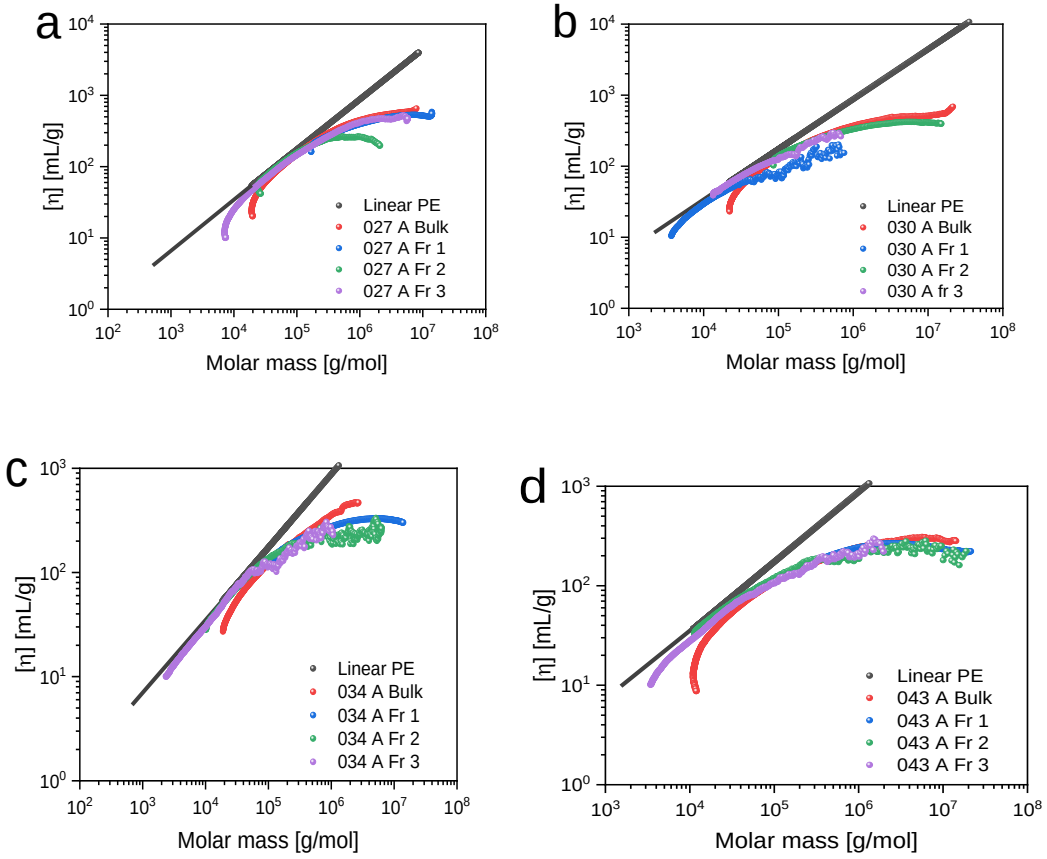

Figure 5.8 MHS plots of p-MMF fractions of 027 A (a), 030 A (b), 034 A (c) and 043 A (d) obtained from HT-SEC-d4.

From literature, the lowest intrinsic viscosities are characteristic of highly branched samples since they form compact coils in solution.[8] For low p-MMF fractions, it was observed that at high molar mass regions, Fr 1 and 3 have similar MHS behaviour, indicating similar branch distribution.

Fr 2 plot lies lower than that of the bulk, thus an increase in intrinsic viscosity. This is also seen in Fr 2 of 034 A but not in the same fraction of 043 A. Intrinsic viscosity increases from Fr 1 to 3 indicating a high LCB density. The results acquired on the branch density correlate with ^{13}C-NMR results as will be discussed in the next section. A dependence in molar mass is seen for LCBPE p-MMF fractions; a significant decrease in branching is seen as the fraction number decreases. This means, there is more branching in the low molar mass fractions compared to high molar mass fractions as long chain branch incorporation into a polymer is highly dependent on the synthesis conditions used and molar mass.

5.3.2 Branching analyses

^{13}C-NMR was employed to determine the type and quantity of branching structures of the p-MMF fractions. The calculated results obtained are reported in Tables 5.5 and 5.6. The predominant types of short chain branches are butyl and amyl, with a smaller content of ethyl for all samples. These findings agree well with literature data (see Appendix A1).[16] It is noteworthy that the short chain branch frequencies of the LDPE p-MMF fractions do not show a significant dependence on molar mass. This is seen as the total SCB for the fractions increase from Fr. 1 to 3 and then decrease from Fr 4 to 8 for LDPE 1 fractions. Whereas for LDPE 2 and 3 fractions, fluctuations are observed. This is expected as p-MMF is not sensitive to chemical composition or branching distributions but rather to molar mass.

The short chain branches were found to decrease with increase in molar mass for Fr 6 to 8. From the number of branches in these fractions, it is evident that the fractions were not fractionated according to branching. As expected, the LCB content in the LDPE fractions was low. High molar mass fractions of LDPE 1 had a high content of LCB which is also seen in the MHS plots. Therefore, the overall high LCB content in the bulk LDPE 1 as reported in Chapter 4 is confirmed in the fractions.

The p-MMF fractions of LCBPEs do not contain any short chain branches (see Appendix A2); this was also reported for the bulk samples in Chapter 4. The LCB/1000C increases with increase in fraction number (from high to low molar mass fractions). A clear dependence of branching on molar mass is seen from the ^{13}C-NMR results. The third fraction from all four samples had the highest LCB content except in 034 A. This indicates a rather uniform branching distribution in the fractions as well as the bulk samples. The low LCB content in Fr 3 of 034 A is also observed in the MHS and conformation plots (Fig. 5.8).

Table 5.5 Summary of branch types and Br/1000C in the LDPEs. The branch contents were calculated from ^{13}C-NMR spectra.

	$2B_3$	**$1B_2$**	**$2B_4$**	**$3B_5$**	**$3B_{6-n}$**		
Sample name	Methyl	Ethyl	Butyl	Amyl	LCB	SCB total	Total branches
LDPE 1 (bulk total branching 17.7)							
Fr 1	0.0*	0.0*	10.7	2.1	1.0	12.8	13.8
Fr 2	1.8	2.4	8.7	3.1	2.9	16.0	18.9
Fr 3	2.2	2.7	8.1	2.9	1.5	15.9	17.4
Fr 4	1.6	2.2	7.6	2.2	1.1	13.6	14.7
Fr 5	1.8	1.9	7.2	2.5	2.0	13.4	15.4
Fr 6	2.1	0.0*	6.6	1.9	2.3	10.6	12.9
Fr 7	2.3	0.0*	6.3	2.1	2.6	10.7	13.3
Fr 8	1.7	0.0*	6.5	2.5	3.2	10.7	13.9
LDPE 2 (bulk total branching 13.1)							
Fr 1	3.7	0.0*	5.6	2.1	1.8	11.4	13.2
Fr 2	3.3	0.0*	4.7	1.5	0.0	9.5	9.5
Fr 3	5.1	0.0*	5.8	1.3	0.0	12.2	12.2
Fr 4	4.5	0.0*	6.8	2.4	0.6	13.7	14.3
Fr 5	4.4	0.0*	5.4	1.8	1.4	11.6	13.0
Fr 6	5.7	0.0*	5.4	2.9	2.2	14.0	16.2
Fr 7	4.9	0.0*	5.0	1.5	1.8	11.4	13.2
Fr 8	4.0	0.5	3.9	1.1	1.0	9.5	10.5
LDPE 3 (bulk total branching 10.2)							
Fr 1	0.0*	0.0*	7.8	1.7	1.3	9.5	10.8
Fr 2	0.0*	0.0*	6.7	1.3	0.7	8.0	8.7
Fr 3	0.0*	1.0	7.5	1.1	0.3	9.6	9.9
Fr 4	0.0*	0.0*	7.0	2.6	2.0	9.6	11.6
Fr 5	0.0*	2.3	6.8	2.3	3.5	11.4	14.9
Fr 6	0.0*	0.0*	6.1	2.0	2.5	8.1	10.6
Fr 7	0.0*	0.0*	5.7	1.6	2.5	7.3	9.8
Fr 8	0.0*	0.0*	4.3	1.1	1.5	5.4	6.9
δ_{exp}	20.2	11.2	23.4	32.7	32.3		
δ_{lit}	20.3	11.3	23.6	32.6	32.2		

Table 5.6 Summary of branch types and Br/1000C in the p-MMF fractions of LCBPEs. The branch contents were calculated from ^{13}C-NMR spectra.

	$3B_{6-n}$[a]	**Weighted ($3B_{6-n}$)[b]**
Sample name	LCB	
027 A Bulk total	**2.7**	**1.60**
Fr 1	0.012	0.002
Fr 2	0.982	0.451
Fr 3	3.491	1.106
030 A Bulk total	**3.7**	**2.71**
Fr 1	0.413	0.120
Fr 2	1.482	0.477
Fr 3	5.641	2.115
034 A Bulk total	**4.2**	**3.36**
Fr 1	0.022	0.003
Fr 2	1.801	0.797
Fr 3	6.471	2.562
043 A Bulk total	**5.7**	**5.82**
Fr 1	0.803	0.078
Fr 2	1.612	0.414
Fr 3	8.681	5.330
δ_{exp}	32.25	
δ_{lit}	32.18	

[a] Calculated from ^{13}C-NMR spectra; [b] Average branching × weight fraction from pMMF.

The total branching obtained from the weighted LCB contents shows some disparities with the totals obtained directly from the bulk ^{13}C-NMR spectra. We attribute this to the possible detection problems at low LCB contents especially in the first fractions. In addition, from our observations, high molar mass components/fractions are much more challenging to put into solution at 120 °C in comparison to fractions of 043A.

5.3.3 Thermal analyses

Thermal analysis provides crucial information on the effects of SCB and LCB on crystallization behaviour of polyethylene. DSC crystallization curves of the LDPE p-MMF fractions in comparison to their respective bulk samples are shown in Fig. 5.9 a-c. All fractions for LDPE samples show a rather similar trend when their crystallinities are compared to their respective bulk

sample. The influence of molar mass and branching is seen in the crystallization exotherms. For LDPEs, crystallization temperatures increase with increase in molar mass that is from Fr. 1 to 3 and then decrease as the fraction number increases, from Fr. 4 to 8. This can be attributed to the rearrangement of structure and packing due to the type of branches involved.[17] The summary of their thermal properties is shown in Table 5.5.

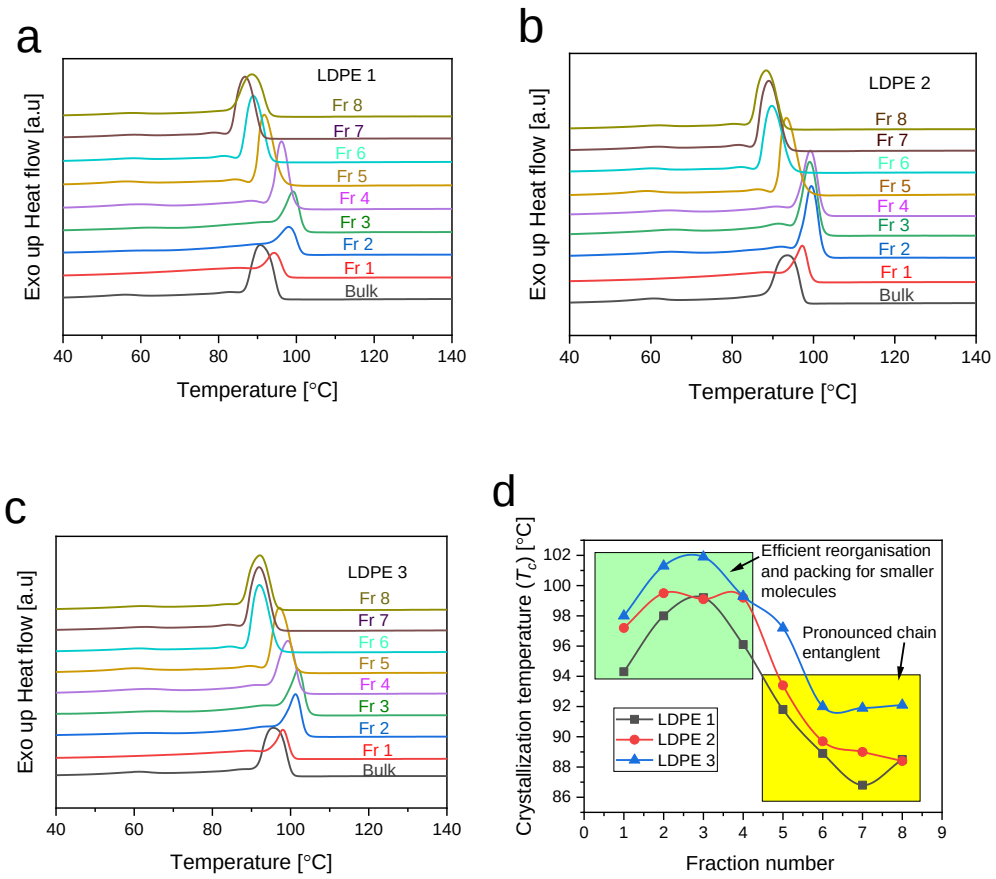

Figure 5.9 DSC thermograms of the p-MMF fractions of LDPE 1 (a), LDPE 2 (b) and LDPE 3(c). Plot of crystallization temperature (T_c) as a function of fraction number (d).

The crystallization temperature (T_c) as a function of fraction number is shown in Fig. 5.9 d. Here, it is visible that the low molar mass fractions have higher crystallization temperatures in comparison to high molar mass ones. Smaller molecules can easily reorganize themselves even in

the presence of SCB. Larger molecules, however, get entangled preventing efficient reorganization. This gets pronounced in the presence of both SCB and LCB as seen in Fig. 5.9 d.

Table 5.7 Summary of thermal properties of p-MMF fractions of LDPEs.

Fraction	**T_c[a]**	**T_m[a]**	**ΔH_m[a]**	**X_c[a,b]**
		LDPE 1		
Fr 1	94.3	104.1	97.1	33.2
Fr 2	98.0	107.2	106.8	36.5
Fr 3	99.2	108.0	106.7	36.4
Fr 4	96.1	107.5	112.1	38.3
Fr 5	91.8	107.3	103.1	35.2
Fr 6	88.9	106.6	113.5	38.7
Fr 7	86.8	106.0	103.7	35.4
Fr 8	88.5	107.9	97.7	33.3
		LDPE 2		
Fr 1	97.2	108.4	105.2	35.9
Fr 2	99.5	110.6	143.2	48.9
Fr 3	99.1	111.9	144.4	49.3
Fr 4	99.2	111.6	129.5	44.2
Fr 5	93.4	109.4	122.4	41.8
Fr 6	89.7	109.5	113.7	38.8
Fr 7	89.0	108.4	117.0	39.9
Fr 8	88.4	107.9	107.4	36.7
		LDPE 3		
Fr 1	98.0	108.3	93.0	31.7
Fr 2	101.3	110.6	130.6	44.6
Fr 3	101.9	111.5	141.7	48.4
Fr 4	99.3	111.4	157.4	53.7
Fr 5	97.2	111.2	149.1	50.9
Fr 6	92.0	111.3	115.5	39.4
Fr 7	91.9	110.6	121.6	41.5
Fr 8	92.1	110.6	118.0	40.3

[a] determined by DSC
[b] $X_c = (\Delta H_m / \Delta H_m^{\theta} \times 100\ \%)$, $\Delta H_m^{\theta} = 293$ J/g.[18]

Whereas the crystallization exotherms are unimodal, melting endotherms show multimodality which indicates the presence of multiple components in the LDPE fractions, see Fig. 5.10. This is observed across all samples especially for Fr. 1-5. This is due to molar mass effects as well as contribution of SCB distribution. While the T_m of Fr. 5-8 decrease for LDPE 1 and 2, those of LDPE 3 remain almost constant. Here, the contributions of SCB in Fr. 5-8 can be clearly seen; this

helps explain the differences in the mechanical properties of the LDPEs as discussed in Chapter 4. These fractions are important for the structure behaviour of the finished product while the Fr. 1-4 play a part in the processability and product appearance such as gloss and environmental stress resistance.

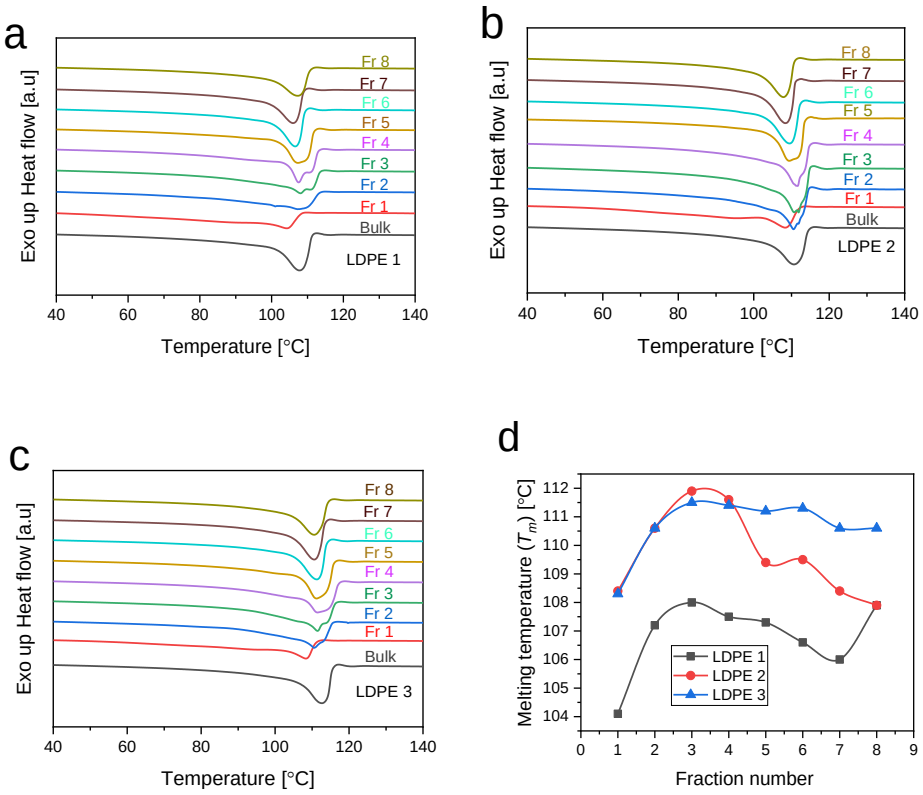

Figure 5.10 DSC thermograms of the prep-MMF fractions of LDPE 1 (a), LDPE 2 (b) and LDPE 3 (c). Melting temperature as a function of fraction number is shown in (d).

Molecular chains possessing various amounts of SCB insertions have different lamellae thickness and crystallisable methylene sequence length.[19] From Figs. 5.11 a-d, it can be seen that thermograms for Fr. 2 and 3 show one main narrow peak which indicates uniformity in the chemical compositions of the fractions. Whereas Fr. 1 in the same samples has thermograms that are broad with low T_c and T_m. As mentioned before, this could be an effect of high molar mass which impacts the molecular size distribution and packing of the molecules within the sample.

For LDPEs, the influence of LCB was observed to be minimal; the thermal behaviour of these fractions was mostly influenced by short chain branches. However, a different case is observed for LCBPE fractions (Table 5.6). The crystallization temperatures were quite interesting, 027 A Fr. 1 to 3 had crystallization temperatures of 111.6, 119.1 and 119.4 °C, respectively. The latter two are particularly high and compare with T_c for linear PE. Whereas for p-MMF fractions of 030 A, 034 A and 043 A, Fr. 2 has the highest crystallization temperature. The first fractions of the LCBPE p-MMF fractions have the lowest T_c which might be due to chain entanglement preventing rapid reorganization during crystallization.

Table 5.8 Summary of thermal properties of p-MMF fractions of LCBPEs.

Fraction	**T_c[a]**	**T_m[a]**	**ΔH_m[a]**	**X_c[a,b]**
		027 A		
Fr 1	111.6	137.8	209.4	71.3
Fr 2	119.1	132.1	220.5	75.3
Fr 3	119.4	128.9	272.2	92.9
		030 A		
Fr 1	116.9	134.0	208.6	71.2
Fr 2	120.5	131.5	248.4	84.8
Fr 3	118.2	127.6	269.4	91.9
		034 A		
Fr 1	116.8	134.7	233.9	79.8
Fr 2	120.5	131.7	254.0	86.7
Fr 3	116.9	126.4	267.9	91.4
		043 A		
Fr 1	114.9	134.8	209.2	71.4
Fr 2	120.8	131.8	251.5	85.7
Fr 3	117.3	126.3	262.7	89.4

[a] determined by DSC
[b] $X_c = (\Delta H_m / \Delta H_m^{\theta} \times 100\ \%)$, $\Delta H_m^{\theta} = 293$ J/g.[18]

To fully understand the behaviour of each fraction in relation to its counterparts, plots of T_m and T_c were constructed as shown in Fig. 5.12. Here, it is visible that as the molecules become larger, crystallization temperature becomes influenced by size due to chain entanglement. However, larger molecules form larger lamella and hence require more energy to melt, as indicated by the decreasing T_m in the order Fr 1>Fr 2>Fr 3.

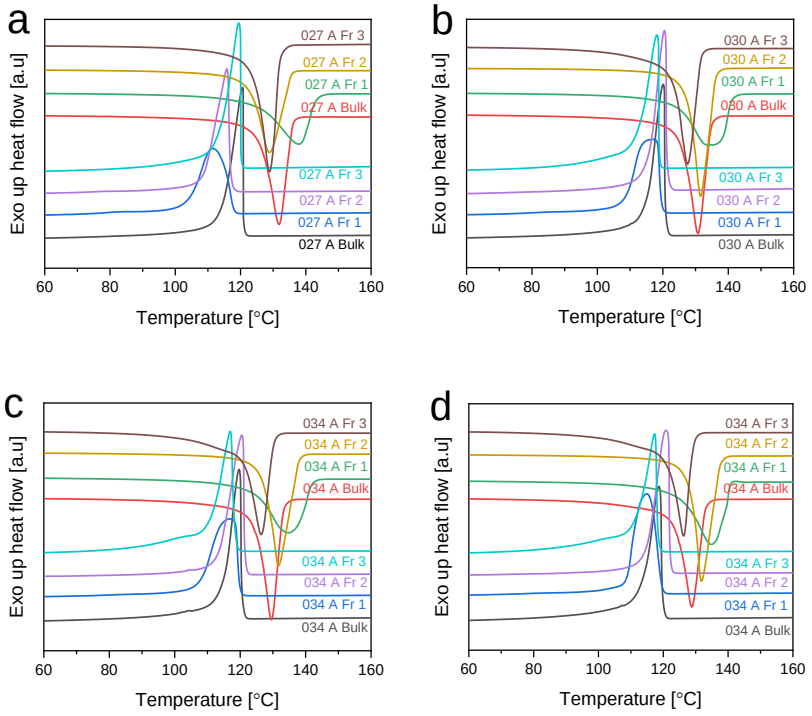

Figure 5.11 DSC thermograms of the p-MMF fractions of 027 A (a), 030 A (b) 034 A (c) and 043 A (d).

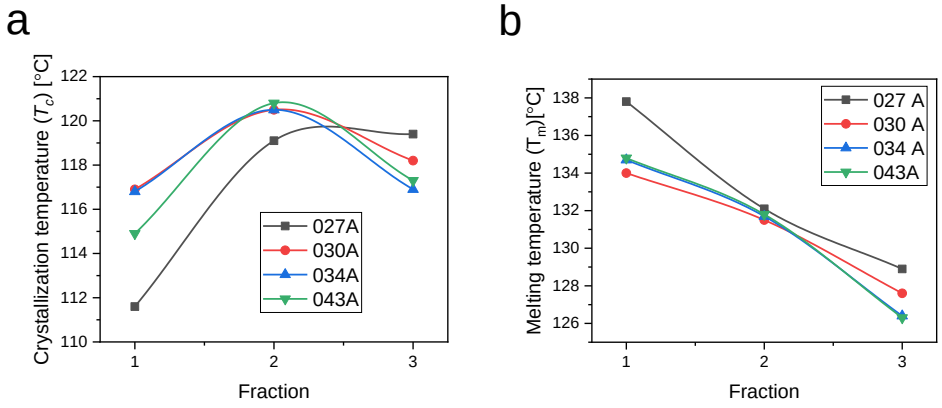

Figure 5.12 Plots of crystallization (T_c) (a) and melting (T_m) temperature (b) as a function of fraction number.

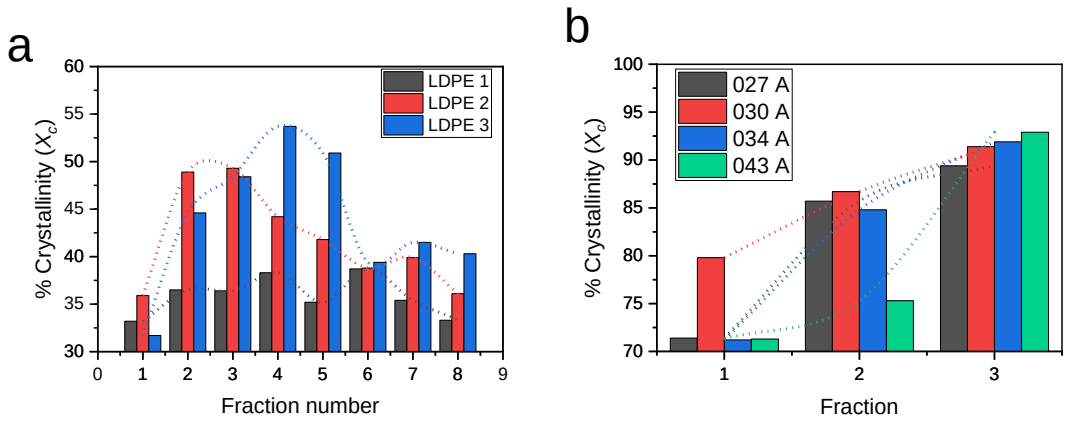

Figure 5.13 Crystallinity of p-MMF fractions of LDPEs (a) and long chain branches PEs (b).

The crystallinities of LDPEs are influenced by SCB and synthesis conditions target creating a balance between SCB and LCB. Fig. 5.13 a shows the calculated crystallinities of the fractions as a function of the fraction number. Fractions of LDPE 1 have the lowest crystallinity, while those of LDPE 2 and 3 show slightly higher values in Fr. 2-4. The low molar mass and low LCB content in these fractions result in slightly higher crystallinities due to reduced chain entanglement.

On the other hand, the crystallinity of LCBPEs increased from Fr. 1 to 3 in all samples as indicated in Fig. 5.13 b. The molar mass of the fractions decreases with fraction number. Therefore, larger molecules of the first fractions show comparably lower crystallinity despite having low LCB levels (refer to Table 5.3). This is because larger chains get entangled quite easily during the reorganisation process upon heating and cooling. Despite having more LCB, smaller molecules have higher crystallinities most probably due to side chain crystallisation which aids in the rapid reorganisation of the macromolecules.

5.3.4 High temperature interaction chromatography (HT-IC)

The interaction chromatography analysis of the fractions was done in two modes. Similar to bulk samples, a solvent gradient of 1-dodecanol→TCB was applied. Ndiripo *et al.*[20] concluded that a 1-dodecanol→$TCB_{30\ min}$ solvent gradient gives better peak-to-peak separation while longer columns promote column efficiency and resolution. The elugrams obtained are shown in Figs. 5.14 and 5.15 for LDPE and long chain branched p-MMF fractions, respectively.

For LDPE 1 fractions (Fig. 5.14 a), the elugrams show broad elution profiles for low molar mass fractions which become narrower as molar mass increases. The same behaviour is seen for LDPE 2 (Fig. 5.14 b) fractions. Low molar mass fractions exhibit complex molecular compositions, and they are eluted first as they have less interaction with the stationary phase. Of interest were LDPE 3 (Fig 5.14 c) fractions of high molar mass (Fr 5, 6, 7 and 8) which showed bimodality in the fractions which was not detected in the previous experiments carried out. This shows the presence of components with different branching densities, see Fig. 5.14 c.

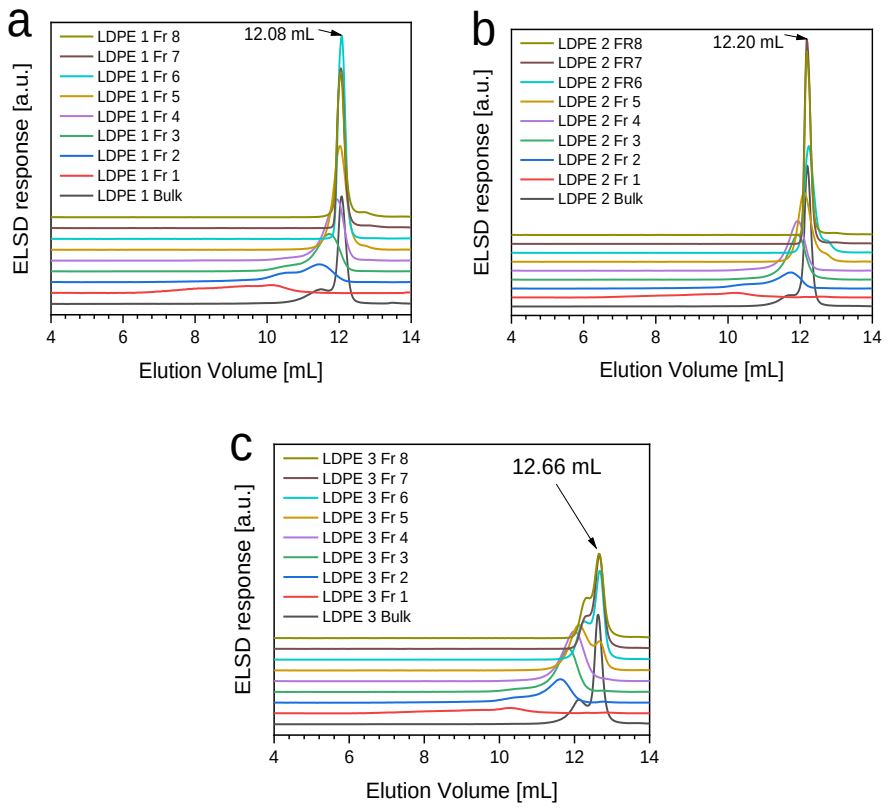

Figure 5.14 Elugrams of p-MMF fractions of LDPE 1 (a), LDPE 2 (b) and LDPE 3 (c) obtained by SGIC using a 1-dodecanol→TCB_{30min} solvent gradient with PGC (Hypercarb® 300 × 4.6 mm^2) as the stationary phase at 160 °C. The ELSD was used for detection.

High molar mass fractions of LDPE 1 and LDPE 2 had elution volumes that are almost the same, indicating similar chemical compositions regardless of the different molar masses. Monrabal *et al.*[21,22] suggested that the adsorption strength of ethylene/1-olefin copolymers on PGC was proportional to the accessible contact surface area of the polymer chain on the flat stationary phase

surface. This indicates that a sample with few on no short chain branches (SCBs) interacts strongly with the support due to longer ethylene sequences resulting to a larger contact surface area. A sample will adsorb on the surface and require a higher volume ratio of TCB to desorb than a sample having more SCBs and shorter ethylene sequences.

The linear PE standard used eluted between 13.0 mL and 14.0 mL (refer to Chapter 4). High molar mass fractions of LDPE 1 and LDPE 2 elute at close volumes as they have lower branch content compared to LDPE 1. The bimodal nature of LDPE 3 Fr. 5 to 8 elugrams shows that these fractions constitute polymer chains with relatively broad chemical composition distributions. Contributions of LCBs could not be deduced because they are very low in these samples. SCBs were much more influential to their retention behaviour.

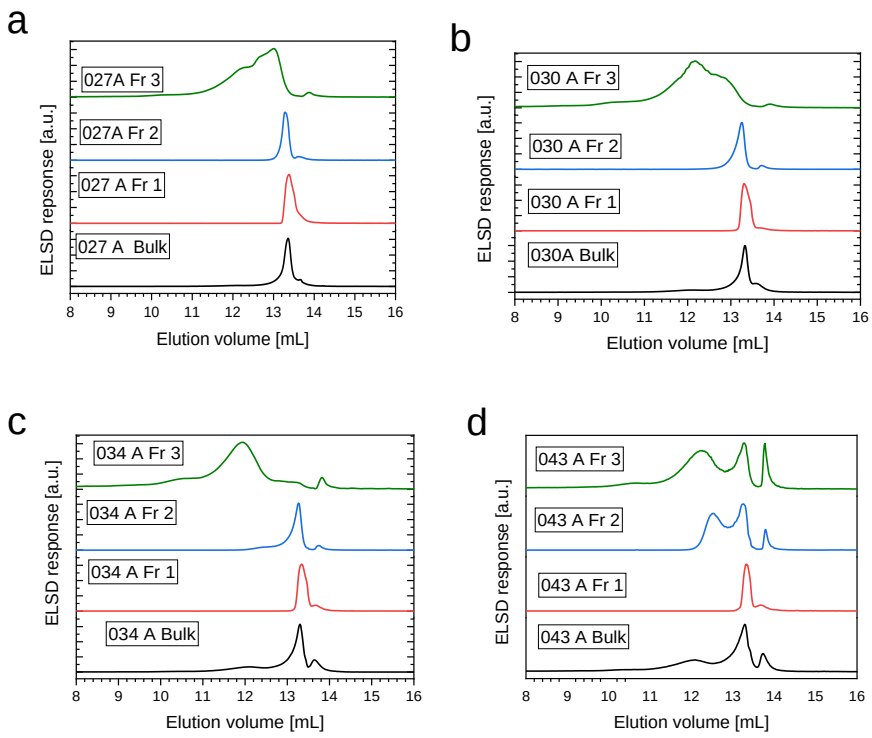

Figure 5.15 Elugrams of p-MMF fractions of 027 A (a), 030 A (b), 034 A (c) and 043 A (d) obtained by SGIC using a 1-dodecanol→TCB_{30min} solvent gradient with PGC (Hypercarb® 300 × 4.6 mm^2) as the stationary phase at 160 °C. The ELSD was used for detection.

The elution behaviour of the LCBPE fractions are shown in Figs. 5.15 a-d. The LCBPE fractions behaved in a rather different manner. Fr. 1 of 030 A and 027 A are narrow, an indication of

homogeneity in terms of molar mass and chemical composition. Fr. 2 of both samples showed 2 peaks, the second peak being a late eluting one. Interestingly eluting at a similar volume as the one from the respective bulk samples. The third fractions for LCBPE samples are quite broad and have components that interact less with the stationary phase; this shows heterogeneity or molecular complexity of these fractions. Fr. 1 of 034 A and 043 A showed a similar behaviour, 2 peaks were observed, and the 043 A fraction had a higher intensity. This indicates that this component is increasing with decrease in molar mass. As also observed from the bulk samples.

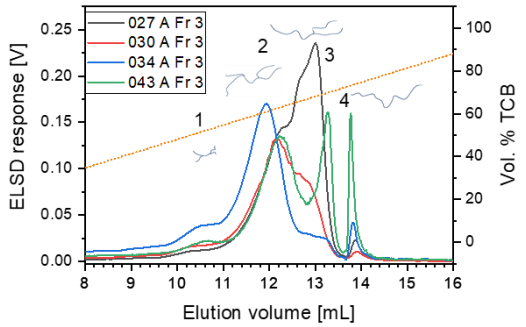

Figure 5.16 Overlays of elugrams obtained from the HT-SGIC of the third fractions of LCBPEs using a 1-dodecanol→TCB_{30min} solvent gradient.

Of interest were the third fractions from all LCBPE samples. The elugrams obtained were broad with Fr. 3 of 043 A having 3 components. A plot of the elugrams of the third fractions is shown in Fig. 5.16. The late eluting peak (4) can be assigned to linear PE molecules. The increase in the LCB content results in the formation of weaker interactions requiring less TCB for redissolution/desorption. This coupled with molar mass effects results in broader elution profiles.

HT-TGIC was used as the second mode utilizing a non-absorptive stationary phase, silica gel. Separations on silica gel using temperature gradient are sensitive to the crystallinity of the polymer. ODCB was used as the mobile phase; the behaviour of the LDPE fractions in TGIC is shown in Fig. 5.17. Two peaks are observed in all the fractions, the first eluting before temperature gradient is applied at 40 °C and the second one appearing after temperature gradient is applied. The decrease in the first peak with fraction number occurs simultaneously with an increase in the second peak. This might be due to low crystallinity components of the fractions which increase with decrease

in molar mass. The broad elugrams indicate the complexity of the branching composition and contribution of molar mass to the elution of the molecules in the column.

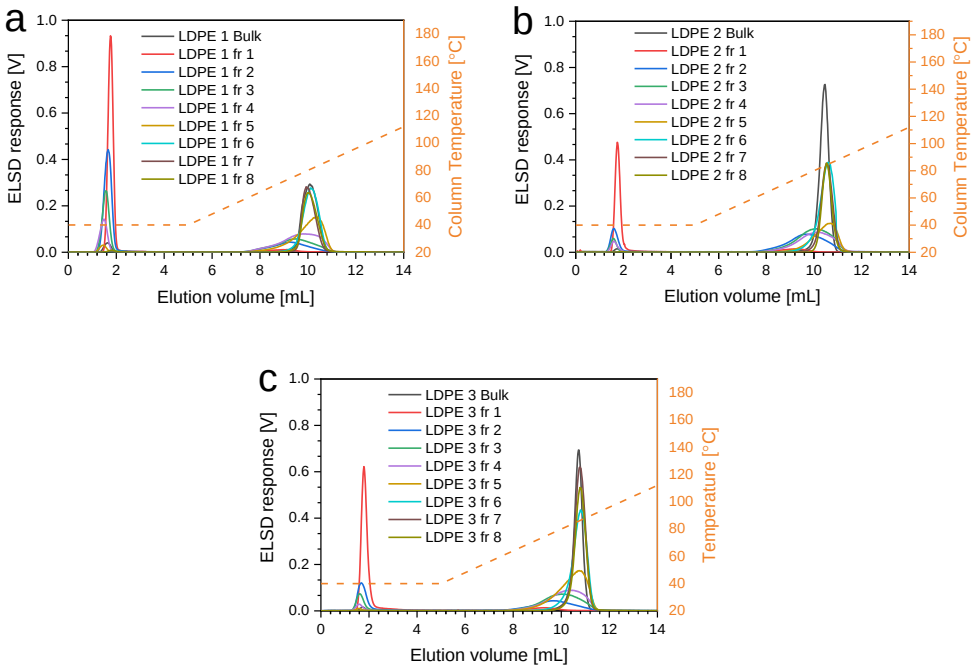

Figure 5.17 HT-TGIC elugrams of p-MMF fractions of LDPE 1, LDPE 2 and LDPE 3 obtained with silica as the stationary phase. ODCB was used as the mobile phase.

Better resolution was observed compared to HT-SGIC though the contribution of LCBs could not be deduced because of the presence of SCBs. The elution behaviour of p-MMF fractions of LCBPEs and their respective bulk samples are shown in Fig. 5.18. The low crystalline components are observed in each set of fractions, the intensity increases with decrease in molar mass (increase in fraction number). Fr. 3 of 043 A has the highest intensity, this could be due to very low MM components. Fr. 1 show unimodal narrow elugrams just like the bulk samples indicating a uniform branching distribution.

At high molar masses, the retention volume of the fractions increases and the peaks are narrow, this can be explained by the specific chemical compositions of the fractions. They have more long undisturbed/uninterrupted methylene sequences which interact more strongly with the stationary phase and have higher melting points. It was observed that the elution behaviour of these fractions

followed similar trends as in DSC. The highly crystalline fractions have a higher LCB content hence a more complex molecular structure and low melting point. Fr. 1 and 2 of all samples have few LCBs and their elution behaviour resembles that of a linear PE due to polymer chains that have methylene sequences long enough to form compact crystallites with high melting points, hence eluting at higher temperatures.

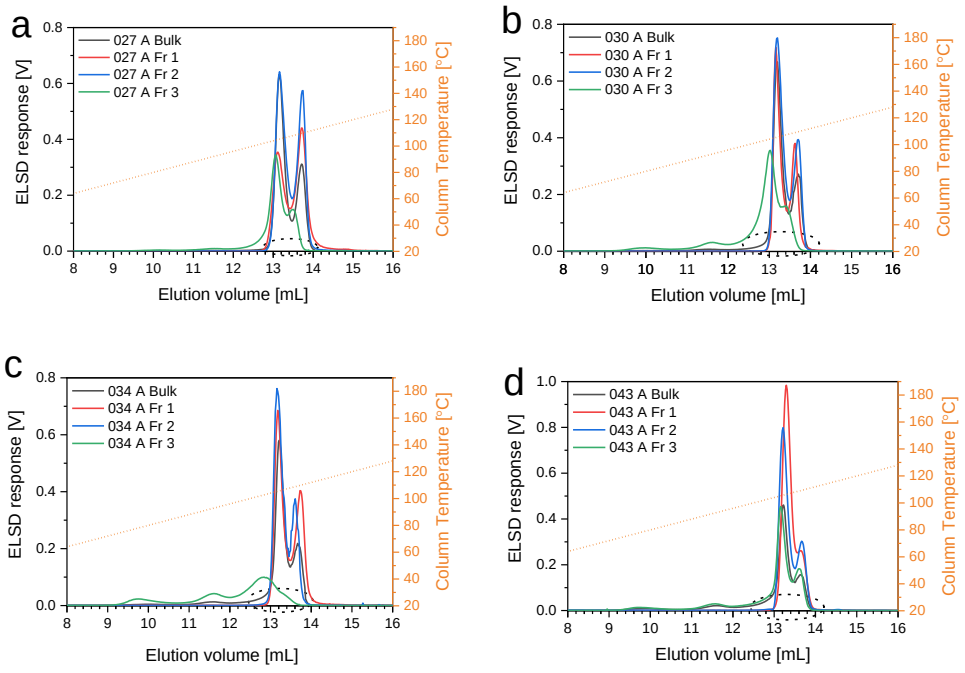

Figure 5.18 HT-TGIC elugrams of p-MMF fractions of 027 A (a), 030 A(b) 034 A (c) and 043 A (d) obtained with silica as the stationary phase. ODCB was used as the mobile phase.

Here, a case of the contribution of long chain branches can be made for Fr. 3 which showed the following LCB contents: 2.74, 3.68, 4.23, and 5.67 for 027 A, 030 A, 034 A and 043 A, as obtained from ^{13}C-NMR, respectively. The last eluting peak (4) is assigned to linear chains which form larger crystallites in solution and require more thermal energy for redissolution see Fig. 5.19. Here we make a clear distinction between HT-SGIC (refer to Fig. 5.16) and HT-TGIC on a non-interactive stationary phase. In HT-SGIC, more compact branched structures with high molar mass require more TCB for redissolution and desorption; hence the chains with long LCBs elute last. Redissolution and desorption require the TCB to penetrate and weaken the intra- and

intermolecular forces together as well as the forces between the polymer and the PGC stationary phase. On the other hand, linear macromolecules form larger crystallites which require higher temperatures to elute in HT-TGIC in comparison to branched structures.

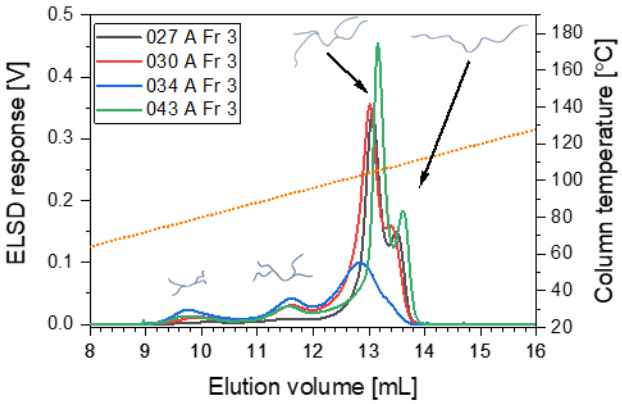

Figure 5.19 Overlays of HT-TGIC elugrams of the third fractions of the LCBPEs obtained from a ODCB solution with silica as the stationary phase.

The multimodality in these fractions is an indication of a complex branching distribution at low molar masses. Long chain branches alter the structure of polymer. This suggests that the long chain branches are quite long and when a branch chain approaches long lengths, it behaves more like an independent chain. In solution, LCBs are highly ordered and have reduced entanglements hence forming more compact molecules with high crystallinity. Crystallinity refers to the orderly arrangements of the polymer chains. A general increase in elution volume of long chain branched fractions compared to LDPE fractions was observed. with lower eluting fractions having broader CCDs compared to the higher eluting fractions. To evaluate the molar masses of the eluting fractions from HT-TGIC, coupling to HT-SEC will be discussed next.

HT-TGIC was coupled to HT-SEC with the use of ODCB as the eluent in the 1st and 2nd dimensions; the contour plots obtained are shown in Fig. 5.20. A slow flow rate was used in the first dimension and a fast one in the second dimension for rapid analysis. The linear PE peak observed is unimodal compared to the one obtained from 1D analyses probably due to the decreased flow rate from 0.5 mL/min to 0.05 mL/min.

5.3.5 HT-2D-LC

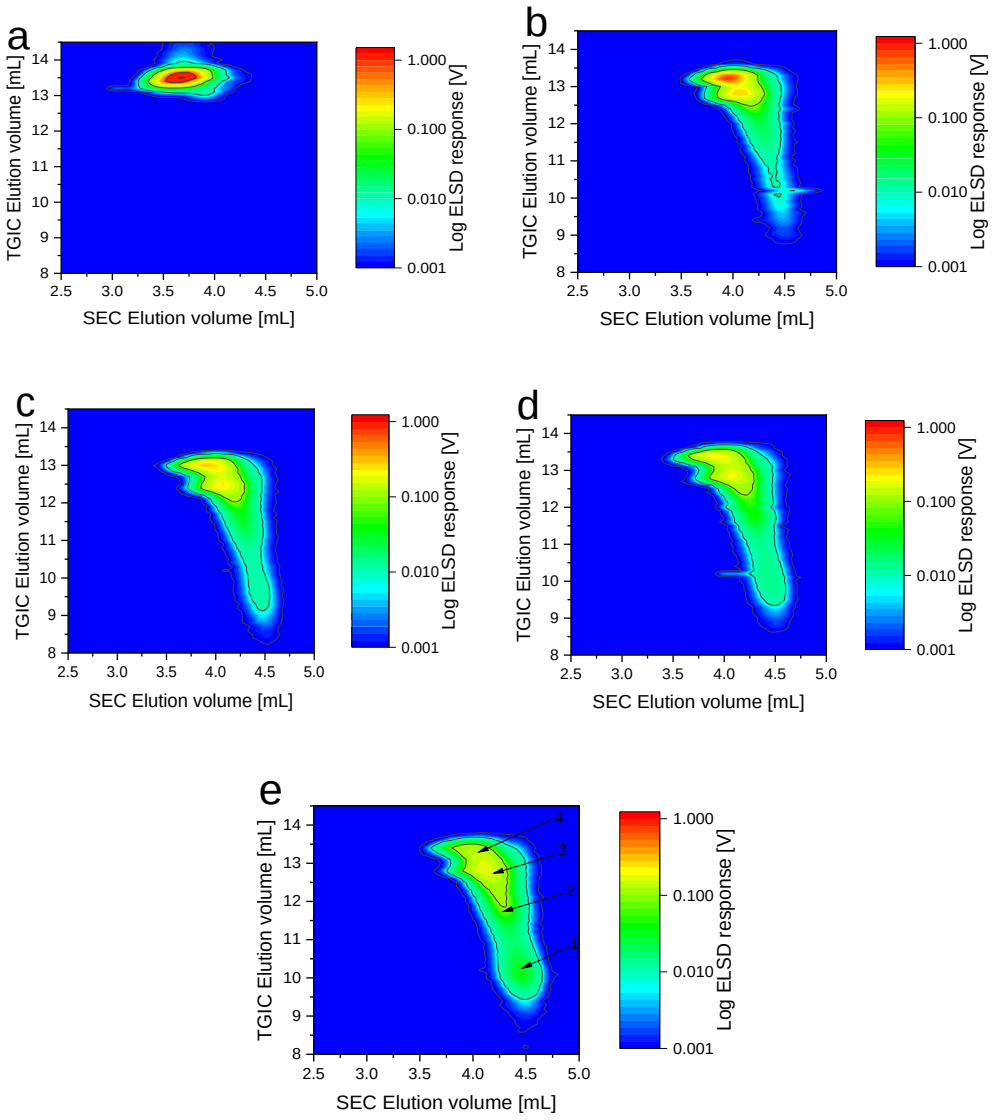

Figure 5.20 TGIC×SEC contour plots of the third fractions LCBPEs 027 A (a), 030 A (b) 034 A (c) and 043 A (d) obtained with a 250 × 4.6 mm silica column in the first dimension and a 100 × 7.5 mm PL Rapide column in the second dimension. A 0.4 °C/min temperature gradient was used in the 1st dimension with a ODCB flow rate of 0.05 mL. ODCB was also used in the 2nd dimension at a flow rate of 2.75 mL/min.

However, the flow rate did not affect the separation of the fractions. All the fractions exhibit a broad branching distribution with a low molar mass component being eluted earlier as the first peak. The intensity of peak 1 increases with increase in fraction number (decrease in molar mass).

As molar mass increases the components are retained more in the 1st dimension. As the intensity of the low molar mass component increases, the intensities of the other peaks decrease. This is clearly seen on Fr 3 of 043 A (Fig. 5.20 e).

The multimodal peak intensity decreases with decrease in fraction number. The second peak in the 1st dimension is observed to increase as fraction number increases. The high molar mass components were rather retained longer in the first dimension. A clear dependency of separation on molar mass with the influence of LCB that are long enough to behave like independent chains as already mentioned before. LCB affects the elution behaviour of molecules in an undistinguishable manner from that of a linear PE. The elution behaviour of these fractions followed the behaviour observed in DSC thermograms and to prove this, sample 043 A bulk was used.

5.3.6 Coupling HT-TGIC to DSC

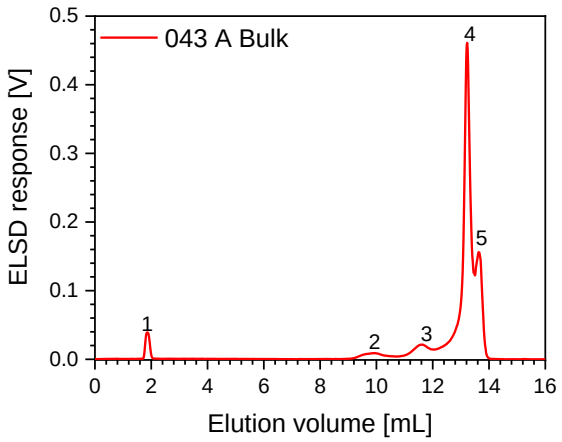

Figure 5.21 TGIC elugrams of the bulk sample 043 A obtained with silica as the stationary phase and ODCB as the mobile phase. Fractions collected as labelled.

Fractions of bulk sample 043 A were collected from HT-TGIC elugrams as shown in Fig. 5.21. Multiple fractionation experiments were conducted to obtain reasonable fraction amounts. The fractions were dried using vacuum and high temperature and analyzed on DSC. All experiments were done under the similar heating and cooling conditions and a fast rate of 20 °C/min for a temperature range of 20 to 200 °C. A faster rate was used as sample size was very small. It was

observed that the melting and crystallization temperatures of the fractions increased as fraction number increased.

Melting points of 117.5, 125.5, 133.0, 133.7, 129.5 and 133.2 ℃ were obtained for Fr. 2, 3, 4, 5, bulk and a reference linear PE, respectively. Fr. 5 and linear PE had melting points that were quite close and eluted at same volumes on HT-TGIC. This means their chemical compositions are almost similar, Fr. 5 has long undisturbed methylene sequences that resemble a linear PE. As elution temperature increases, the chemical composition distribution of the fractions becomes narrower (refer to previous discussion and Fig. 5.18). This is in good agreement with what was observed with DSC crystallization peaks (Fig. 5.22 a and 5.22 b). Fr 2 can be attributed to low molar mass substances and Fr 3 to low LCB substances.

When column temperatures are decreased, silica as a non-adsorptive stationary phase allows polymer chains to gradually crystallize without an interactive force hastening the processes. For LCBPEs, thermal behaviour is mostly influenced by molar mass rather than branching compared to LDPEs.

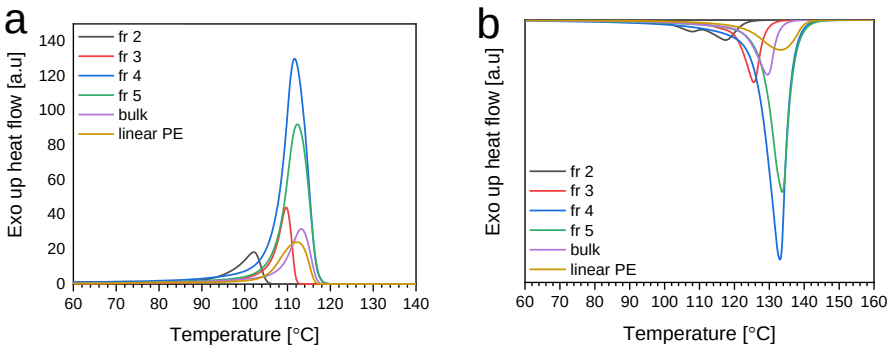

Figure 5.22 DSC thermograms of HT-TGIC fractions of 043 A, bulk and linear PE.

Considering Fr. 1 and 5, their chemical compositions are different. Fr. 1 as the lower eluting polymer has low melting temperatures (lower crystallinity and low LCBs) whereas Fr. 5 as the late eluting fraction has higher melting temperatures (higher crystallinity and more LCBs). These

differences in material can be crucial at the macroscopic level as they influence physical and mechanical properties.

5.4 Conclusions

Preparative molar mass fractionation (p-MMF) on the two sets of polyethylene was carried out to obtain fractions with varying molar masses and chemical compositions. Analyses of the p-MMF fractions with HT-SEC-IR revealed unimodal molar mass distributions in all the fractions. Molar masses increased with fraction number for LDPE samples and decreased with increase in fraction number for LCBPEs; this was due to different p-MMF methods used.

Quadruple-detector high-temperature size exclusion chromatography (HT-SEC-d4) used for molar mass and branching analyses confirmed ^{13}C-NMR findings that short chain branching (SCB) is inherent across the molar mass fractions of the LDPEs. Long chain branching is predominant in fractions with higher molar mass and controls crystallinity. These fractions give the bulk material the required physical and mechanical properties as previously discussed in Chapter 4. For LCBPEs, LCB is the predominant type of branch, and it increases with decrease in the fraction molar mass. Consequently, the crystallinity of the third fractions is higher in comparison to fraction 1 and 2. This is the opposite of what was observed in the LDPEs.

Chemical composition analyses using HT-IC revealed complex elution behaviours for the third fractions indicating complex branching distributions. This can be linked to the coil conformations as influenced by the LCB. LDPE fractions eluted in HT-SGIC with multimodal peaks which resembled the bulk peaks. Here, the presence of less branched components was proved for LDPE 3. These results were in good agreement with ^{13}C-NMR, HT-SEC and DSC. The high elasticity and tensile strength for LDPE 3 could be explained by the presence of the two distinct components.

5.5 References

(1) Sigwinta, M.; Ndiripo, A.; Wewers, F.; Pasch, H. *Polym. Int.* **2020**, *69*, 291–300.

(2) Striegel, A. M. *Anal. Chem.* **2005**, *77*, 104A–113A.

(3) Bungu, P. E.; Pasch, H. *Polym. Chem.* **2018**, *9*, 1116–1131.

(4) Bungu, P. S. E.; Pasch, H. *Polym. Chem.* **2019**, *10*, 2484–2494.

(5) Zhou, X.; Hay, J. N. *Eur. Polym. J.* **1993**, *29*, 291–300.

(6) Eselem Bungu, P. S.; Zentel, K.; Hintenlang, S.; Busch, M.; Pasch, H. *ACS Appl. Polym. Mater.* **2020**, *2*, 5864–5877.

(7) Yu, Y.; DesLauriers, P. J.; Rohlfing, D. C. *Polymer* **2005**, *46*, 5165–5182.

(8) Plüschke, L.; Mundil, R.; Sokolohorskyj, A.; Merna, J.; Sommer, J.-U.; Lederer, A. *Anal. Chem.* **2018**, *90*, 6178–6186.

(9) Podzimek, S. In *Light Scattering, Size Exclusion Chromatography and Asymmetric Flow Field Flow Fractionation: Powerful Tools for the Characterization of Polymers, Proteins and Nanoparticles*; John Wiley & Sons: New Jersey, 2011, pp 99–206.

(10) Plüschke, L. *Advanced Structural Characterization of Dendritic Polyethylene Obtained from Chain Walking Catalysis*. P.h.D. thesis, Technical University of Dresden, Dresden, 2020.

(11) Pasch, H.; Malik, M. I. *Advanced separation techniques for polyolefins*; Springer: Switzerland, 2014, p 179.

(12) Kaspárková, V. R.; Ommundsen, E. *Polymer* **1993**, *34*, 1765–1767.

(13) Xue, Y.-H.; Bo, S.-Q.; Ji, X.-L. *Chin. J. Polym. Sci.* **2015**, *33*, 508–522.

(14) Zentel, K. M.; Bungu, P. S. E.; Pasch, H.; Busch, M. *Polym. Chem.* **2021**, *12*, 3026–3041.

(15) Liu, C.; Wang, J.; He, J. *Polymer* **2002**, *43*, 3811–3818.

(16) Bovey, F.; Schilling, F.; McCrackin, F.; Wagner, H. *Macromolecules* **1976**, *9*, 76–80.

(17) Mirabella Jr, F. M.; Ford, E. A. *J. Polym. Sci., Part B: Polym. Phys.* **1987**, *25*, 777–790.

(18) Mirabella, F. M.; Bafna, A. *J. Polym. Sci., Part B: Polym. Phys.* **2002**, *40*, 1637–1643.

(19) Liu, W.; Zhang, X.; Bu, Z.; Wang, W.-J.; Fan, H.; Li, B.-G.; Zhu, S. *Polymer* **2015**, *72*, 118–124.

(20) Ndiripo, A.; Albrecht, A.; Pasch, H. *RSC Adv.* **2020**, *10*, 17942–17950.

(21) Monrabal, B.; López, E.; Romero, L. *Macromol. Symp.* **2013**, *330*, 9–21.

(22) Monrabal, B. *Macromol. Symp.* **2015**, *356*, 147–166.

Chapter 6 : Conclusions and recommendations

Overall conclusions from the conducted study are presented and recommendations for future work based on the findings are put forward.

6.1 Conclusions

In the present study, low density polyethylene (LDPE) and long chain branched polyethylene (LCBPE) were studied using a combination of multiple advanced fractionation techniques. The molecular heterogeneity of these polyolefins is defined by the molar mass and branching distributions.

Major conclusions and key findings of this study are summarized as follows:

Three commercial LDPEs with distinct branching densities and applications were successfully sourced from Sigma-Aldrich South Africa (LDPE 1), Sabic, Saudi Arabia (LDPE 2), and Sasol Polymers, Secunda, South Africa (LDPE 3). Four lab synthesized polyethylene samples were produced in collaboration with Borealis (Linz, Austria). The lab synthesized samples were synthesized in such a way that only long chain branches were produced unlike in the three LDPE samples which have both long chain and short chain branches (LCB and SCB respectively).

In the first part of the study, bulk samples were successfully characterized using several advanced and hyphenated analytical techniques. The samples are polyethylene homopolymers and major differences in the crystallinities of the two sets were initially revealed using FTIR and DSC. FTIR revealed differences in the spectral region of 1500 – 1420 cm^{-1}, LDPEs had single broad peaks whereas LCBPEs were shown to have long methylene sequences and an apparent absence of SCB. DSC results showed higher melting temperatures (T_m) for LCBPEs compared to LDPEs. The calculated crystallinities obtained by DSC agreed with FTIR findings; LCBPEs had higher crystallinities compared to LDPEs due to differences in branching compositions, specifically the presence SCBs in LDPEs and their absence in LCBPEs. High resolution ^{13}C-NMR revealed the differences in branching, LDPEs contain both SCB and LCB with butyl branches being predominant. LDPE 1 has the highest total number of branches hence having the lowest crystallinity as revealed by DSC whereas LCBPEs have

LCBs only. ^{13}C-NMR could not provide information on the SCB and LCB distributions in the samples, therefore, other methods of branching determination were studied.

The molar mass distributions (MMDs) of these resins were determined using HT-SEC with infrared (IR) detection. For comprehensive branching information, a quadruple-detector high-temperature size exclusion chromatography (HT-SEC-d4) system was used. Unlike LDPEs which showed presence of SCB and LCB, LCBPEs had relatively smaller R_g values and contraction factors with more pronounced co-elution. Furthermore, the Mark-Houwink-Sakurada (MHS) plots of LCBPEs showed a much more pronounced deviation from the linear PE reference behaviour. This was proof of LCB not only being present, but their length was estimated to be significantly longer than 6 carbons. Our estimation is that they are longer than 50 – 60 carbons.

In the second part of the study, preparative fractionation was used to obtain simplified homogenous fractions for studying the branching distributions. The bulk samples were successfully fractionated using preparative molar mass fractionation (p-MMF) to get fractions with varying narrow molar masses. Two different methods of p-MMF were applied for the two sets of polyolefins. Preparative solvent gradient fractionation (p-SCF) was applied for LDPEs and p-MMF by precipitation was applied on the LCBPEs. The latter was used on LCBPEs as it allows for handling smaller sample sizes of less than 1 g as the LCBPEs were small in quantity. HT-SEC was used to validate the fractionation and it was shown that fractions with distinctly different molar masses and molar mass distributions were obtained.

The fractions obtained were analyzed using advanced analytical techniques. HT-SEC-d4 used for molar mass and branching analyses of the fractions confirmed ^{13}C-NMR findings that SCB is inherent across the molar mass fractions of LDPEs. As observed from the bulk samples, no SCBs could be detected in LCBPEs. The sensitivity limits of light scattering and viscometry detectors were a major challenge when analyzing low molar mass fractions. LDPE fractions had low crystallinities as influenced by SCBs, and LCBPEs had high crystallinities which increased with an increase in LCB as was observed with the bulk samples.

Mechanical analyses were successfully conducted on the LDPEs. However, due to limitations in the amount of the material for the LCBPEs, mechanical analysis could not be conducted. Tensile strength and Young's moduli of the LDPE samples could be linked to crystallinity and

total branching differences. The contributions of SCB overshadow those of LCB, but when SCB is comparable, more LCB results in higher tensile strength.

Tailored conditions for comprehensive branching analysis of the bulk PEs were successfully developed and implemented. It is known that SCBs alter the crystallinity of PE, this was seen for LDPEs, but LCBPEs showed significantly higher crystallinities due to the presence of LCB that cause "side chain crystallization". Polyolefins can be separated according to their chemical composition using high temperature interaction chromatography (HT-IC). Porous graphitic carbon (PGC) was used as an adsorptive stationary phase for the analyses of both sets of PEs, but single components of the samples could not be separated efficiently using a temperature gradient (TGIC). This was attributed to: (1) the interactive force disturbing the crystallization and redissolution processes or (2) the interactive force being too strong and indiscriminating between chains with small LCB differences. However, when a solvent gradient (SGIC) was applied at 160 °C using 1-dodecanol and TCB as the adsorption and desorption promoting solvents, respectively, components in LCBPEs could be resolved and LDPES could be distinguished.

To enhance separation in the TGIC setup, silica was used as a non-adsorptive stationary phase to allow for only crystallization and redissolution processes to influence interaction. It was observed that the separation of LDPEs is dependent on SCB whereas for LCBPEs it was molar mass and LCB content dependent. In the presence of SCB, it was shown that the contributions of LCB are negligible or cannot be seen. LCBPEs were retained longer as seen by high redissolution temperatures which were influenced by the presence of LCB. The behaviours of these branches indicated that their length could be $> C_{50}$ and contribute to side chain crystallization. High-temperature two-dimensional liquid chromatography analyses (HT-2D-LC) confirmed the increase in molar mass of the components with increasing elution volume/column temperature when both SGIC and TGIC were used in the first dimension.

The contributions of LCB towards chromatographic behaviour could not be elucidated in the LDPE fractions in terms of separation in HT-IC due to SCB content. Their separation was based on SCB with low molar mass components having broader peaks. On the other hand, LCBPEs showed multiple peaks on the silica stationary phase with low molar mass fraction having four distinct peaks. Generally, increased retention times were a notable characteristic of LCBPE fractions in comparison to LDPE fractions. This behaviour was also confirmed in

HT-2D-LC; the intensity of low eluting peaks from the 1st dimension increased with increase in LCB content. Preparative fractionation was, therefore, crucial in the better description of the LDPE and LCBPE microstructure.

6.2 Future work

1. LCBPEs have shown interesting thermal and crystallization behaviours. To further study the influence of LCB on crystallinity and crystalline arrangements, microscopy and spectral techniques can be used. Atomic force microscopy (AFM) has become one of the most frequently used tools for studying polymer crystallization and direct observation of long branches.[1,2]. Raman spectroscopy and X-ray diffraction techniques can be also used to study the crystalline nature of the samples.[3]
2. It will be interesting to understand the impact of LCB in LCBPE samples on mechanical properties such as tensile strength, Young's modulus and toughness. In the absence of large quantities of sample, microhardness tests and other mechanical analysis tools that rely on minute amounts of samples can be applied.
3. The fractions from the observed peaks of LCBPEs in HT-TGIC analyses can be collected and analyzed on HT-SEC-d4. This can then allow the separated fractions from HT-IC to be conclusively analyzed for LCB content in HT-SEC-d4.
4. A characteristic bimodal elution behaviour of linear polyethylene was observed in HT-TGIC using silica as the stationary phase and ODCB as the mobile phase. Further studies can be done to elucidate this behaviour of PE on silica.

6.3 References

(1) Hobbs, J. K.; Farrance, O. E.; Kailas, L. *Polymer* **2009**, *50*, 4281–4292.

(2) Shinohara, K.-i.; Yanagisawa, M.; Makida, Y. *Sci. Rep.* **2019**, *9*, 9791.

(3) Paradkar, R.; Sakhalkar, S.; He, X.; Ellison, M. *J. Appl. Polym. Sci.* **2003**, *88*, 545–549.

Appendix A ^{13}C-NMR data

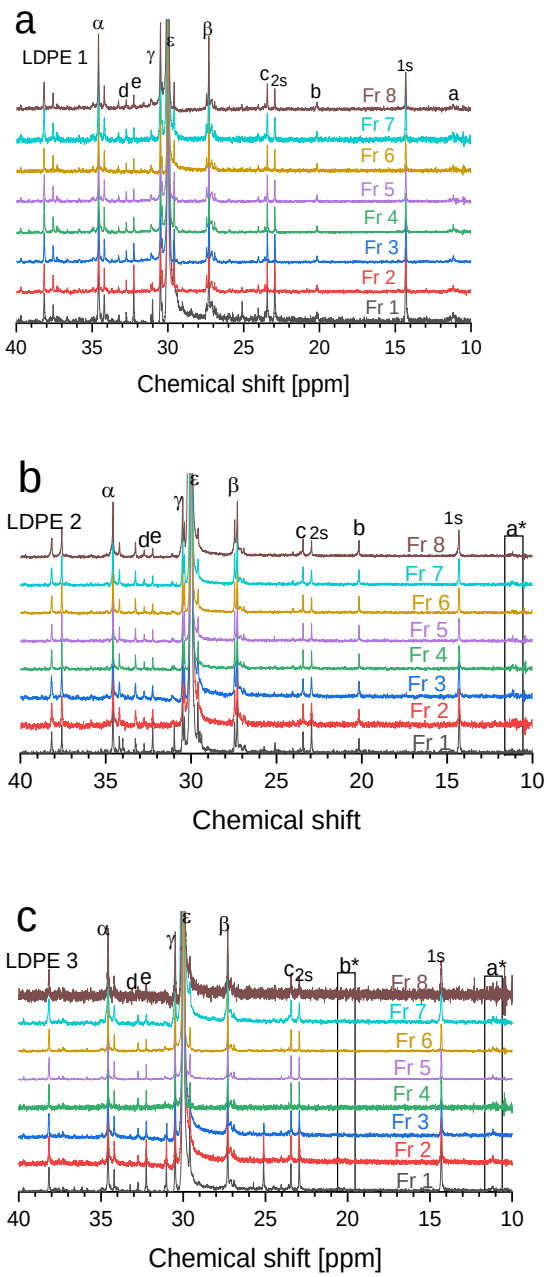

Figure A1 Normalised ^{13}C-NMR spectra LDPEs of p-MMF fractions of LDPEs. The spectra of the fractions of LDPE 1-LDPE 3 are shown in a-c respectively. (*) Peak absent.

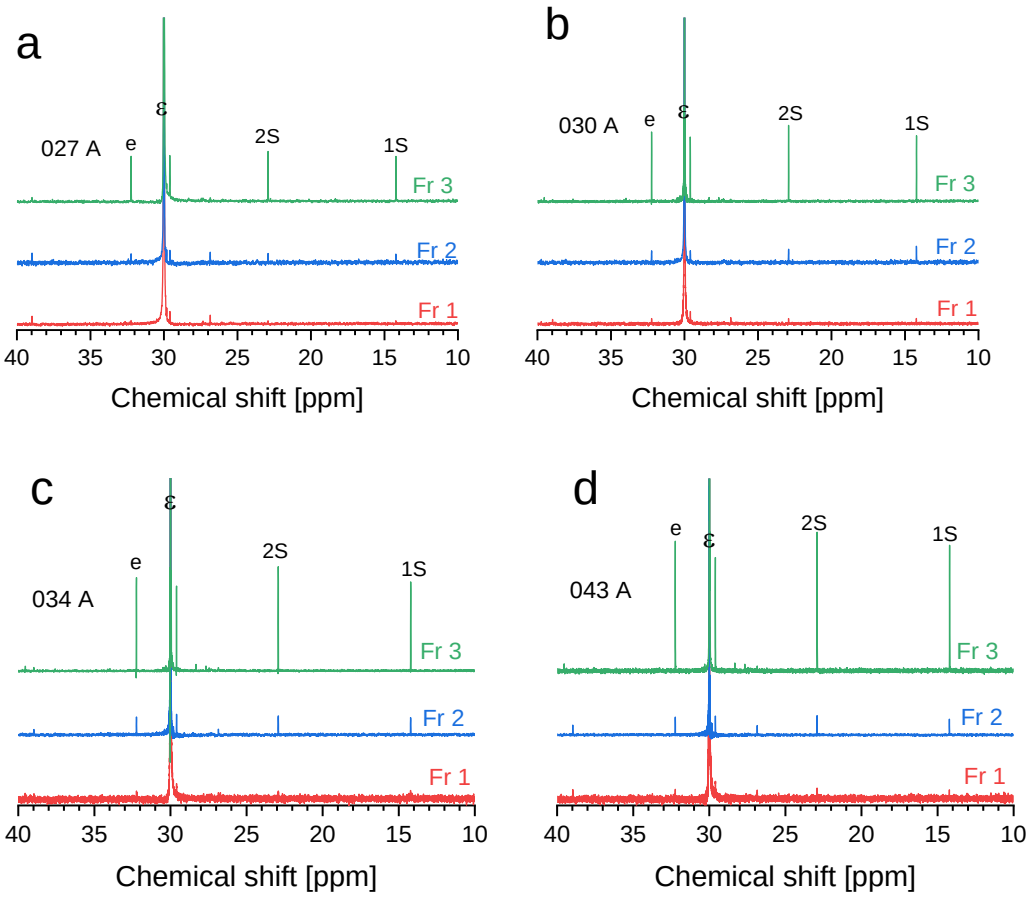

Figure A2 Normalised ^{13}C-NMR spectra of p-MMF fractions of LCBPEs. The spectra of the fractions of 027A-043A are shown in a-d respectively.

Appendix B Mechanical properties data

Commercial LDPEs were sourced for the present work in larger quantities and supplied enough material for mechanical testing. LCBPEs could not be tested due to insufficient sample. The detailed description of the mechanical testing procedure and the test strip moulding is provided in Chapter 3.

A summary of the tensile strength and the Young's moduli is presented in Table B 1. Fig. B 1 a compares the tensile strengths of the LDPEs, as expected, tensile strengths of the resins increase with decrease in the short chain branching (SCB), see Table B 1 The main difference in the tensile strengths of LDPE 2 and 3 can be attributed to the branching distribution across the molar mass distribution. Findings from HT-SEC clearly show higher contraction factors and slightly higher LCB content for LDPE 3 which is most probably designed for applications such as buckets and high strength containers. In addition, DSC findings also point to a higher crystallinity of LDPE 3 in comparison to LDPE 2. As expected, the same observation was made when Young's moduli of the samples were compared. Young's modulus increases with increase in tensile strength (Fig. B 1).

From literature, it has been established that tensile strength and Young's modulus are dependent on the crystallinity of the polyolefin resin as the different components play a part in the final mechanical properties.[1]

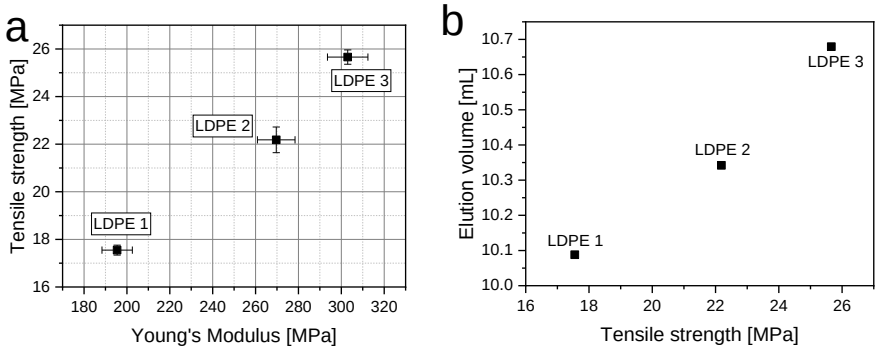

Figure B1 Relationship between tensile strength and Young's modulus of LDPE 1, 2 and 3 (a); relationship between elution volume obtained from $TGIC_{silica\ (ODCB)}$ and tensile strength for the same samples (b).

Recently, Amjadi *et al.*[2] concluded that while the ultimate tensile strength is dependent on the crystallinity level, it is independent of molar mass. As previously stated, the distribution of SCB and LCB is important.

Table B1 Summary of mechanical properties of LDPEs.

	LDPE 1	**LDPE 2**	**LDPE 3**
Young's modulus [MPa]	195.4±7.08	269.7±8.78	302.9±9.43
Tensile strength [MPa]	17.6±0.21	22.2±0.54	25.7±0.30

However, at elevated temperatures, tensile strength depends on the MMD. This results in higher strength due to the reduced capability of macromolecules sliding over each other and increased chain entanglemnt.[2] For the three LDPE samples, tensile strength and TGIC elution volume correlate well, see Fig. B 1 b. This could be due to the total branching as shown from ^{13}C-NMR results. Molar mass in the present case plays a lesser role in influencing tensile strength.

The melt flow index (MFI) decreased with an increase in tensile strength. This is explained best by the differences in the LDPE's branching structures, which are depicted by the MHS plots as well as ^{13}C-NMR. Long chain branching has a direct effect on the polymer melt and viscosity properties by promoting molecular entanglements. Accordingly, the branching characteristics have a direct association with the MFI of the LDPEs. If the SCB is comparable between two samples e.g., LDPE 2 and 3, the differences in the LCB play a major role.

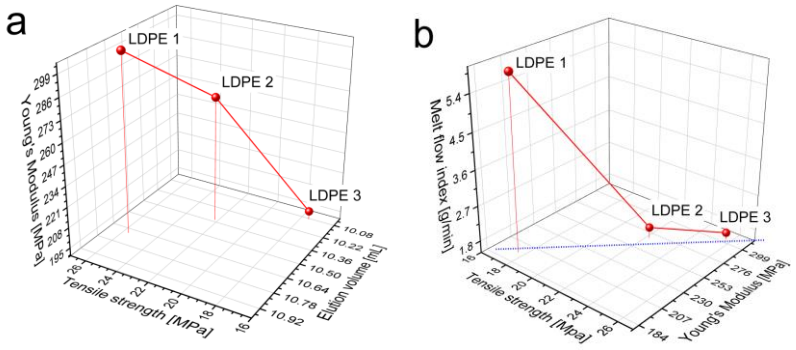

Figure B2 Correlation between Young's modulus, tensile strength, and $TGIC_{silica\ (ODCB)}$ elution volume (a) melt flow index, tensile strength, and young's modulus of LDPE 1, 2 and 3 (b). The dotted blue line (·····) in (b) shows the linear corelation between tensile strength and Young's modulus.

However, SCB has a significant impact on the melt flow properties as in the case of LDPE 1. SCB alters the crystalline structure of the molecules by folding into layers hence reorientation when under a tensile load.

There is a direct linear relationship of Young's modulus, tensile strength, and elution volume (Fig. B 2 a). Elution volume in TGIC increases with increase in tensile strength and Young's modulus. Similar plots can be constructed using DSC data instead of TGIC elution volume. The correlation between Young's modulus, tensile strength, and melt flow is plotted in Fig. B 2 b. This is different with the MFI; the MFI decreases with an increase in tensile strength and Young's Modulus. LDPE 1 has a significantly higher MFI which is due to a high degree of long chain branching compared to the other LDPEs.

References

(1) Huff, T.; Bushman, C.; Cavender, J. *J. Appl. Polym. Sci.* **1964**, *8*, 825–837.

(2) Amjadi, M.; Fatemi, A. *Polymers* **2020**, *12*, 1857.